NASA Technical Paper 3525

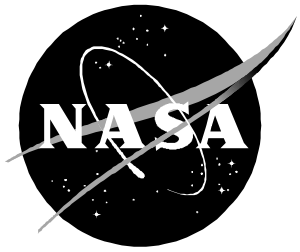

Investigation of Piloting Aids for Manual Control of Hypersonic Maneuvers

David L. Raney, Michael R. Phillips, and Lee H. Person, Jr.
Langley Research Center • Hampton, Virginia

National Aeronautics and Space Administration
Langley Research Center • Hampton, Virginia 23681-0001

October 1995

Available electronically at the following URL address: http://techreports.larc.nasa.gov/ltrs/ltrs.html

Printed copies available from the following:

NASA Center for AeroSpace Information
800 Elkridge Landing Road
Linthicum Heights, MD 21090-2934
(301) 621-0390

National Technical Information Service (NTIS)
5285 Port Royal Road
Springfield, VA 22161-2171
(703) 487-4650

Abstract

An investigation of piloting aids designed to provide precise maneuver control for an air-breathing hypersonic vehicle is described. Stringent constraints and nonintuitive high-speed flight effects associated with maneuvering in the hypersonic regime raise the question of whether manual control of such a vehicle should even be considered. The objectives of this research were to determine the extent of manual control that is desirable for a vehicle maneuvering in this regime and to identify the form of aids that must be supplied to the pilot to make such control feasible. A piloted real-time motion-based simulation of a hypersonic vehicle concept was used for this study, and the investigation focused on a single representative cruise turn maneuver. Piloting aids, which consisted of an autothrottle, throttle director, autopilot, flight director, and two head-up display configurations, were developed and evaluated. Two longitudinal control response types consisting of a rate-command–attitude-hold system and a load-factor-rate–load-factor-hold system were also compared. The complete set of piloting aids, which consisted of the autothrottle, throttle director, and flight director, improved the average Cooper-Harper flying qualities ratings from 8 to 2.6, even though identical inner-loop stability and control augmentation was provided in all cases. The flight director was determined to be the most critical of these aids, and the cruise turn maneuver was unachievable to adequate performance specifications in the absence of this flight director.

Introduction

Many recently proposed hypersonic vehicle concepts present significant problems in guidance, flight control, and flying qualities, which must be addressed if such designs are to be viable. These air-breathing vehicle designs traverse a broader range of flight regimes than aircraft which have flown in the past and must emphasize performance during all phases of flight to achieve their mission. Stringent constraints on angle of attack, sideslip, and dynamic pressure must be observed because hypersonic propulsion system performance will be strongly dependent on flight condition and may suffer dramatically if excessive variation is experienced. (See refs. 1 and 2.) Yet, such vehicles will be required to perform at least several basic maneuvers at high-speed flight conditions. The anticipated sensitivity of hypersonic propulsion systems makes precise regulation of flight condition imperative, while the high degree of aero-propulsive interaction makes such tight control difficult to achieve. These factors, together with nonintuitive effects associated with maneuvering in the hypersonic regime, raise the question of whether manual control of such a vehicle should even be considered. Therefore, the extent of manual control which is desirable for a vehicle maneuvering in this regime must be determined, and the form of aids that should be supplied to the pilot to make such control feasible must be identified.

Previous work by Berry (ref. 3) involved a piloted simulation of a hypersonic configuration in which numerous handling qualities issues relevant to maneuvering in high-speed flight were examined. Because of propulsion constraints and a number of high-speed flight effects, pilots encountered considerable difficulty controlling the vehicle even through relatively benign maneuvers. Subsequent work elaborated on aspects of the hypersonic flight regime that were responsible for the observed difficulties and targeted specific areas in need of additional research. (See refs. 4–6.) These investigations noted that the reduced-g environment of the hypersonic flight regime requires the vehicle to come to bank angles greater than 60° to execute a level 2g turn. This effect has been referred to as "centrifugal relief." Also, regulation of dynamic pressure during the maneuvers was particularly difficult because small errors in flight path angle produced large dynamic pressure excursions due to density variation with altitude. The dynamic pressure excursions were difficult to arrest because of the path-attitude decoupling that occurs at hypersonic speeds. This phenomenon tends to make control of flight path very difficult if a pitch-rate-command–attitude-hold response type is used. (See ref. 6.) McRuer and Myers (ref. 7) further examined the manner in which physical characteristics of hypersonic air breathers and the associated flight regime would impact flying qualities specifications for this class of vehicle.

Concurrent research by Lallman and Raney (refs. 8–12) focused on regulation of trajectory parameters during hypersonic maneuvers at cruise flight conditions, but maneuvers were restricted to the vertical plane. A follow-on investigation (ref. 13) addressed the problem of coordinated control of maneuvers in both the vertical and lateral planes at hypersonic cruise flight conditions. An approach was presented that provided maneuver

coordination through the resolution of altitude and cross-range errors into a normal load factor and bank angle command combination. The research of reference 13 yielded an automatic control design for executing coordinated maneuvers in hypersonic flight while regulating key parameters such as angle of attack, sideslip, and dynamic pressure.

This report describes an investigation in which the control laws and guidance concepts presented in reference 13 were implemented in a real-time simulation of an air-breathing hypersonic vehicle with the objective of development and evaluation of a set of piloting aids that could provide desired maneuver performance with an acceptable pilot workload. The real-time experiment consisted of two parts. The first part of the experiment was intended to identify the pilots' preferences from a set of two response types and two head-up display configurations designed to permit satisfactory manual control of the hypersonic vehicle. The second part of the experiment examined the degradation in task performance and pilot satisfaction as various pilot aids were removed and compared the resulting performance with maneuver performance in the fully automatic mode. The experiment provided information regarding the level of assistance that must be supplied to the pilot to achieve desired maneuver constraints and the form that the assistance should take.

The report begins with a description of the aircraft model used in the real-time simulation. The physical configuration of the simulator itself, in terms of displays and control inceptors, is briefly presented. Next, the report describes the real-time experiment design, describes the evaluation criteria, and discusses the experiment results. A concluding section summarizes the observations and presents several implications for vehicles maneuvering in the hypersonic regime.

Symbols

g	acceleration due to gravity, ft/sec^2
h	altitude, ft
n	normal load factor, g units
$\bar{q}$	dynamic pressure, lb/ft^2
R	altitude measured to center of Earth, ft
$t_{\theta 2}$	flight path-attitude lag time constant
V	total velocity relative to air mass, ft/sec
α	angle of attack, deg
γ	flight path angle, deg
Δ	perturbation from trim conditions
ρ	density, slug/ft^3
ϕ	bank angle, deg

Abbreviations:

APAS	aerodynamic preliminary analysis system
CDU	cockpit display unit
CGI	computer-generated image
CHR	Cooper-Harper rating
EADI	electronic attitude display indicator
HSI	horizontal situation indicator
HUD	head-up display
LFRC	load factor rate command
PAL	pilot assistance level
POST	Program to Optimize Simulated Trajectories
RBFD	resolver-based flight director
RCAH	rate-command–attitude-hold
rms	root-mean-square
SPI	surface position indicator
VMS	Visual/Motion Simulator

Aircraft Model

The vehicle concept used in this study is an air-breathing single-stage-to-orbit configuration designed to operate from a conventional runway. Planform and profile views of this hypersonic winged cone configuration are presented in figure 1. The fuselage has a conical forebody half angle of 5° with wrap-around engine nacelles and a 75° swept delta wing. The configuration includes elevons and a rudder for longitudinal and lateral-directional control. The overall vehicle length is 200 ft with a wing span of 60 ft; the weight of the fully fueled vehicle is approximately 300 000 lb with a fuel load of 110 000 lb. The pilot is located 101 ft ahead of the vehicle center of gravity at takeoff. A summary of geometric characteristics for this vehicle is presented in table 1.

A full-envelope database has been generated for the configuration as a result of extensive wind tunnel testing combined with analytical investigations using the aerodynamic preliminary analysis system (APAS). (See ref. 14.) The development of this inertial, propulsive, and aerodynamic database is detailed in references 15 and 16. The data provided in reference 15 were used to represent the aerodynamic characteristics of this configuration for the real-time simulation.

The variation of inertial characteristics and center of gravity with total vehicle weight is shown in figure 2. All maneuvers presented in this report were initiated with a vehicle weight of 250 000 lb. Although mass reduction due to fuel burn was modeled, inertial characteristics and

center-of-gravity location did not vary significantly during the real-time maneuver simulations.

The engine model used in this investigation does not include propulsion sensitivities to angle-of-attack variation. For this particular configuration, the wrap-around engine nacelles may tend to reduce the effect of propulsion sensitivity to angle of attack, but more typical configurations often include an underslung engine nacelle located on the lower surface of the fuselage. Such configurations would likely exhibit a greater propulsion sensitivity to angle-of-attack variation and thereby complicate longitudinal control of the vehicle. (See ref. 17.) Details of the engine model are presented in appendix A.

The simulation model used in this study is a rigid-body approximation, although recent analytical investigations using other hypersonic configurations have indicated that the aeroelastic modes have significant potential impact on all aspects of control for this type of vehicle. (See refs. 18 and 19.) The impact of aeroelasticity on the manual control of such configurations is a topic worthy of real-time research, but such a study would require a motion-based simulator with a bandwidth that exceeds the capabilities of the facility used in this investigation.

Simulation Facility

A real-time simulation of the hypersonic aircraft model was implemented on the NASA Langley Visual/Motion Simulator (VMS). The Langley VMS is a six-degree-of-freedom hexapod with performance characteristics described in table 2. During this investigation, the approximate time delay for the motion cues was 82 msec ($\pm$30 msec) and for the visual cues was 170 msec ($\pm$35 msec). Detailed specifications of the Langley VMS facility and motion algorithms are provided in references 20 and 21. The spherical rotational Earth equations of motion that were used to drive the simulator visual displays and motion cues are drawn primarily from reference 22. The general interior layout of the cockpit is shown in figure 3. The test pilot occupied the left station and the research engineer occupied the right station for all of the maneuvers described in this report. Descriptions of individual control and display features shown in figure 3 follow.

HUD and Out-the-Window Scene

The out-the-window scene used for the visual component of this simulation was a computer-generated image (CGI) produced by an Evans & Sutherland CT-6 system. Because the maneuvers in this investigation took place at an altitude of approximately 85 000 ft, the out-the-window visual scene produced by the CGI system simply consisted of dark blue sky showing a cloud layer to provide an indication of roll attitude with respect to the horizon. The image was presented on three cockpit windows (two forward and one left side) with an arrangement of three video monitors and a mirror beam splitter. Further details regarding the physical arrangement of the components of this display system are available in reference 23.

The primary cockpit flight instrument used in this investigation consisted of a head-up display (HUD). The HUD image was generated by a Terabit Eagle 100 symbology generator and then superimposed on the out-the-window scene generated by the Evans & Sutherland CGI system. This combined image was then presented to the pilot on the forward cockpit window video monitor. Although the HUD contained all information necessary to perform the hypersonic maneuver tasks, pilots indicated that inclusion of the out-the-window scene provided reassurance of the vehicle attitude with respect to the horizon.

The baseline HUD, which was used in this experiment, is shown in figure 4 and contains information relevant to the flight condition and vehicle attitude. A conventional pitch ladder with attitude indicator is provided at the center of the display. An artificial horizon line and flight path marker are also included as shown in figure 4. To the right of the horizon line is a digital altitude indicator and to the left of the horizon line are digital indicators for equivalent airspeed, angle of attack, Mach number, dynamic pressure, and normal load factor. A bank angle index is provided in the form of radial tick marks distributed in an arc around the bottom of the display in increments of 30°. As shown in figure 4, minor tick marks occur in increments of 10° between bank angle indices of $\pm$30°. A triangular symbol travels around the perimeter of the bank angle index to indicate the vehicle roll attitude. At the top of the display is a heading indicator and index with tick marks spaced at intervals of 2° and labeled at intervals of 10°. A throttle level indicator depicts the current throttle setting on a vertical scale shown in the upper left corner of figure 4.

Two radically different forms of flight director symbology were used with this basic HUD layout. As part of this experiment, the pilot's ability to perform the hypersonic maneuver task with different types of director symbology was compared. Specific components of these two flight director formats and the algorithm used to drive them will be discussed later in this report.

Head-Down Displays

Figure 3 shows the location of the electronic attitude display indicator (EADI) on the cockpit instrument panel. The EADI contains much of the same information presented on the basic HUD previously described but

without the presence of the out-the-window scene. A diagram of the EADI is shown in figure 5. The pilots who participated in this experiment indicated that they rarely, if ever, referred to the EADI during the maneuvers, and then, only to obtain gross confirmation of the information being displayed on the HUD.

Figure 3 also shows the location of the horizontal situation indicator (HSI) and surface position indicator (SPI). The HSI is shown in figure 6. Only the compass and heading readouts of this display were driven during this experiment, and pilots indicated that this instrument was not needed during the execution of the up-and-away maneuvers as long as they could rely on the heading index shown on the HUD.

A diagram of the SPI, which is shown in figure 7, depicts the magnitude and sense of the various control surface deflections with a color code for rate or position saturation. The control surfaces are colored green during nominal operation. If an actuator experiences a rate limit, the corresponding control surface is colored yellow; if a position limit is experienced, the surface turns red. Readouts of fuel flow rate and total fuel consumption are included on this instrument as well as a fill line, which shades the fuselage to provide a general indication of the amount of fuel remaining. This instrument was used primarily by the research engineer during control system checkout and diagnostic activities. Pilots did not use this display during execution of the maneuvers.

Cockpit Controls

The cockpit controls available to the pilot consisted of a left-side stick controller and a single throttle lever. The general location of the side stick is shown in figure 3. Force gradient and breakout settings of the McFadden hydraulic control loader used for this side stick are shown in table 3. An adjustable armrest was provided adjacent to the controller, and pilots indicated that no discomfort or awkwardness was experienced with the use of this type of control inceptor.

The throttle lever controlling total fuel flow rate was located to the pilot's right as shown in figure 3. The pilot of such a vehicle would not likely exercise independent control over fuel flow rate to individual combustor modules, so a single throttle lever was provided to the pilot for this study. An aural cue was provided in the form of engine noise that was scaled with fuel flow rate. (The noise was actually an afterburner sound effect, so turbine spooling sounds were intentionally absent.) The throttle lever had a total throw of 52.5°, and the corresponding fuel flow rate varied from 10 lb/sec in the aft position to 200 lb/sec in the full-forward position. Appendix A illustrates the manner in which the commanded fuel flow rate was used in the engine model.

The level of throttleability that would be possible for a scramjet propulsion system operating at hypersonic speeds is uncertain. Uninterrupted operation of the propulsion system would be of paramount importance during a hypersonic maneuver, which would place constraints on allowable magnitudes and rates of change of fuel flow settings. Such constraints will depend on configuration and flight condition. However, the severity of these constraints is highly uncertain, and information is not currently available on the throttleability of potential hypersonic propulsion systems. In the interest of ascertaining what the pilot would prefer to do in the absence of constraints, no limits were placed on allowable throttle lever angle variation when the throttle was under manual control.

Additionally, a cockpit display unit (CDU) was used by the research engineer to configure the simulator. The location of this device is shown in figure 3. The CDU was programmed to permit the researcher to select command response type, flight director type, and pilot assistance level (PAL) from the cockpit prior to each maneuver. (Pilot assistance level refers to the number and type of aids supplied to the pilot during the maneuver and will be described in greater detail later in this report.) Specific target flight conditions for the maneuver were also input to the CDU, and initiation of the task was manually triggered from the CDU. The CDU program included maneuver task completion criteria (table 4) that could provide a visual cue upon successful completion of a maneuver. The exact values from table 4 were selected somewhat arbitrarily, but they still provided a consistent definition of task completion for use when comparing time histories of a given maneuver under differing control configurations.

Preliminary Simulation Sessions

At the outset of this investigation, a series of real-time simulation sessions were conducted in which two Langley test pilots performed several of the hypersonic maneuver tasks described in reference 3. These consisted of constant dynamic pressure ascents and descents, decelerating turns, and cruise turns. The control system was a rate-command–attitude-hold response type for both the pitch and roll axes. (The design of this control law is described in appendix B.) No flight director or autothrottle was provided, but the baseline HUD shown in figure 4 was presented. When attempting to perform the maneuvers, the pilots experienced numerous difficulties associated with the peculiarities of the hypersonic flight regime that were revealed during earlier hypersonic simulation work conducted by Berry. (See refs. 3 and 4.) The intent of these preliminary simulation sessions was to reproduce these effects so that potential solutions to the problems could be developed. The

hypersonic cruise turn maneuver was selected for this experiment because it required coordination of lateral and longitudinal inputs as well as considerable throttle activity. To the test pilots, this task represented a fundamental maneuver with a high degree of difficulty.

The hypersonic cruise turn maneuver consisted of a heading change of 30° at constant altitude and dynamic pressure and was executed at a load factor of 2*g*. The maneuver was initiated from a level trimmed flight condition at Mach 7.86 at an altitude of 85 040 ft and dynamic pressure of 2000 lb/ft^2. The normal load factor required to maintain straight and level flight at this condition was approximately 0.84*g* because of the centrifugal relief effect. Centrifugal relief refers to a reduction in the normal load factor required for level flight that is experienced as a vehicle approaches orbital velocity. (See refs. 4 and 5.) The hypersonic cruise turn task definition was adapted from reference 3 and is summarized as follows:

1. Hold Mach number, altitude, and dynamic pressure
2. Bank to initiate maneuver
3. Establish steady 2*g* turn
4. Attain required heading change
5. Roll-out on desired heading

When asked to perform this maneuver with no flight director or autothrottle, the pilots indicated that the task was not reliably achievable. Note that the pilots felt that they had good control over the aircraft attitude; the rate-command–attitude-hold control law was doing its job. Figure 8 shows typical time histories of the cruise turn executed by two different pilots using the rate-command–attitude-hold system without autothrottles or flight director guidance. The target heading for this maneuver was 120°. From the heading time histories shown in figure 8, the pilots clearly did not have precise control over this parameter. The bank angle traces also show that there was a considerable uncertainty associated with the timing of the roll-out needed to arrest turn rate at the target heading.

The target altitude for the cruise turn was 85 000 ft and dynamic pressure was 2000 lb/ft^2. Figure 8 shows that significant excursions also occurred in these parameters during the maneuver. The pilots apparently were not able to control flight path sufficiently to perform the desired maneuver. Both pilots noted that arresting flight path deviations during the cruise turn was particularly difficult. The primary difficulty arises from the decoupling of path and attitude that occurs for this vehicle at the chosen flight condition. This result was not unexpected because it has been repeatedly alluded to in earlier research (refs. 3, 5, and 6). In fact, the development by Chalk in reference 6 regarding rate of change of flight path for a hypersonic vehicle equipped with a pitch rate-command–attitude-hold system predicted that extremely low-bandwidth control of flight path rate would result. The reason for this is illustrated by equations (1) and (2).

$$\frac{1}{t_{\theta 2}} = \frac{g}{V}\frac{n}{\alpha} \tag{1}$$

$$\dot{\gamma} = \frac{g\Delta n}{V} \tag{2}$$

where Δn is the normal load factor perturbation from trim.

The parameter $1/t_{\theta 2}$ is referred to as the flight path-attitude lag and can be interpreted as the frequency above which $\Delta\theta = \Delta\alpha$ and below which $\Delta\theta = \Delta\gamma$. (See ref. 6.) Note in equation (1) that, for a given n/α, $1/t_{\theta 2}$ tends to zero as V increases. Equation (2) further illustrates that, for a given change in normal load factor, the resulting rate of change in flight path angle is inversely proportional to velocity. Therefore, pitch attitude changes in hypersonic flight take an excessively long time to produce flight path changes. (The value of $1/t_{\theta 2}$ for the subject vehicle at the Mach 7.86 flight condition is approximately 0.084 sec^{-1}.) This effect is referred to as "path-attitude decoupling." The plots of pitch attitude and flight path angle time histories shown in figure 9 illustrate the impact of this decoupling. This figure shows that flight path angle was relatively unaffected by the pilots' higher frequency pitch inputs, while the flight path response to the pilots' lower frequency pitch inputs was virtually 90° out of phase. The resulting angle-of-attack perturbations shown in figure 8 are clearly not desirable from the standpoint of minimizing disturbances to the propulsion inlet conditions.

Equation (3) further illustrates the importance of flight path in regulating dynamic pressure. At hypersonic speeds, the V^3 multiplier of density gradient becomes the dominant factor in this equation. As flight path errors developed during the turn, the pilots noted a dynamic pressure error, which they then attempted to null with the use of throttle inputs. This significantly increased pilot workload during the maneuver. The time histories in figure 8 show that pilot B increased fuel flow rate in an unsuccessful attempt to compensate for dynamic pressure errors resulting from a positive altitude excursion.

$$\dot{\bar{q}} = \rho V\dot{V} + \frac{V^3}{2}\frac{\partial\rho}{\partial h}\gamma \tag{3}$$

The next section of this report describes several piloting aids that were developed to address the

difficulties that the pilots experienced during the preliminary simulation sessions.

Description of Piloting Aids

The difficulties encountered during manual control of the cruise turn maneuver precipitated an informal development phase in which the research engineer worked together with the project pilots to develop a series of aids in the form of guidance laws, flight directors, autothrottle, and throttle director that would help the pilots cope with the hypersonic flight environment. This part of the research involved discussions with the pilots, development and implementation of solutions, and precursory evaluation of these solutions leading to further refinement of the concepts. These piloting aids were then systematically evaluated in a formal real-time experiment. The following paragraphs describe the aids that were developed to assist the pilots in conducting the hypersonic maneuvers. The formal experiment that was designed to evaluate and quantify the benefits derived from use of these aids will be described later in this report.

Autopilot and Flight Director Guidance

Trajectory control was recognized to be the primary difficulty that the pilots would encounter during the cruise turn. Chalk noted in reference 6 that direct piloted control of flight path will not be practical because of the slow response rate; a better approach may be for the pilot to exert direct control over angle of attack or load factor and to modulate his inputs in response to flight director displays for trajectory control. Later work by Raney and Lallman (ref. 13) acknowledged this and addressed the problem by using a guidance approach that resolved vertical and lateral trajectory deviations into a lift vector command that would null the errors.

The primary element of the guidance law developed in reference 13 was a simple coordinate transformation referred to as a "resolver" that converted vertical and lateral flight path corrections into a desired bank angle and normal load factor subject to vehicle constraints. The guidance law was applied to an example configuration identical to the configuration used in this study, and its performance was demonstrated in an unpiloted digital simulation. The algorithm could be used either to drive inner-loop flight controls directly as an autopilot or to drive a cockpit flight director that could guide the pilot through a hypersonic maneuver. The guidance law was implemented in the real-time simulation for this study so that it could operate in either of these two modes. Detailed development of this guidance strategy is presented in reference 13.

The advantage of this guidance concept for driving a flight director, rather than simply presenting a flight path error to the pilot, is that flight path dynamics are effectively removed from the immediate control task that the pilot is attempting to perform. This is achieved because the guidance law specifies flight director cues in the form of normal load factor and bank angle, which are two parameters over which the pilot has relatively high-bandwidth control even at hypersonic flight conditions. The effect of path-attitude decoupling is thereby eliminated from the pilot's flight director tracking task, and the problems of a conventional flight path director are avoided. This is precisely the approach envisioned by Chalk in reference 6.

Flight Director Symbology

Two forms of flight director symbology were compared for use in executing the hypersonic maneuvers. The two flight directors differed only in the graphical presentation of the load factor and bank angle cues to the pilot. The first director symbology is referred to as the "conventional flight director" in this report, and the second is referred to as the "resolver-based flight director" (RBFD). The same algorithm was used to compute the desired load factor and bank angle in both cases.

The symbology for the conventional flight director used in this investigation consists of a director diamond superimposed on the head-up display from figure 1 as shown in figure 10. The vertical offset of the director symbol from the flight path marker is driven by the normal load factor error, which is the difference between the actual load factor normal to the velocity vector and the desired load factor computed according to the algorithm described in reference 13. Likewise, the lateral offset of the flight director symbol from the flight path marker is driven by the bank angle error, which is the difference between the actual bank angle of the vehicle and the desired bank angle generated by the guidance law. The director diamond in figure 10 flashes from hollow to solid for 2 sec prior to the initiation of the roll-out during the cruise turn maneuver.

Because the flight path angle was no longer the parameter being directly pursued by the pilot, revision of the visual cue used to depict the control task was also appropriate. The resolver-based flight director (RBFD) presents the pilot with a graphical depiction of the magnitude and direction of the vehicle actual lift vector instead of the desired lift vector specified by the guidance law. The display is simply a pictorial representation of the resolver element of the guidance algorithm described in reference 13.

Primary elements of the RBFD symbology consist of the load factor director circle, bank angle director, and

the lift vector arrow shown in figure 11. The load factor circle is centered on the flight path marker symbol. The radius of the load factor circle is proportional to the magnitude of the desired load factor computed by the resolver element of the guidance algorithm. The load factor circle contracts or expands to indicate the variation of the desired load factor. The bank angle director symbol moves around the perimeter of the load factor circle to indicate the desired bank angle computed by the resolver. A faint dashed line runs from the center of the flight path marker to the bank angle director symbol. A lift vector arrow is shown in figure 11 pointing vertically upward from the origin of the flight path marker symbol. The length of the lift vector arrow is proportional to the actual load factor acting normal to the vehicle flight path based on accelerometer measurements. The lift vector arrow always points straight up from the flight path marker.

To execute a desired maneuver with the RBFD, the pilot manipulates the control stick to place the tip of the lift vector arrow at the location on the perimeter of the load factor circle indicated by the bank angle director. In this way the pilot achieves the load factor and bank angle that will cause the flight path to move in the desired fashion. As the desired load factor and bank angle vary, the pilot tracks the RBFD symbology by attempting to maintain contact between the tip of the lift vector arrow and the bank angle director on the perimeter of the load factor circle. The dashed line between the bank angle director and the center of the flight path marker permits the pilot to ascertain whether he has precisely matched the desired bank angle. The dashed line will be completely obscured by the lift vector arrow when the bank angle error is nulled.

After the two test pilots performed several maneuvers with the RBFD, they suggested a refinement to the symbology, which resulted in a fixed-radius version of the RBFD shown in figure 11. The load factor circle was fixed at a constant radius, and the lift vector arrow shortened or lengthened to reflect the error between the desired load factor and the commanded load factor rather than having the load factor circle contract or expand according to desired load factor. The test pilots indicated that too much appeared to be happening at the same time when the load factor director circle and the load factor arrow were both changing size in the original RBFD.

The nominal bank angle indicator shown in figure 11 is another refinement based on pilot suggestions and is used only during maneuvers for which a prescribed nominal bank angle can be defined; the level 2*g* turn is such a maneuver. In this case, the nominal bank angle indicator appears at the nominal bank angle for the turn on the inner perimeter of the load factor circle at the instant the maneuver is initiated. The bank angle director then moves around the outer perimeter of the load factor circle at the desired roll rate until it is aligned with the nominal bank angle indicator. The pilot tracks the bank angle director during the roll-in. The nominal bank angle for a level 2*g* turn at hypersonic speeds is calculated from equation (4).

$$\phi_{nom} = \cos^{-1}\left[0.5\left(1 - \frac{V^2}{Rg}\right)\right] \tag{4}$$

During the turn, the bank angle director may call for minor deviations from the nominal bank angle indicator to null slight altitude errors. The nominal bank angle indicator symbol was added to provide the pilots with an anticipation cue that would warn them to prepare to arrest their roll rate. The bank angle director triangle in figure 11 flashes from hollow to solid for 2 sec prior to the initiation of the roll-out during the cruise turn maneuver.

The specific symbology of the RBFD is designed to represent the physical orientation of the vehicle lift vector in relation to the desired load factor and bank angle. In this way the RBFD relates directly to the fundamental forces, which act on the aircraft and which the pilot must manipulate in order to effectively control the trajectory.

Command Response Types

Two command response types were compared for use in executing the hypersonic maneuver tasks. The first response type was a pitch rate-command–attitude-hold (RCAH) system. This is the same system that was used to perform the maneuvers during the preliminary simulation sessions. Because the guidance laws were designed to drive the flight director based on desired load factor, the pilots were then provided with another response type option that might provide better harmony with such a director. Accordingly, a second control law was designed to provide a load-factor-rate-command (LFRC)–load-factor-hold response type. Note that such a system would be self-trimming in the sustained 2*g* turn and should require less pilot attention than the rate-command–attitude-hold system. The LFRC system was also well suited to the incorporation of load factor limits. In both cases, the lateral control law was a roll-rate-command–attitude-hold system. A description of the control laws for the two response types is provided in appendix B.

The set of two flight director symbologies and two response types yielded four combinations for use in the piloted evaluations. The combination of the conventional director symbology with the RCAH response type represented a relatively familiar configuration to the test pilots, while the combination of the resolver-based flight

director and the LFRC response type represented a considerable departure from convention.

Autothrottle and Throttle Director

Another piloting aid that was designed for this investigation consisted of an autothrottle that regulates dynamic pressure during hypersonic maneuvers. Pilots had indicated a high degree of difficulty associated with regulating dynamic pressure during the cruise turns in the preliminary simulation sessions. An autothrottle, which compensated for density variation with altitude, was formulated to maintain dynamic pressure during ascending or descending flight. The design of this autothrottle was developed in reference 13.

A throttle director was also provided on the left wingtip of the flight path marker to provide a speed control cue in the absence of the autothrottle system. This element of the display is shown in figures 10 and 11. The throttle director consists of a shaded bar which appears above or below the left wingtip of the flight path marker. The vertical length of the bar is proportional to the fuel flow error, which is the difference between the actual fuel flow rate and the desired fuel flow rate to the propulsion system. The desired fuel flow rate is computed with the same algorithm that drives the autothrottle. The bar drops below the wingtip to indicate that the actual fuel flow rate is less than the desired rate and rises above the wingtip when the actual fuel flow rate is greater than the desired rate. The pilot is then able to null the fuel flow error by adjusting the throttle controls accordingly. An identical throttle director was used with the conventional flight director symbology and the RBFD symbology.

Pilot Assistance Levels

To ascertain the form and degree of assistance that must be supplied to the pilot to achieve satisfactory maneuver performance, the pilot assistance level (PAL) concept was developed. The numerical PAL designation represents the level of assistance provided to the pilot in the form of directors and automation. A flowchart that depicts the manner in which the various piloting aids were integrated with other elements of the real-time simulation is shown in figure 12. Table 5 defines the set of numerical PAL designations and presents the associated switch configurations for the flowchart. The autopilot and autothrottle elements shown in figure 12 are thoroughly described and demonstrated in reference 13. A description of the inner-loop pitch, roll, and yaw control elements is presented in appendix B. Figure 12 shows that the basic inner-loop stability augmentation system (SAS) was provided with all PAL conditions and that only outer-loop elements were added or removed as the pilot assistance level was varied.

Prior to initiation of a run, the pilot assistance level was selected by entering the appropriate numerical PAL designation from table 5 into the CDU. This process selected which piloting aids would be supplied by appropriately configuring the switches shown in the flowchart. The CDU was then used to select which of the two HUD's and two longitudinal control response types would be used.

After designating the PAL setting, the maneuver task was input to the CDU by specifying desired changes in altitude, dynamic pressure, and heading. The cruise turns that were performed in this study consisted of a heading change of 30° at constant altitude and dynamic pressure. The maneuver was then initiated by pressing the "execute" button on the CDU. The guidance laws then drove the flight director, autothrottle, or autopilot corresponding to the PAL setting. If the PAL setting was 0, then neither the autopilot, flight director, autothrottle, nor throttle director was driven, and the pilot had full manual control of the vehicle using the side-arm control stick and throttle levers.

From the comparison of performance metrics for a given task executed with different PAL configurations, identification of those tasks which require automation or flight director cues to achieve the desired performance is possible. This information is necessary to define the types of tasks that can and cannot be performed under degraded control configurations and to determine the level of automation that should be provided for controlling the vehicle during nominal execution of a hypersonic maneuver.

Experiment Design

The hypersonic cruise turn maneuver was used to compare the various control designs and piloting aids in a formal real-time experiment. When comparing the control and flight director features, the pilot was asked to focus on the following two main issues: Does the feature improve the ease with which the task is executed? and Does the feature improve the precision with which the task is executed? After each task, the pilot was asked to evaluate the vehicle control systems using the Cooper-Harper flying qualities rating scale shown in figure 13. Subjective comments on displays and response types were also requested. During each run, a videotape of the front cockpit monitor showing the CGI and HUD was made, which included an audio recording of the pilot's remarks.

The real-time experiment consisted of two segments. Part 1 of the experiment was designed to identify the pilot's preferred command response type and flight director symbology from a set of four combinations for

use in the hypersonic cruise turn maneuver. The designations for these four response type and HUD combinations are shown in table 6. Part 1 of the experiment was conducted with PAL 3 so that autothrottles were active at all times. This permitted the pilot to focus on the specific features of the response type and the flight director symbology. At the conclusion of part 1, the pilot was asked to select his preferred flight director and response type combination.

Part 2 of the experiment was intended to assess the degradation in task performance and Cooper-Harper flying qualities ratings as the pilot assistance level was reduced from 4 (fully automated) to 0 (no automation). This segment of the experiment was conducted with the pilot's preferred director symbology and command response type from part 1. When the maneuver was executed with PAL 4, the pilots simply observed the automatic systems while paying special attention to the timing and magnitude of throttle inputs. This provided them with an opportunity to train for the task of conducting the maneuver when the autothrottle and flight director would not be present.

Four Langley test pilots were asked to participate in the experiment. All four pilots were familiar with a wide range of configurations including both transport and fighter aircraft. Each pilot was briefed on the purpose of the experiment prior to participation. This briefing also included a discussion of the flying qualities and control issues associated with maneuvering in hypersonic flight. Prior to each simulation session, the pilot was supplied with a specific session itinerary, run log, and comment pages. These materials described the maneuver tasks and objectives of the simulation session. A typical session itinerary is shown in figure 14.

Specific criteria were necessary for judgment of desired and adequate task performance. Information on tolerances of hypersonic propulsion systems to angle-of-attack and dynamic pressure perturbations and permissible range of throttleability was not available at the time of this investigation. Therefore, relatively stringent performance criteria were specified in the interest of providing a conservative assessment of the errors that the propulsion system and trajectory parameters might tolerate. Figure 14 includes the criteria used to define desired and adequate task performance for dynamic pressure and altitude regulation as well as heading capture. Note that neither of the time histories shown in figure 8 satisfied even the adequate performance criteria. Desired and adequate tolerances for the tracking of guidance commands were also specified to let the pilots know how aggressively they should pursue the director symbology.

To assess the merits of the various piloting aids, maneuver tasks were compared on the basis of two criteria. The first means of comparison was pilot workload metrics, and the second was task performance metrics. These metrics are listed as follows:

1. Pilot workload metrics
   - A. Flying qualities ratings using Cooper-Harper scale
   - B. Longitudinal stick rms deviation from mean
   - C. Flight director rms tracking errors
   - D. Subjective comments
2. Performance metrics
   - A. Peak absolute error measurements in dynamic pressure and altitude
   - B. Dynamic pressure and altitude rms error
   - C. Fuel consumption during task
   - D. Acquisition and regulation of target parameters

The pilot workload metrics addressed the question of whether or not a particular feature being examined improved the ease with which the pilot was able to perform a given maneuver, while the performance metrics addressed the question of whether or not the feature improved the precision with which the pilot could perform the maneuver. The following section of the report describes the results of the real-time experiment and presents comparisons in terms of these metrics.

Discussion of Part 1 Results

The first part of the experiment was intended to identify the pilots' preferences for the response type and HUD combination. Each pilot performed the hypersonic cruise turn maneuver several times with each of the four combinations. The authors emphasize that this part of the experiment was conducted with the use of PAL 3 in all cases, that is, with the autothrottle activated. Table 7 shows the pilots' final choices for their preferred response type and HUD symbology. A clear preference was demonstrated for the LFRC response type over the RCAH. Pilots indicated that the workload was much lower with this response type but that the need to push the stick forward in the roll-out to unload the vehicle was disconcerting at first. The harmony of the flight director with this response type was understandably much greater because the flight director symbology for either HUD configuration is driven by a load factor error signal. Table 7 shows no consistent preference for one flight director symbology over the other, although each pilot cited significant reasons for his choice. Appendix C contains a transcript of each pilot's comments regarding the basis for the selection of the preferred response type and HUD combination. The following sections examine the

variation in pilot workload metrics and task performance metrics with the response type and the HUD symbology.

Workload Metrics

The test pilots were asked to assign a Cooper-Harper flying qualities rating (CHR) to each of the response type and HUD combinations. These ratings are shown in figure 15. The data show an improvement in pilot satisfaction with the LFRC response type when compared with the RCAH response type. The pilots generally indicated that the LFRC control system permitted the flight director signal to be followed with greater ease. Pilots also commented that the LFRC response type provided greater ability to carefully control and arrest the *g*-onset than the RCAH system during roll-in and roll-out maneuvers.

Figure 15 shows that pilot C awarded the LFRC–HUD-1 combination a CHR of 2.5, while awarding the LFRC–HUD-2 combination a CHR of 4. Pilot C expressly noted that the source of this rating difference was a hardware issue and felt the basic symbology elements of HUD 2 provided the pilot with better awareness than HUD 1. However, as the large circular element of HUD 2 (the load factor circle shown in fig. 11) traversed the horizontal scan lines of the cockpit window video monitor, the curved line appeared to stair-step. This effect proved particularly distracting to pilot C, which resulted in lowering the rating of HUD 2. This effect is an artifact of the hardware configuration of the Langley VMS, which mixes the HUD with an out-the-window scene for display on a video monitor. Pilot C indicated that, although the conceptual depiction of the task was better with HUD 2 (the RBFD), the higher resolution of the display symbols provided by the HUD 1 implementation was preferred.

The combination that received the best average CHR was the LFRC response type with the HUD-1 symbology. Each of the test pilots awarded this combination a level-1 flying qualities rating (CHR $\leq$ 3). As table 7 indicated, this combination was selected as the most preferable by two of the test pilots.

Figure 16 shows a comparison of the rms longitudinal stick deflections associated with each of the four response types and HUD combinations for the cruise turn task. To produce this graph, the rms deviation from the mean stick deflection was computed for each of the time histories in the entire set of real-time runs conducted by all four test pilots. The average rms stick deflection was then computed for each response type and HUD combination as shown in figure 16. The maximum and minimum rms deflections are also shown in the figure. The values represent the general level of stick activity about the mean stick deflection. Approximately twice as much stick activity resulted from the RCAH system than from the LFRC system. However, a few comments regarding possible bias in this observation should be noted.

First, the basic nature of the cruise turn task, which requires the pilot to maintain 2*g* through the turn while regulating altitude (and thereby dynamic pressure) with bank angle, makes the LFRC response type ideally suited to this task. Other tasks not requiring sustained periods of constant *g* may have resulted in less pronounced differences in stick activity between the RCAH and LFRC control systems. Also, the LFRC response type permits the pilot to carefully control the rate of *g*-onset, set load factor, and then get out of the longitudinal control loop during the steady segment of the maneuver. But the RCAH system did not include a trim control and, therefore, required the pilot's constant attention to maintain 2*g* during the steady segment of the maneuver. Inclusion of a trim button on the stick for use with the RCAH system might have reduced this effect, although the pilots commented that they would be hesitant to set such a trim device at the value required for the 2*g* turn.

Further insight into these effects is provided in figure 17, which presents a comparison of time histories from typical maneuvers conducted by pilot A using each of the four response type and HUD configurations. The figure shows that similar levels of altitude and dynamic pressure errors were experienced for all four configurations, and these errors were well within the tolerances specified for desired performance. However, figure 17 also shows that normal load factor was relatively quiet during the steady segment of the maneuver for the runs conducted with the LFRC response type and that considerably greater activity was experienced with the RCAH system. Figure 17 also shows the associated angle-of-attack time histories. Although the magnitudes of the angle-of-attack variation during the maneuvers are the same, the time histories show that the runs conducted with the RCAH system were much noisier. The pilots commented that the RCAH response type required continual inputs on their part and that the precision of the maneuver was not as good as with the LFRC system. Anticipated propulsion system sensitivity to angle of attack makes minimization of perturbations during the maneuver desirable; the benefit of the LFRC response type, which allows the pilot to extract himself from the longitudinal task during the steady segment of the maneuver, is clear.

Figure 17 also shows that about the same level of bank angle activity was experienced during the maneuver for all four configurations. The small bank angle perturbations are called for by the guidance algorithm to regulate altitude and dynamic pressure during the maneuver. A comparison of load factor and bank angle time

histories in figure 17 clearly indicates the necessity to roll and pull simultaneously to track flight director guidance during the roll-in and roll-out segments of this maneuver.

A comparison of the heading, altitude, and dynamic pressure time histories in figure 17 with those in figure 8 clearly shows that use of the flight director and guidance algorithm developed after the preliminary simulation sessions provided the pilot with significantly greater control over the vehicle trajectory. In particular, the heading time histories in figures 8 and 17 indicate that the piloting aids, which consisted of the autothrottle and flight director, permitted the maneuver to be performed in a consistent and repeatable manner. A quantitative comparison of maneuver performance with and without the various piloting aids was conducted in the second part of the real-time experiment and will be discussed later in this report.

Another metric used to compare the four response type and HUD combinations was the rms tracking error of the actual normal load factor from the desired normal load factor commanded by the guidance algorithm. This metric provides a relative assessment of how closely a particular configuration enables the pilot to achieve the conditions called for by the guidance algorithm. The pilots were asked to track the load factor director as closely as possible. Flight director tracking tolerances were specified as 0.1*g* for desired performance and 0.2*g* for adequate performance as noted in figure 13. Figure 18 again indicates a clear improvement of the LFRC response type over the RCAH response type. When using the LFRC system, the pilots experienced an average rms load factor error of roughly 0.05*g*, while the RCAH system resulted in an average rms load factor error of roughly 0.12*g*. The LFRC system permitted the pilots to track the load factor guidance cue more precisely, regardless of the HUD symbology.

A similar comparison of rms tracking error in bank angle is shown in figure 19. The flight director tracking tolerances specified in figure 14 for bank angle were 5.0° for desired performance and 10° for adequate performance. Figure 19 shows that the performance for all four HUD and response type combinations was well within the desired tolerance.

Performance Metrics

To compute the dynamic pressure performance metrics, the peak absolute value of the dynamic pressure error was first determined for each of the real-time runs. The average peak absolute dynamic pressure error was then computed for each of the response type and HUD configurations. The average, maximum, and minimum values of the peak absolute dynamic pressure error are shown in figure 20. Error tolerances were specified as 20 lb/ft^2 for desired task performance and 30 lb/ft^2 for adequate performance. An analogues plot of the mean dynamic pressure error is shown in figure 21.

Figure 20 shows that desired performance was achieved in all runs (recall that autothrottles designed to regulate dynamic pressure were active in all runs during this part of the experiment). A slight increase in both the peak and the mean dynamic pressure errors is apparent when the RCAH response type is compared with the LFRC response type. An identical trend in terms of variation in peak and mean absolute altitude errors with response type and HUD configuration is shown in figures 22 and 23. The altitude error tolerance for desired performance was 200 ft, and all runs achieved desired performance. The HUD symbology appeared to have no appreciable impact on maneuver precision as judged by the magnitude of altitude and dynamic pressure errors.

Fuel consumption during the maneuver is another factor to consider when comparing the performance metrics for the four response type and HUD combinations. Figure 24 shows the variation in fuel consumption with configuration. On average, the RCAH response type resulted in slightly greater fuel expenditure during the maneuver due to increased activity in terms of angle-of-attack variation and associated control surface deflections. This maneuver represents only a small segment of the entire mission for an air-breathing hypersonic vehicle, and the relatively small difference in fuel consumption could be significant when integrated over the duration of the mission. Current air-breathing hypersonic vehicle concepts must emphasize fuel efficiency throughout the flight envelope to retain any hope of a achieving a reasonable payload capacity, so the apparent reduction in fuel consumption provided by the LFRC system is an attractive feature of this response type.

In summary, part 1 of the real-time experiment indicated that all four pilots preferred the LFRC response type over the RCAH response type. Pilot comments emphasized that the load-factor-oriented control system provided greater harmony with the flight director cue, which was driven with a load factor command specified by the guidance system. The impetus for providing a load-factor-oriented director instead of flight-path-oriented director stems from the hypersonic path-attitude decoupling effect, which was elaborated on earlier in this report. The LFRC response type provided the pilots greater ease and slightly improved precision in control of the maneuver based on Cooper-Harper ratings, pilot comments, workload metrics, and task performance metrics. This response type also relieved the pilot of the longitudinal control task once the steady turn was established thereby producing fewer angle-of-attack perturbations, less associated control activity, and

slightly lower average fuel consumption. Note that this effect was somewhat influenced by the lack of a trim button in the RCAH implementation and that a different trend might be observed for other maneuvers that don't involve such sustained periods at elevated load factor as does the cruise turn.

No consistent preference for either HUD was identified because two pilots preferred the conventional symbology and two preferred the resolver-based symbology. Desired performance specifications were achieved with both HUD's, and no significant differences in maneuver precision or workload were noted. Although no consistent preference for either HUD symbology could be identified, each pilot had good justification for the particular symbology selection. Each of the four test pilots awarded at least one response type and HUD combination a level-1 flying qualities rating (CHR $\leq$ 3) for the cruise turn maneuver and selected a preferred combination for use in part 2 of the real-time experiment.

Discussion of Part 2 Results

The second part of the real-time experiment examined the degradation in task performance and flying qualities ratings as various piloting aids were removed. This was accomplished by asking the pilots to perform and compare the maneuver using their preferred flight director and response type under each of the pilot assistance level (PAL) conditions described earlier in this report. The PAL setting was varied from 4 (full autopilot task execution) to 0 (manual control of stick and throttle with no directors). The intent was to identify the degree of assistance that must be supplied to the pilot in order to achieve desired task performance with an acceptable workload. This section presents the variation with PAL of pilot workload metrics and of task performance metrics.

Workload Metrics

The test pilots were asked to assign a Cooper-Harper flying qualities rating to each of the PAL conditions. These ratings are shown in figure 25. The PAL 4 runs involved fully automatic execution of the maneuver with autopilot and autothrottles, so no Cooper-Harper ratings were assigned for that condition. Figure 25 shows that the task was rated as level 1, with an average CHR equal to 2.6, when PAL 3 was used. The PAL 3 condition corresponds to manual stick control with a flight director and autothrottle. (See table 5.) When the autothrottle was deactivated and the throttle director cue was provided with PAL 2, the average CHR increased to 4. Pilot comments indicate that a considerable workload increase was associated with tracking the throttle director cue. This results is due, at least in part, to the fact that the throttle director calls for a thrust increase during the roll-in phase of the maneuver, when a relatively high workload is already required to track the flight director cue. With the autothrottle deactivated, the pilot is required to roll, pull, and add power simultaneously during this portion of the maneuver.

Figure 25 shows that the average CHR awarded was 3.5 when the throttle director cue was removed with PAL 1. Pilot comments indicated a slight improvement in the perception of workload when the throttle director was removed. With PAL 1 the pilots used the digital readout on the HUD to provide feedback for the manual regulation of dynamic pressure with throttle. All four pilots indicated that they were essentially operating the throttles in an open-loop fashion during the roll-in, relying on their training from earlier observations of the autothrottle. After the roll-in was completed, they could check the dynamic pressure readout on the HUD to affect minor corrections to the throttle setting during the steady turn, which was part of the maneuver that required much less attention to the flight director. So, with PAL 1, the pilots appeared to demote throttle control from a pursuit task to an open-loop-memorized task during the roll-in, which could explain the slight reduction in the perceived difficulty of the task. However, two of the pilots specifically commented that they would prefer the presence of the throttle director if they were performing an unfamiliar task. All of the pilots commented that, although they could perform the maneuver satisfactorily with manual throttle control, they felt that autothrottles should be provided (as with PAL 3) for routine execution of such a maneuver.

The most notable feature in figure 25 is the dramatic degradation in acceptability ratings when PAL was reduced from 1 to 0, which corresponded to removal of the flight director cue. With PAL 1, the average Cooper-Harper rating (CHR) assigned by the pilots was 3.5, whereas with PAL 0 the average increased to 8. This occurred in spite of the considerable training that the pilots received in performing the task while using the higher pilot assistance levels. The pilots indicated that the task simply could not be performed to adequate specifications on a reliable basis with PAL 0, as had been noted earlier during the preliminary simulation sessions. This condition persisted in spite of the change from the RCAH control system that was used in the preliminary sessions to the LFRC control system that had been unanimously chosen by the pilots during part 1 of the formal real-time experiment.

Figure 26 shows the average, maximum, and minimum rms longitudinal stick deflections for the combined set of real-time runs for all four pilots. The data corresponding to the PAL 4 fully automated runs are included

for completeness. The trends observed in figure 26 agree completely with those in figure 25 and provide an objective confirmation of the assigned pilot ratings. Figure 27 shows a plot of time histories of longitudinal stick deflection from two typical runs conducted by pilot B with PAL 3 and PAL 0. The pilot was using the LFRC response type in both runs. A dramatic increase in stick activity is apparent when the autothrottle and flight director piloting aids are removed, which further corroborates the trend shown in figure 25.

Performance Metrics

The variation in the task performance metrics with pilot assistance level generally followed the same trends that were observed for the workload metrics. Figure 28 shows the average, minimum, and maximum of the peak absolute value of dynamic pressure error compiled from the complete set of piloted real-time runs. Bounds that define desired and adequate task performance are also indicated in this figure. The PAL 4 fully automatic runs are included for comparison purposes.

Figure 28 shows that all runs conducted with PAL 3 achieved desired performance specifications, while none of the runs conducted with PAL 0 achieved even adequate performance specifications. Figure 29 shows the analogous plot for the peak absolute altitude error. Once again, none of the runs conducted with PAL 0 achieved even adequate performance. The variation of the mean absolute dynamic pressure error with PAL is shown in figure 30, and mean absolute altitude error is shown in figure 31. The mean errors shown in these plots follow the same trends observed in the peak error plots in figures 28 and 29. A significant increase in altitude error is evident when the maneuver is conducted with manual stick control and autothrottles (PAL 3) instead of the full autopilot (PAL 4), but desired task performance is still achieved. No significant variation is observed in task performance with PAL's 3, 2, and 1. Although the pilot comments reflected a preference for autothrottles, only minor differences were apparent in the task performance metrics.

Time histories from typical runs with the LFRC response type and PAL 0 for each of the four pilots are plotted in figure 32. The time histories show that none of the PAL 0 cases satisfied the adequate performance tolerances. Apparently the failure of the pilot to meet dynamic pressure task performance specifications with PAL 0 is related to a basic inability of the pilot to adequately regulate the vehicle vertical flight path through the turn. The poor task performance is due to the same path-attitude decoupling phenomenon that was noted in the preliminary simulation sessions, although a pitch-rate-command–attitude-hold (RCAH) system was used in those sessions. Equation (3) illustrated that even minor vertical flight path perturbations can yield extreme dynamic pressure perturbations at hypersonic speeds. Figure 32 shows that the pilots were attempting to counter the resulting altitude and dynamic pressure perturbations with longitudinal stick (normal load factor) and throttle inputs, which lead to a very high perception of workload and poor task performance. The bank angle and heading time histories illustrate the lack of precision and repeatability that is experienced when the maneuver is conducted without the aid of a flight director. Excessive angle-of-attack perturbations also resulted from the frequent longitudinal inputs. Note that the pilots had an opportunity to observe the fully automatic execution of the maneuver with PAL 4 in the simulator prior to conducting the maneuver themselves with PAL 0.

Figure 33 presents time history plots of typical maneuvers executed by pilot D using each of the pilot assistance levels with his preferred HUD and response. The PAL 4 fully automatic execution is included for comparison. The flight director guidance supplied in the PAL settings of 1–3 permitted the pilot to effectively cope with the high-speed path-attitude decoupling and to achieve desired performance as indicated by the dynamic pressure and altitude time histories. Recall that the flight director cue (regardless of the pilot's preferred symbology) is driven by the load factor command specified by the guidance algorithm rather than by a vertical flight path error. Examination of the altitude, bank angle, and load factor time histories for PAL's 1–4 in figure 33 shows that the problem of vertical flight path control is solved by the flight director guidance strategy of minor bank angle adjustments to regulate altitude through the turn, while a normal load factor of $2g$ is maintained. A significant reduction in angle-of-attack perturbations is realized when compared with the PAL 0 (no flight director) case. Throttles are used primarily to counter the drag increment produced by the load factor increase from $1g$ to $2g$. This is in contrast to the pilot's intuitive strategy of modulating load factor to regulate altitude through the turn while using throttle to null dynamic pressure perturbations as the PAL 0 traces show. A comparison of the heading time histories in figure 33 with those in figure 32 indicates the improvement in task repeatability that is gained through the use of the flight director with PAL's 1–4.

The variation in fuel required to complete the maneuver is plotted versus PAL in figure 34. The figure shows that dramatic fuel savings is realized as a result of following the guidance strategy described previously. In fact, the average fuel savings for this maneuver, which lasts approximately 90 sec, is greater than 1000 lb and is a substantial fraction of the payload capacity for such a configuration.

A more subtle trend is also apparent when comparing fuel consumption of PAL 4 (full autopilot and autothrottle) with that of PAL 2 (manual throttle with throttle director). The maneuvers executed with PAL 2 consistently used about 40 lb less fuel than those executed with PAL 4. Because fuel efficiency is a key factor in the feasibility of the hypersonic air-breathing vehicle concept, the answer to why the pilots were able to manually achieve slightly better efficiency than the autothrottles while still achieving desired performance is important. A comparison of the mean dynamic pressure errors in figures 30 and 34 reveals the reason. With the larger mean dynamic pressure excursions permitted through the maneuver, which did not violate the task performance specifications, the pilots achieved desired performance and realized a fuel savings. This practice is illustrated by the dynamic pressure time history for the PAL 2 case in figure 33, which shows a dynamic pressure deficiency of approximately 8 lb/ft^2 throughout the steady segment of the maneuver. The propulsive efficiency of the engine model used in this investigation was not significantly penalized in response to off-nominal dynamic pressure conditions, so the pilots' technique resulted in a slight fuel savings. The actual sensitivity of propulsive performance to flight condition for this type of engine is highly uncertain. Given an accurate propulsive model, a fuel-optimal guidance algorithm can be envisioned which would direct the pilot along the most efficient trajectory subject to propulsive performance and aerodynamic heating constraints. This topic is currently the subject of considerable research. The guidance algorithm described in reference 13 includes no such considerations, and the autothrottles merely sought to regulate dynamic pressure at the prescribed reference value of 2000 lb/ft^2. The observation emphasizes the importance of fuel-optimal trajectory determination for this type of configuration.

The analysis of pilot workload metrics and task performance metrics from part 2 of the real-time experiment indicates which aids must be provided to the pilot to achieve desired task performance with an acceptable workload. The complete set of piloting aids, which consist of the autothrottle, throttle director, and flight director, improves the average of Cooper-Harper ratings from 8 to 2.6. Level-1 flying qualities ratings (CHR $\leq$ 3) and desired task performance were achieved when the maneuver was performed with PAL 3, that is, with the flight director and autothrottle provided to the pilot. Level-2 flying qualities ratings (4 $\leq$ CHR $\leq$ 6) and desired task performance were achieved when the flight director was provided and the throttles were under manual control (PAL 1), as long as the pilot had a digital readout of dynamic pressure and had received sufficient training. In the absence of the autothrottle, throttle director, and flight director cues (PAL 0), the flying qualities were rated level 3 (7 $\leq$ CHR $\leq$ 9) or worse, and achievement of even adequate task performance was never possible. These results suggest that a flight director driven by a guidance algorithm tailored to the specific characteristics of high-speed flight should be considered a flight-critical element of the control system for an air-breathing hypersonic vehicle. Autothrottles should be provided to reduce pilot workload and should probably be treated as flight-critical control elements based on pilot comments. When sufficient training was provided, the pilot was able to maintain adequate control of the vehicle trajectory during the cruise turn in the absence of the autothrottle, but this is contingent upon the throttleability of scramjet propulsion systems at hypersonic speeds and their operational sensitivity to flight condition perturbations.

Concluding Remarks

An investigation has been conducted to develop and evaluate a series of piloting aids for maneuver control of an air-breathing hypersonic vehicle. Stringent propulsion constraints and nonintuitive high-speed flight effects associated with maneuvering in the hypersonic regime raise the question of whether manual control of such a vehicle should even be considered.

The objectives of this research were to determine the extent of manual control that is desirable for a vehicle maneuvering in this regime and to identify the form of aids that must be supplied to the pilot to make such control feasible. A piloted real-time motion-based simulation of an air-breathing hypersonic vehicle concept was used for this study, and the investigation focused on a single representative cruise turn maneuver at a Mach number of 7.86 and an altitude of 85 000 ft.

Several maneuver control aids were developed as a result of pilot comments and control problems encountered during a series of preliminary maneuver simulation sessions. These aids consisted of an autothrottle, throttle director, autopilot, flight director, and two head-up display (HUD) configurations. The first of the two HUD configurations contained relatively conventional flight director symbology elements. The second HUD presented a graphical representation of the vehicle lift vector in terms of normal load factor and bank angle. The algorithm, which was used to drive both HUD configurations, was based on a normal load factor specified by the guidance law. The impetus for providing the load-factor-oriented guidance instead of flight-path-oriented guidance stems from the hypersonic path-attitude decoupling effect. This effect introduces a significant lag into the vehicle's flight path response to attitude changes, which makes direct manual control of flight path impractical. Two longitudinal control response types consisting of a

rate-command–attitude-hold (RCAH) system and a load-factor-rate–load-factor-hold (LFRC) system were also developed.

A formal real-time experiment was then conducted which included two parts and the participation of four NASA test pilots. The first part of the experiment identified the pilots' preferences from a combined set of the two response types and the two HUD configurations to determine which combination provided the greatest ease and precision of control. The second part of the experiment examined the degradation in task performance and pilot satisfaction as various aids were removed from the pilot's use; these results were compared with maneuver performance in the fully automatic mode.

The first part of the real-time experiment revealed that all four pilots preferred the LFRC response type over the RCAH response type. This preference was due in part to the greater harmony of the load-factor-oriented control system with the flight director cue, which was driven with a load factor command specified by the guidance system. This response type also provided pilot relief from the longitudinal control task after the steady turn was established, which thereby produced fewer angle-of-attack perturbations, less associated control activity, and slightly lower fuel consumption. Note that this effect was somewhat influenced by the lack of a trim button in the RCAH implementation and that a different trend might be observed for other maneuvers that do not involve such sustained periods at elevated load factor as does the cruise turn. The LFRC response type provided pilots greater ease and slightly improved precision in control of the maneuver on the basis of pilot comments, Cooper-Harper flying qualities ratings, workload metrics, and task performance metrics.

No consistent preference for either HUD was identified because pilot opinions were evenly split between the two symbologies. Desired performance specifications were achieved with both HUD's, and no significant differences in maneuver precision or workload were noted. Each of the four test pilots awarded at least one response type and HUD combination a level-1 flying qualities rating (CHR $\leq$ 3) for the cruise turn maneuver and selected a preferred combination for use in the second part of the real-time experiment.

The second part of the experiment indicated which aids must be provided to the pilot to achieve desired task performance with an acceptable workload. The complete set of piloting aids, which consisted of the autothrottle, throttle director, and flight director, improved the average of Cooper-Harper ratings from 8 to 2.6. The flight director was the most critical of these aids, and the cruise turn maneuver became essentially unachievable to adequate performance specifications in the absence of this flight director. Level-1 flying qualities ratings and desired task performance were achieved when the flight director and autothrottle were provided to the pilot. Level-2 flying qualities ratings and desired task performance were achieved when the flight director was provided and the throttles were under manual control, as long as the pilot had a digital readout of dynamic pressure. In the absence of the autothrottle, throttle director, and flight director aids, the flying qualities were rated level 3 or worse, and achievement of even adequate task performance was never possible.

Hypersonic maneuver control will be significantly complicated by high-speed flight effects such as path-attitude decoupling and centrifugal relief. Propulsion system sensitivity to flight condition perturbations will present additional challenges to the pilot of such a vehicle. The severity with which these nonintuitive effects alter the pilot's ability to control the vehicle makes some form of assistance imperative. This investigation focused on the execution of a single representative cruise turn maneuver at a Mach number of 7.86 and an altitude of 85 000 ft. The results indicate that a flight director driven by a guidance algorithm tailored to the specific characteristics of high-speed flight should be considered a flight-critical element of the control system for an air-breathing hypersonic vehicle. Autothrottles should be provided to reduce pilot workload and, on the basis of pilot comments, be treated as a flight-critical control element for an air-breathing hypersonic vehicle.

NASA Langley Research Center
Hampton, VA 23681-0001
July 14, 1995

Appendix A

Propulsion Model

The hypersonic propulsion model used in this simulation was based primarily on the propulsive database provided in reference 15. However, the propulsive database supplied by reference 15 contains several somewhat artificial and unrealistic features required for operation of the Program to Optimize Simulated Trajectories (POST). For example, the winged cone propulsive database includes data points at fuel equivalence ratios as high as 100 to prevent POST from extrapolating to negative specific impulses in the lower fuel equivalence ratio regions. Such high fuel equivalence ratios are unrealistic and were not included in the Langley Visual/Motion Simulator (VMS) hypersonic propulsion model. A modified engine model was developed that was based on only the most reliable data presented in reference 15. This appendix describes the characteristics of the modified propulsion model.

Symbols

$f1$	interpolation table function number 1
$f2$	interpolation table function number 2
ISP	specific impulse, sec
ISP′	specific impulse for equivalence ratio of 1, sec
M	Mach number
$\bar{q}$	dynamic pressure, lb/ft^2
s	Laplace transform parameter
T	axial thrust, lb
V	inertial velocity, ft/sec
W_F	fuel flow rate, lb/sec
$W_{F\|\eta=1}$	fuel flow rate for equivalence ratio of 1, lb/sec
η	fuel equivalence ratio
τ_{eng}	engine response time constant

Subscripts:

cmd	commanded value
max	maximum allowable value

Model Description and Implementation

This modified propulsion model includes a suitable input for use by the autothrottle control law. A penalty is applied for fuel equivalence ratios $\eta > 1.0$; equivalence ratio information is included up to 10.0, although excursions as high as 10.0 would be extremely inefficient and improbable. A flowchart of the modified engine model is shown in figure A1.

The original propulsive database presented in reference 15 also included a weak dependence on dynamic pressure, which forced the interpolations for specific impulse and thrust coefficient to be three-dimensional. The dynamic pressure dependence has been eliminated from the interpolations because this was a weak and somewhat uncertain effect, although dynamic pressure remains in the model as a multiplier of thrust coefficient.

The revised propulsion model yields a net thrust which acts along the vehicle body X-axis. The effects of angle of attack and sideslip, body angular rates, and control surface deflections on thrust and specific impulse are not accounted for in this model. In this simulation, fuel flow rate can be commanded by the pilot or by an autothrottle feedback control law; the choice depends on the mode selected. This fuel flow rate command is then used with Mach number and dynamic pressure to compute a fuel equivalence ratio. The equivalence ratio is then used in a one-dimensional interpolation table to compute a specific impulse that is valid for equivalence ratios ≤1. A penalty is then applied for equivalence ratios >1 in the form of an upper limit on specific impulse. This specific impulse is then multiplied by fuel flow rate to determine the resultant thrust. The procedure for calculation of equivalence ratio, specific impulse, and thrust from commanded fuel flow rate is as follows:

1. Determine fuel flow rate W_F from commanded fuel flow rate $W_{F_{cmd}}$ by simulation of engine fuel flow dynamics (a value of $\tau_{eng} = 0.5$ was used in the simulation)

$$W_F = \frac{W_{F_{cmd}}}{\tau_{eng} s + 1}$$

2. Use natural log of Mach number in figure A2 to interpolate for the quantity $f1(M)$, which is a one-dimensional interpolation.

3. Determine ideal fuel flow rate $W_{F|\eta=1}$ from $f1(M)$ as follows:

$$W_{F|\eta=1} = \bar{q} \exp[f1(M)]$$

where exp is the inverse of the natural log.

4. Determine fuel equivalence ratio η as follows:

$$\eta = \frac{W_F}{W_{F|\eta=1}}$$

5. Use Mach number in figure A3 to interpolate for the specific impulse ISP′ achieved by this propulsion system when the fuel equivalence ratio $\eta = 1$.

6. Use the fuel equivalence ratio with figure A4 to interpolate for the specific impulse limit penalty below and

apply limit as shown in the block diagram in figure A1 to determine actual specific impulse ISP.

$$\mathrm{ISP}_{\max} = f2(M)/\eta$$

7. Multiply specific impulse ISP by fuel flow rate W_F to determine axial thrust T.

An explanation of steps (5) and (6) follows. Specific impulse is a measure of fuel efficiency in an air-breathing engine. For hypersonic propulsion systems, the best efficiency occurs at a fuel equivalence ratio of 1. Figure A3 (step 5) shows the specific impulse that is achieved by this propulsion system at various Mach numbers when the fuel equivalence ratio is set to 1. As equivalence ratio is adjusted above 1, the fuel efficiency drops off (i.e., specific impulse decreases). Step (6) applies a correction factor to the specific impulse from step (5) to reflect this decrease in efficiency. Figures A2–A4 are based on the most realistic segments of the original winged-cone database provided in reference 15. Interpolation data are included in figures A2–A4.

Two limiters are included in the block diagram shown in figure A1 to ensure that Mach number and fuel equivalence ratio remain within the limits of this model. This model is appropriate for Mach numbers between 0.3 and 25 and fuel equivalence ratios between 0.1 and 10.

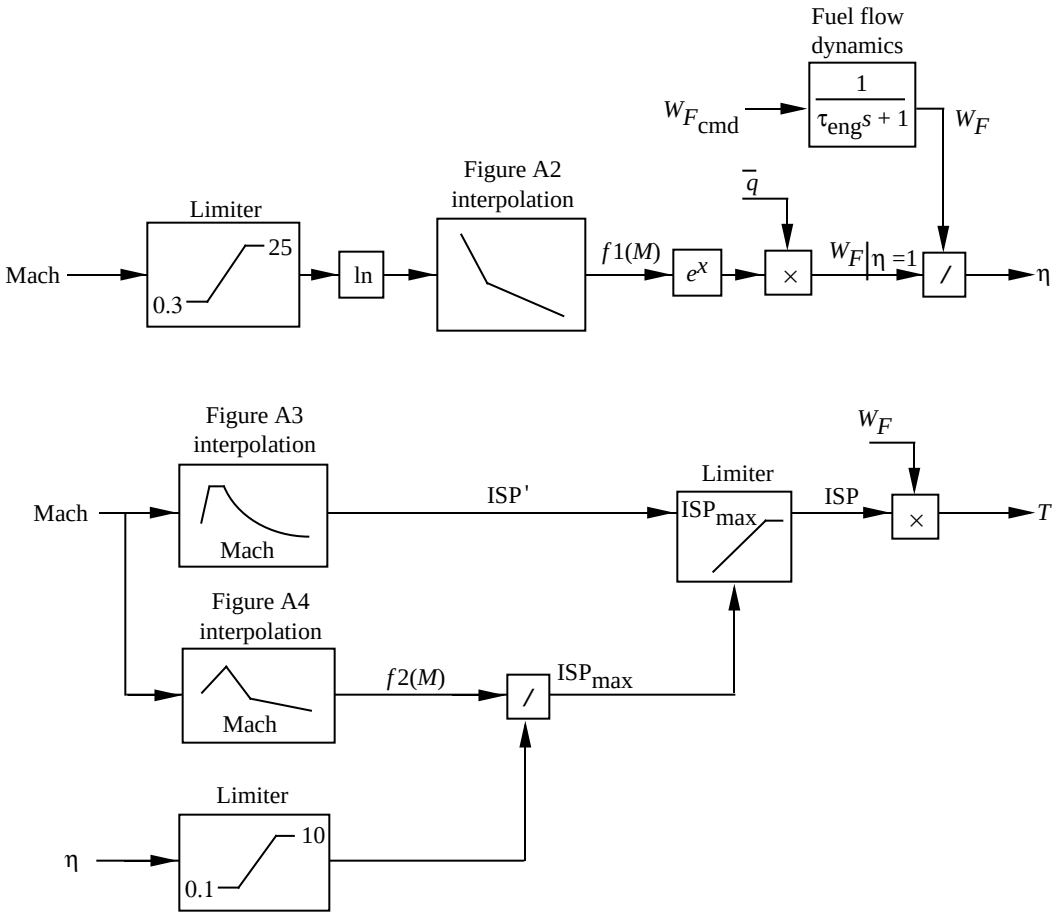

Figure A1. Block diagram of propulsion model.

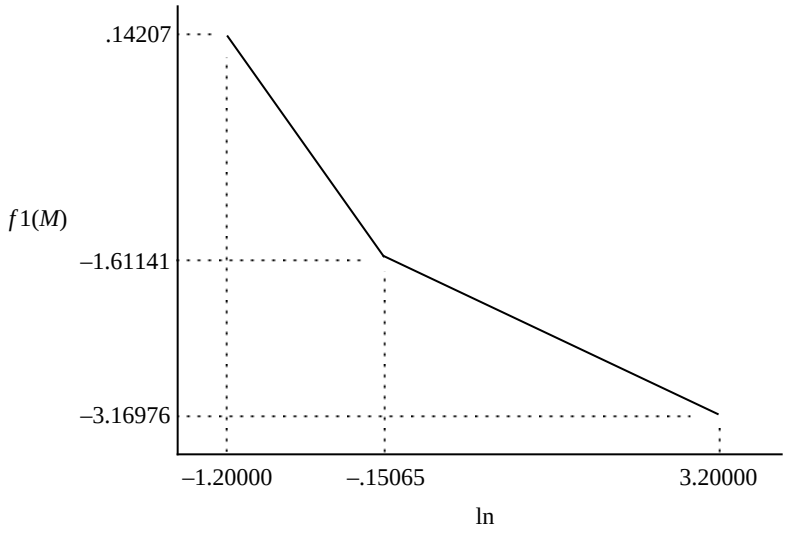

Figure A2. Interpolation data for function *f1(M)*.

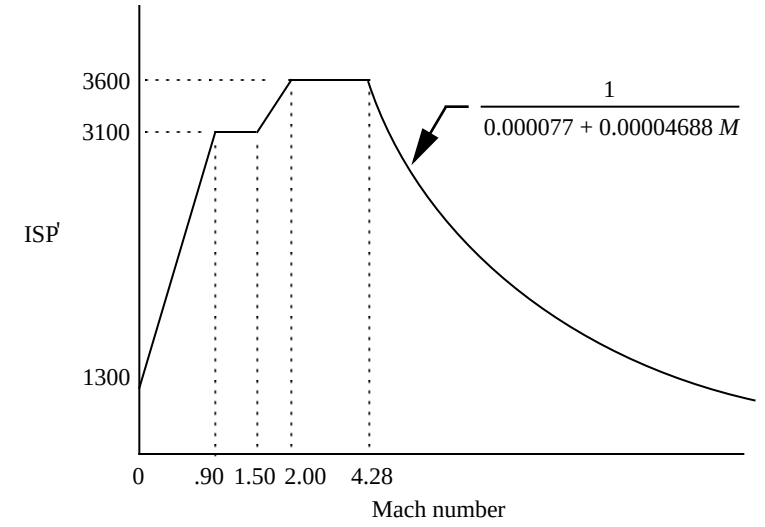

Figure A3. Specific impulse function data.

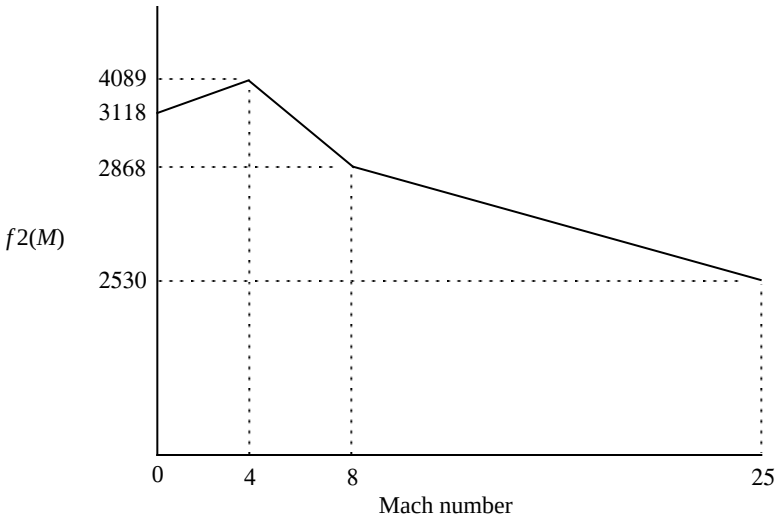

Figure A4. Interpolation data for function $f2(M)$.

Appendix B

Description of Inner-Loop Flight Control Laws

This appendix describes the derivation of the inner-loop flight control laws, which stabilize the vehicle dynamics, track load factor and bank angle commands from the pilot or autopilot, and maintain zero sideslip during maneuvers. A simple pole-placement technique is used, which allows specification of the inner-loop responses in terms of desired frequency and damping. Figure 12 shows a flowchart of the real-time simulation, which depicts the relation of the inner-loop flight controls in relation to other components of the simulation. Three separate inner-loop control laws are synthesized to drive the symmetric elevon, differential elevon, and rudder deflections for pitch, roll, and yaw control. The estimation of sideslip angle with a lateral accelerometer and the concept of a complementary filter to reduce high-frequency control action resulting from atmospheric disturbances are also described.

Symbols

A_Y	lateral acceleration in body-axis coordinate system, ft/sec^2
b	wing span, ft
g	acceleration due to gravity, ft/sec^2
I_X	rolling moment of inertia, slug-ft^2
I_{XZ}	product of inertia, slug-ft^2
I_Z	yawing moment of inertia, slug-ft^2
K_1	effective pitch loop proportional gain
K_2	effective pitch loop integral gain
K_{a_β}	sideslip feedback gain to aileron
$K_{a_{\delta_r}}$	rudder deflection crossfeed gain to aileron
K_{a_ϕ}	bank angle feedback gain to aileron
$K_{a_{\dot{\phi}}}$	roll rate feedback gain to aileron
K_q	pitch rate feedback gain to elevons
K_{r_β}	sideslip feedback gain to rudder
K_{r_r}	yaw rate feedback gain to rudder
K_{sE1}	longitudinal stick gain for RCAH system
K_{sE2}	longitudinal stick gain for LFRC system
L, M, N	rolling, pitching, and yawing moments, ft-lb
m	mass, slug
N_V	normal load factor with respect to velocity vector, g units
n	normal load factor, g units
p	roll rate in body-axis coordinate system, deg/sec
q	pitch rate in body-axis coordinate system, deg/sec
$\bar{q}$	dynamic pressure, lb/ft^2
r	yaw rate in body-axis coordinate system, deg/sec
s	Laplace transform parameter
u, v, w	body-axis velocities, ft/sec
V	inertial velocity, ft/sec
W	weight, lb
x_b, y_b, z_b	vehicle body axes
x	actuator feedback signal
X, Y, Z	body-axis force components, lb
α	angle of attack, deg
β	sideslip angle, deg
Δ	characteristic equation
δ_a	aileron deflection, positive right trailing edge down, deg
δ_e	elevon deflection, positive trailing edge down, deg
δ_r	rudder deflection, deg
ζ_{OL}	open-loop damping ratio (pitch)
ζ_a	aileron control loop damping ratio
ζ_r	rudder control loop damping ratio
ζ_{sp}	short-period damping ratio
ζ_0	damping ratio of introduced actuator and filter dipole
θ	pitch angle, deg
λ	distance from c.g. to lateral accelerometer, positive forward, ft
τ_L	actuator feedback filter time constant
τ_a	actuator lag time constant
τ_β	sideslip complementary filter time constant
τ'	effective pitch loop filter time constant
ϕ	roll angle, deg
ω_{OL}	open-loop natural frequency (pitch), rad/sec
ω_a	aileron control loop natural frequency, rad/sec
ω_r	rudder control loop natural frequency, rad/sec
ω_{sp}	short-period natural frequency, rad/sec

ω_0 frequency of introduced actuator and filter dipole, rad/sec

Superscripts:

· first derivative with respect to time

·· second derivative with respect to time

^ estimated value

~ complementary filtered value

Subscripts:

acc accelerometer signal

cmd commanded value

err error signal

RW relative to wind

0 nominal or trim value

Pitch Control[1]

The primary element of the longitudinal control architecture is a pitch rate command loop. The object is to control pitch rate for a plant with dynamics that are approximated by the second-order system given in equation (B1).

$$\begin{bmatrix} \dot{w} \\ \dot{q} \end{bmatrix} = \begin{bmatrix} Z_w & V \\ M_w & M_q \end{bmatrix} \begin{Bmatrix} w \\ q \end{Bmatrix} + \begin{bmatrix} Z_{\delta_e} \\ M_{\delta_e} \end{bmatrix} \delta_e \tag{B1}$$

The basic pitch rate command architecture is shown in figure B1. The pitch rate error is multiplied by gain K_q and then fed into a first-order actuator model with time constant τ_a. Equation (B2) expresses the control deflection-to-pitch rate error transfer function for the network shown in figure B1. This transfer function can be manipulated to achieve equations (B3)–(B6), which illustrate that the addition of the pitch control filter loop around the actuator shown in figure B1 effectively produces a proportional-integral control action on the pitch rate error signal.

$$\frac{\delta_e}{q_{\text{err}}}(s) = \frac{K_p\left(\frac{1}{\tau_a s + 1}\right)}{1 - \left(\frac{1}{\tau_a s + 1}\right)\left(\frac{1}{\tau_L s + 1}\right)} \tag{B2}$$

$$\frac{\delta_e}{q_{\text{err}}}(s) = \left(K_1 + \frac{K_2}{s}\right)\left(\frac{1}{\tau' s + 1}\right) \tag{B3}$$

[1]Adapted from unpublished notes by Frederick J. Lallman, "Hypersonic Pitch Control Laws," April 19, 1990.

where

$$K_1 = K_p\left(\frac{\tau_L}{\tau_a + \tau_L}\right) \tag{B4}$$

$$K_2 = K_p\left(\frac{1}{\tau_a + \tau_L}\right) \tag{B5}$$

$$\tau' = \frac{\tau_a \tau_L}{\tau_a + \tau_L} \tag{B6}$$

The dynamics of the closed-loop system are described by equation (B7) and the associated characteristic equation (B8).

$$\begin{bmatrix} \dot{w} \\ \dot{q} \\ \dot{\delta}_e \\ \dot{x} \end{bmatrix} = \begin{bmatrix} Z_w & V & Z_{\delta_e} & 0 \\ M_w & M_q & M_{\delta_e} & 0 \\ 0 & \frac{K_p}{\tau_a} & -\frac{1}{\tau_a} & \frac{1}{\tau_a} \\ 0 & 0 & \frac{1}{\tau_L} & -\frac{1}{\tau_L} \end{bmatrix} \begin{Bmatrix} w \\ q \\ \delta_e \\ x \end{Bmatrix} - \begin{bmatrix} 0 \\ 0 \\ \frac{K_p}{\tau_a} \\ 0 \end{bmatrix} q_{\text{cmd}} \tag{B7}$$

$$\Delta = s\left(s + \frac{1}{\tau_a} + \frac{1}{\tau_L}\right)(s^2 + 2\zeta_{\text{OL}}\omega_{\text{OL}} s + \omega_{\text{OL}}^2) - \frac{K_p M_{\delta_e}}{\tau_a}\left(s + \frac{1}{\tau_L}\right)\left(s + \frac{1}{t_{\theta 2}}\right) \tag{B8}$$

where

$$\omega_{\text{OL}}^2 = Z_w M_q - V M_w \tag{B9}$$

$$2\zeta_{\text{OL}}\omega_{\text{OL}} = -(Z_w + M_q) \tag{B10}$$

$$\frac{1}{t_{\theta 2}} = \frac{Z_{\delta_e}}{M_{\delta_e}} M_w - Z_w \tag{B11}$$

The standard form of the fourth-order characteristic equation for the short-period pitch mode and the introduced actuator and filter quadratic is given by equation (B12), and the associated closed-loop pitch rate transfer function is given by equation (B13).

$$\Delta = (s^2 + 2\zeta_{\text{sp}}\omega_{\text{sp}} s + \omega_{\text{sp}}^2)(s^2 + 2\zeta_0\omega_0 s + \omega_0^2) \tag{B12}$$

$$\frac{q}{q_{\text{cmd}}}(s) = \frac{\frac{K_p M_{\delta_e}}{\tau_a}\left(s + \frac{1}{\tau_L}\right)\left(s + \frac{1}{t_{\theta 2}}\right)}{(s^2 + 2\zeta_{\text{sp}}\omega_{\text{sp}} s + \omega_{\text{sp}}^2)(s^2 + 2\zeta_0\omega_0 s + \omega_0^2)} \tag{B13}$$

Values for the pitch rate error gain K_q and the filter time constant τ_L may be obtained by prescribing desired values for the closed-loop short-period characteristics and equating coefficients of like powers in equations (B8) and (B12).

A simple modification of the architecture shown in figure B1 will eliminate the zero in the pitch rate transfer function at $1/\tau_L$. The elimination of this zero will provide the system with more desirable transient response characteristics. This is achieved by moving the pitch rate command signal from driving the actuator directly through gain K_q to a position where it enters the actuator through the control filter and a duplicate of the gain K_q. This modification is shown in figure B2. The resulting pitch rate transfer function is shown in equation (B14).

$$\frac{q}{q_{\text{cmd}}}(s) = \frac{\frac{K_p M_{\delta_e}}{\tau_a}\left(s + \frac{1}{t_{\theta 2}}\right)}{(s^2 + 2\zeta_{\text{sp}}\omega_{\text{sp}}s + \omega_{\text{sp}}^2)(s^2 + 2\zeta_0\omega_0 s + \omega_0^2)} \quad \text{(B14)}$$

Other elements were added to the pitch control architecture to provide the pitch-rate-command–attitude-hold and load-factor-rate–load-factor-hold response types. These additions are shown in the complete pitch control block diagram in figure B3. The pitch rate command input to the system shown in this figure was generated by one of three sources, which depends upon the response type and pilot assistance level selected. First, figure B3 shows that if the autopilot was not active (PAL < 4) and the response type selected was RCAH, the pitch rate command was generated by the pilot's longitudinal stick deflection through a scaling gain K_{sE1}. A proportional-integral (PI) network on pitch angle error was used to provide the attitude-hold control action. A detent region of ±0.2 deg/sec was placed on the pilot's pitch rate command signal to delimit the operation of this pitch attitude-hold feature. When the pitch rate command produced by the pilot's stick deflection was outside the detent region, the reference pitch attitude θ_0 was set equal to the actual pitch attitude, so that the error signal being fed through the attitude-hold PI network was zero. When the stick entered the detent region, the pitch attitude was sampled, and this value was used as the pitch attitude reference for the PI network. The gains in the PI attitude-hold network were tuned to provide good response in turbulence, and the integrator was limited at 10°. A delay of 0.5 sec between the instant the stick enters the detent and the instant the reference pitch attitude is sampled was necessary to prevent an excessively abrupt arrest of the pitch rate with an associated overshoot of the reference value.

The second possible source of the pitch rate command signal shown in figure B3 was selected if the autopilot was not active and the designated response type was load factor rate command (LFRC) hold. In this case, the longitudinal stick deflection was fed through a scaling gain K_{sE2} and integrated to produce a load factor command, which was then differenced from an estimate of the actual load factor based on accelerometer signals and angle of attack. This load factor error was then fed through a PI network and converted into a pitch rate command by equation (B15). Gains in the PI network were tuned according to pilot preference during the preliminary simulation sessions. Limits were placed on the load factor command to prevent the signal from exceeding 2*g*.

$$q_{\text{cmd}} = -N_{V\text{err}}\left(\frac{g}{V}\right)\left(\frac{180}{\pi}\right)\left(\frac{1}{Z_w}\right) \quad \text{(B15)}$$

The final source of the pitch rate command shown in figure B3 was selected if the autopilot was activated. In this case, the load factor command from the guidance law described in reference 13 was differenced from the estimated load factor signal and fed through the same PI network used in the LFRC response type. Because the same signal that had been used to drive the flight director while the vehicle was in manual control was used to drive the autopilot, the pilots felt that the automatic systems performed in a predictable and familiar fashion.

Yaw Control

The rudder is used to maintain zero sideslip during a maneuver. Figure B4 shows a block diagram of the yaw control law. The yaw rate and sideslip equations are given by

$$\dot{r} = N_\beta\beta + N_p p + N_r r + N_{\delta_a}\delta_a + N_{\delta_r}\delta_r + \frac{I_{XZ}}{I_Z}\dot{p} \quad \text{(B16)}$$

$$\dot{\beta} = Y_\beta\beta + Y_p p + Y_r r + Y_{\delta_a}\delta_a + Y_{\delta_r}\delta_r - r + \frac{g}{V}\cos\theta_0 \sin\phi \quad \text{(B17)}$$

The final term in equation (B17) involving gravity will be negligible in hypersonic flight because the velocity is very high. Also, the effect of rotary derivatives is often small at hypersonic speeds, because velocity is in the denominator of the dimensionalizing expression. Neglection of the rotary derivative and inertial coupling terms in equations (B16) and (B17) and a Laplace transformation yield the following dynamic system:

$$sr(s) = N_\beta\beta(s) + N_{\delta_a}\delta_a(s) + N_{\delta_r}\delta_r(s) \quad \text{(B18)}$$

$$s\beta(s) = Y_\beta\beta(s) + Y_{\delta_a}\delta_a(s) + Y_{\delta_r}\delta_r(s) - r(s) \quad \text{(B19)}$$

A rudder deflection command is defined with yaw rate and angle-of-sideslip feedback in the following form:

$$\delta_r(s) = K_{r\beta}\beta(s) + K_{r_r} r(s) \tag{B20}$$

Substitution of the rudder deflection command into equations (B18) and (B19) and neglection of yaw and side forces due to aileron deflection yield

$$sr(s) - N_\beta\beta(s) - N_{\delta_r}[K_{r\beta}\beta(s) + K_{r_r} r(s)] = 0 \tag{B21}$$

$$s\beta(s) + r(s) - Y_\beta\beta(s) - Y_{\delta_r}[K_{r\beta}\beta(s) + K_{r_r} r(s)] = 0 \tag{B22}$$

This system can be expressed in matrix form as

$$\begin{bmatrix} s - N_{\delta_r}K_{r_r} & -N_\beta - N_{\delta_r}K_{r\beta} \\ 1 - Y_{\delta_r}K_{r_r} & s - Y_\beta - Y_{\delta_r}K_{r\beta} \end{bmatrix} \begin{Bmatrix} r(s) \\ \beta(s) \end{Bmatrix} = \begin{bmatrix} 0 \\ 0 \end{bmatrix} \tag{B23}$$

This matrix yields the following second-order characteristic equation for the closed-loop system:

$$s^2 - (Y_\beta + Y_{\delta_r}K_{r\beta} + N_{\delta_r}K_{r_r})s + [N_\beta + N_{\delta_r}K_{r\beta} + K_{r_r}(N_{\delta_r}Y_\beta - Y_{\delta_r}N_\beta)] = 0 \tag{B24}$$

The coefficients of this characteristic equation are expressed in equations (B25) and (B26) in terms of frequency ω_r and damping ζ_r for the second-order system.

$$-(Y_\beta + Y_{\delta_r}K_{r\beta} + N_{\delta_r}K_{r_r}) = 2\zeta_r\omega_r \tag{B25}$$

$$N_\beta + N_{\delta_r}K_{r\beta} + K_{r_r}(N_{\delta_r}Y_\beta - Y_{\delta_r}N_\beta) = \omega_r^2 \tag{B26}$$

Neglection of the relatively small terms and solution of the feedback gains $K_{r\beta}$ and K_{r_r} in terms of frequency and damping yield

$$K_{r\beta} = \frac{\omega_r^2 - N_\beta}{N_{\delta_r}} \tag{B27a}$$

$$K_{r_r} = \frac{2\zeta_r\omega_r + Y_\beta + Y_{\delta_r}K_{r\beta}}{-N_{\delta_r}} \tag{B27b}$$

The feedback gains required to produce a given closed-loop frequency and damping combination can now be quickly determined. This permits the designer to place the closed-loop poles at a location which might be desirable from a handling qualities perspective.

Angle-of-Sideslip Estimation

The reliability of air data measurements during some phases of hypersonic flight may be uncertain. The control system designed in this report will utilize an angle-of-sideslip feedback that is constructed from a lateral accelerometer reading rather than an air data sensor array. The lateral accelerometer will be placed at the instantaneous center of rotation in response to a rudder deflection, which eliminates the need to correct the accelerometer reading for rudder effects. In actual practice, the signal needs to be filtered appropriately to eliminate corruption of the measurement due to structural vibrations. The equation for the lateral acceleration measured by an accelerometer located a distance λ forward of the c.g. is given by

$$A_{Y\text{acc}} = V_0\left(Y_\beta\beta + Y_{\delta_r}\delta_r\right) + \lambda\left(N_\beta\beta + N_{\delta_r}\delta_r\right) \tag{B28}$$

The solution of this expression for β yields an angle-of-sideslip measurement in terms of the accelerometer reading and the rudder deflection

$$\hat{\beta} = \frac{A_{Y\text{acc}} - \delta_r\left(V_0 Y_{\delta_r} + \lambda N_{\delta_r}\right)}{V_0 Y_\beta + \lambda N_\beta} \tag{B29}$$

By placing the accelerometer at the lateral center of rotation, the influence of rudder deflection on the angle-of-sideslip measurement is eliminated. Selection of λ so that

$$\lambda = \frac{-V_0 Y_{\delta_r}}{N_{\delta_r}} \tag{B30a}$$

yields

$$\hat{\beta} = \frac{A_{Y\text{acc}}}{V_0 Y_\beta + \lambda N_\beta} \tag{B30b}$$

This expression for sideslip can be substituted into equation (B20) to make the lateral inner-loop controller independent of air data measurements. Note that the expression for λ depends on parameters which change with flight condition, i.e., the lateral center of rotation is not constant over the range of hypersonic flight conditions which the vehicle will experience. Because relocation of the accelerometer as flight condition varies is unreasonable, the instrument should probably be placed at some location that represents the average position of the center of rotation for those flight conditions at which the air data system measurements are the least reliable. For the simulated time histories presented in this report, which include flight conditions at Mach 6, 10, 15, and 20, the lateral accelerometer was placed at the center of rotation for the Mach 6 flight condition.

Complementary Filter

Sudden crosswind gusts would be fed directly into the lateral control surface deflections by sideslip feedback under the rudder control law shown in equation (B20). To avoid sharp peaks in the commanded position of control surfaces, a low-pass filter is added to the sideslip angle feedback loop. The filter is complemented with derivative feedback to produce a unity transfer function, which eliminates the filter effect on the stability of the closed-loop system and prevents it from interfering with the response to pilot or guidance system commands. Because of the derivative feedback through the filter, this network is referred to as a "complementary filter." The expression for the filtered angle-of-sideslip feedback is

$$\tilde{\beta} = \frac{\tau_\beta \hat{\dot{\beta}}}{\tau_\beta s + 1} + \frac{\hat{\beta}}{\tau_\beta s + 1} \tag{B31}$$

where $\hat{\beta}$ is obtained from equation (B29), and $\hat{\dot{\beta}}$ is given by

$$\hat{\dot{\beta}} = Y_\beta \hat{\beta} + Y_{\delta_a} \delta_a + Y_{\delta_r} \delta_r - r \tag{B32}$$

Rotary derivatives have been neglected in equation (B32). The time constant can be selected to provide a reasonable amount of disturbance rejection and a favorable response characteristic. Equation (B31) can be substituted for sideslip feedback in the rudder control law equation (B20). Ideally, the complementary filter has a unity transfer function and does not affect the stability of the closed-loop system. In actual practice, the degree to which the transfer function of equation (B31) differs from unity depends on the accuracy of the estimated derivative signal used in this equation. To this extent, the complementary filter acts only to reduce high-frequency control action in response to atmospheric disturbance inputs but not to commanded control inputs.

Roll Control

Roll control is addressed with the use of ailerons as the primary control effector to track bank angle commands issued by the pilot or autopilot. Figure B5 shows a block diagram of the basic roll control law. The roll rate and bank angle equations are given by

$$\dot{p} = L_\beta \beta + L_p p + L_r r + L_{\delta_a} \delta_a + L_{\delta_r} \delta_r + \frac{I_{XZ}}{I_X} \dot{r} \tag{B33}$$

$$\dot{\phi} = p + r \tan \theta_0 \cos \phi \tag{B34}$$

Neglection of the rotary derivative and inertial coupling terms in equation (B33) yields

$$\dot{p} = L_\beta \beta + L_{\delta_a} \delta_a + L_{\delta_r} \delta_r \tag{B35}$$

The simplifying assumption is made that $\dot{\phi} \approx p$ in equation (B34). A feedback control law for aileron deflection is now defined, which will permit decoupling of yawing and rolling motions by elimination of the effect of rudder deflection and angle of sideslip in equation (B35).

$$\delta_a = K_{a_\beta} \beta + K_{a_{\delta_r}} \delta_r + K_{a_\phi} \phi_{\text{err}} + K_{a_{\dot{\phi}}} \dot{\phi} \tag{B36}$$

In this expression, ϕ_{err} is defined as the commanded bank angle minus the actual bank angle. This control law also includes roll attitude and rate feedback and provides a means to specify frequency and damping in roll response. The angle-of-sideslip signal used in this expression will be the lateral accelerometer complementary filtered estimate in equation (B31). Note that the rudder deflection command is also used in this control law. Substitution of the aileron control law into equation (B35) yields

$$\ddot{\phi} = L_\beta \beta + L_{\delta_r} \delta_r + L_{\delta_a} (K_{a_\beta} \beta + K_{a_{\delta_r}} \delta_r + K_{a_\phi} \phi_{\text{err}} + K_{a_{\dot{\phi}}} \dot{\phi}) \tag{B37}$$

To achieve the desired decoupling of roll and yaw responses, define

$$K_{a\beta} = \frac{-L_\beta}{L_{\delta_a}} \tag{B38a}$$

$$K_{a\delta_r} = \frac{-L_{\delta_r}}{L_{\delta_a}} \tag{B38b}$$

which, upon substitution into equation (B37), produces the expression

$$\ddot{\phi} = L_{\delta_a} K_{a_\phi} \phi_{\text{err}} + L_{\delta_a} K_{a_{\dot{\phi}}} \dot{\phi} \tag{B39}$$

A Laplace transform of equation (B39) yields the following second-order characteristic equation:

$$s^2 - L_{\delta_a} K_{a_{\dot{\phi}}} s - L_{\delta_a} K_{a_\phi} = 0 \tag{B40}$$

The feedback gains in this expression are easily solved for in terms of desired frequency and damping of the closed-loop system to yield

$$K_{a_\phi} = \frac{\omega_a^2}{-L_{\delta_a}} \tag{B41a}$$

$$K_{a_{\dot{\phi}}} = \frac{2\zeta_a \omega_a}{-L_{\delta_a}} \tag{B41b}$$

These gains, along with those in equations (B38), are used in equation (B34) to produce the final aileron control law. The rotary terms neglected in the derivation of this control law were of little significance at the hypersonic flight conditions which were simulated. The inherent aerodynamic roll damping of the vehicle is negligible at these flight conditions, so most of the damping is supplied by the roll rate feedback loop in the aileron control law.

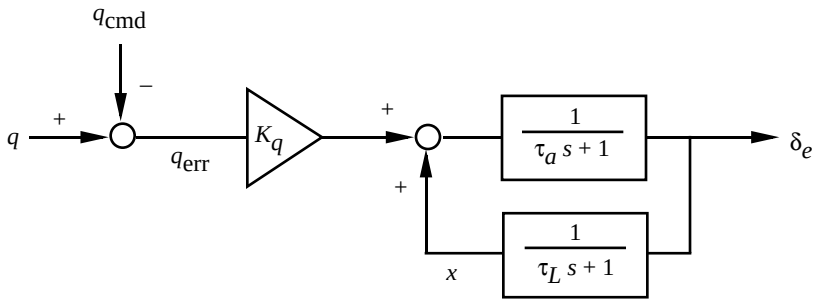

Figure B1. Basic architecture of pitch rate control loop.

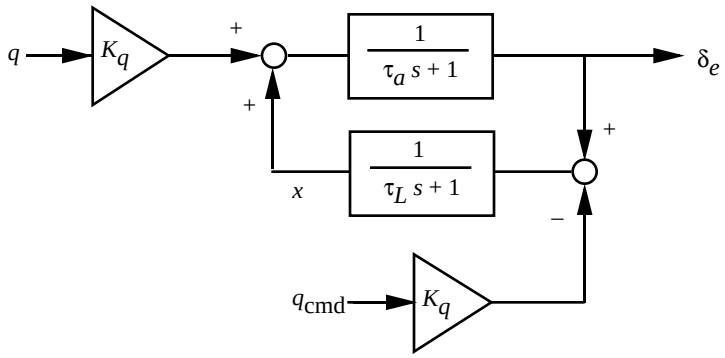

Figure B2. Diagram of modified pitch rate control loop.

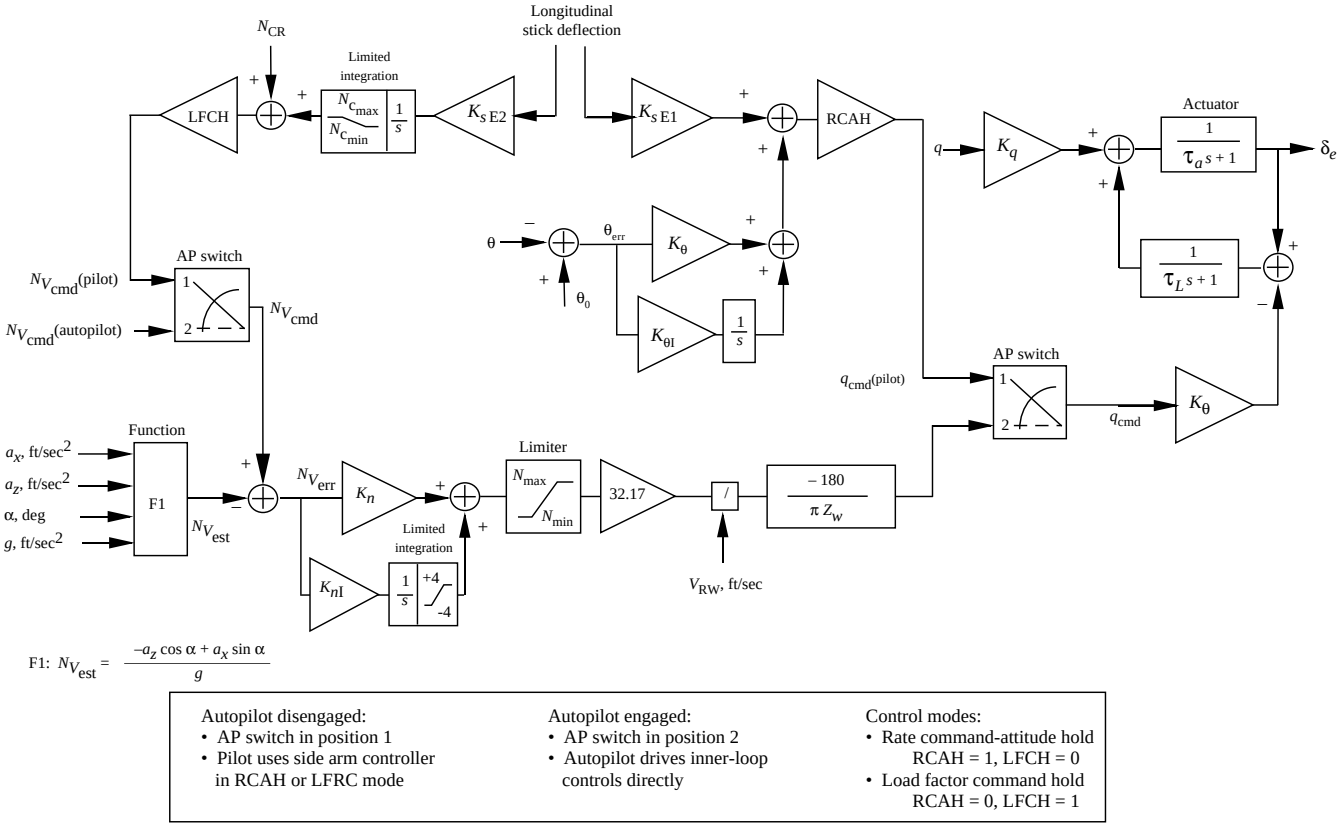

Figure B3. Pitch control law used in real-time simulation.

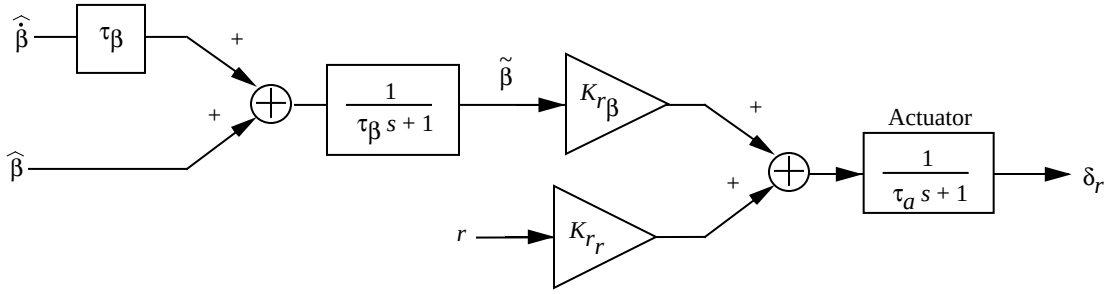

Figure B4. Yaw control law used in real-time simulation.

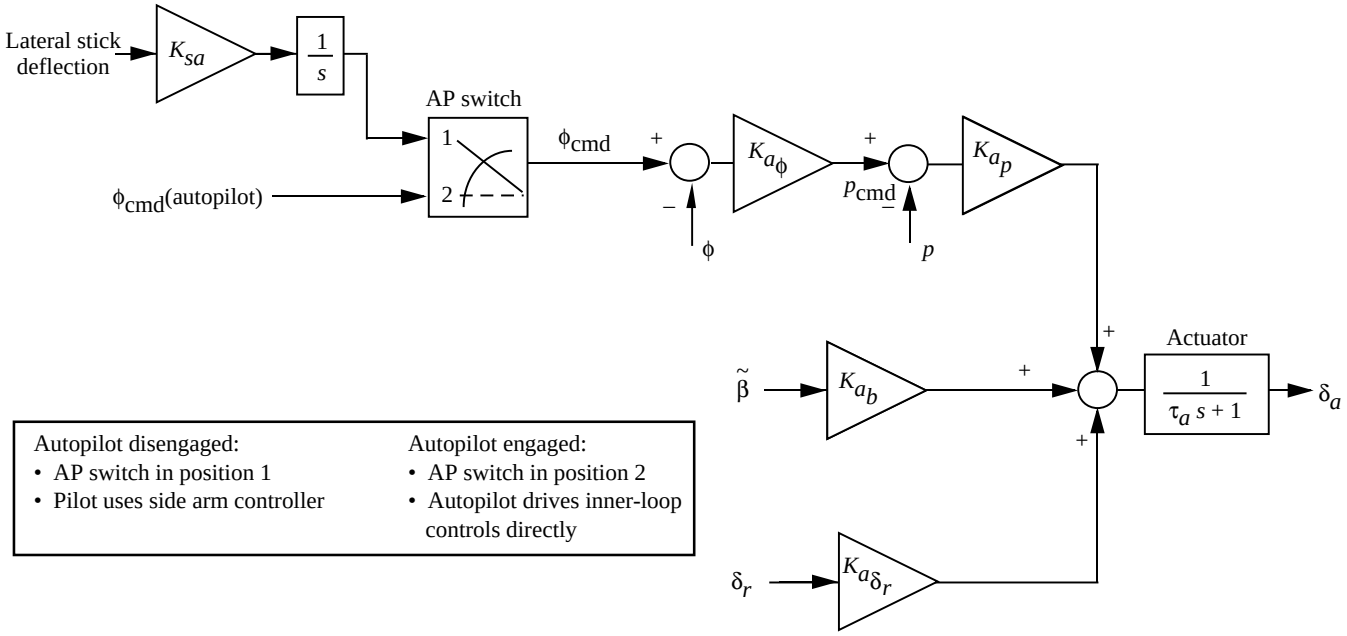

Figure B5. Roll control law used in real-time simulation.

Appendix C

Pilot Written Comments

Abbreviations:

CHR	Cooper-Harper rating
HUD	head-up display
LFRC	load factor rate command
PAL	pilot assistance level
RBFD	resolver-based flight director
RCAH	rate-command–attitude-hold
VMS	Visual/Motion Simulator

Pilot A Comments

Experiment Part 1

HUD. Of the HUD options, I prefer the resolver-based flight director (RBFD). The guidance for bank angle and normal load factor is easy to use and provides good performance. The reticle (load factor circle) diameter could be larger. If there is a problem with this system, it occurs when I am trying to close on the *g*-command guidance cue while using the rate-command–attitude-hold (RCAH) response type. The conventional HUD is a bit difficult to sort out. Although the director cue can be tracked, tracking is never really smooth, and one frequently overbanks.

Response type. Pilot performance with the resolver-based flight director was very good, and as stated before, this flight director seems to be well suited for the cruise turn task, especially when matched to the load factor rate command flight control law (LFRC). The LFRC system enabled the pilot to get out of the loop during the steady part of the turn after having established the proper bank angle and load factor. The requirement for an initial forward longitudinal input when starting the roll-out of the turn was not intuitive and required some pilot adjustment. With the RCAH system, the pilot merely relaxes aft stick pressure during the roll-out.

Table C1. Cooper-Harper Ratings for PAL 3 (autothrottles on):

[HUD and response type preference: RBFD and LFRC]

HUD	Response type	Rating
Conventional	RCAH	4
Conventional	LFRC	3
RBFD	RCAH	3
RBFD	LFRC	2

Experiment Part 2

PAL 3. Easy, fairly precise, good performance with some spare time remaining (CHR 2).

PAL 2. Throttle director is too busy; constant correction required. Still good performance in load factor and bank angle tracking. Control somewhat degraded; little spare time (CHR 5).

PAL 1. No throttle director; not too shabby. Learning curve remembered for approximate throttle settings. Real workload involved when bank angle is greater than 45° to 50° on both roll-in and roll-out. Satisfactory performance on bank angle and load factor. Throttle motion much less than with the throttle director of PAL 2, and performance with dynamic pressure was almost as good. A piece of cake during steady segment of turn (CHR 4).

PAL 0. Control of vehicle trajectory will be lost without flight director (CHR 10).

General comments. For the cruise turns that I performed, task performance clearly deteriorated and my workload increased with lower PAL settings where less guidance information was provided. Dynamic pressure control was particularly erratic because I really didn't have an accurate idea of power requirements at lower PAL's. Pilot workload during the cruise turns was highest during the roll-in and roll-out, regardless of PAL setting. In PAL's 2 and 3, the workload during the steady segment of the turn was very low because the LFRC flight control system eliminated the longitudinal part of the task.

Table C2. Pilot A Cooper-Harper Ratings With Preferred HUD and Response Type

PAL	Rating
3	2
2	5
1	4
0	10

Pilot B Comments

Experiment Part 1

Conventional HUD-RCAH flight control law. For the cruise turn task, this display and flight control law combination seems well matched and level-1 flying qualities were achieved with PAL 3. Demands on the pilot were relatively low during roll-in and roll-out of the turns, and maintainability of 2*g* while established in the

turn was not difficult. As already noted, discrimination between the lateral and the longitudinal cues is difficult when established in the 2*g* turn (CHR 3).

Conventional HUD-LFRC flight control law. This combination was obviously not as well matched as the previous control law; pilot demands were definitely higher during roll-in and, especially, during roll-out when the pilot had to push forward to follow the longitudinal cue. After the turn was established at 2*g*, pilot demands were low because the pilot could essentially get out of the loop in the longitudinal axis (CHR 3+).

RBFD-RCAH flight control law. This flight director and control law combination was the least well matched of any evaluated. Longitudinal demands on the pilot were higher during roll-ins, roll-outs, and while established in the turns (CHR 4).

RBFD-LFRC flight control law. This is a good combination. Although this flight director is not conventional and I had not flown it for some time, I felt very comfortable with it immediately and my performance with PAL 3 was definitely level 1. Performance would be even better if HUD symbology resolution could be improved to enable better discrimination of the intersection of the lift arrow and the bank angle index. This was the best flight director and flight control law combination for the cruise turn task and was therefore chosen for subsequent tasks during this session (CHR 3).

My order of preference for the four combinations is as follows:

1. RBFD-LFRC
2. Conventional HUD-RCAH
3. Conventional HUD-LFRC
4. RBFD-RCAH

Experiment Part 2

Next the pilot assist level was stepped down from 4 to 0 during the use of the RBFD-LFRC flight control law.

PAL 4. When completely automatic, I observed power movements and requirements that the autopilot used to accomplish the maneuver.

PAL 3. With autothrottles and flight director, performance was the same as in experiment part 1 (CHR 3).

PAL 2. Without the autothrottle, I used the flight director power-required cue to set power to the desired level to maintain dynamic pressure to within the specified level. My performance was usually within the desired criteria, but pilot demands definitely increased, especially during roll-in and roll-out (CHR 4).

Table C3. Cooper-Harper Ratings for PAL 3 (autothrottles on):

[HUD and response type preference: RBFD and LFRC]

HUD	Response type	Rating
Conventional	RCAH	3
Conventional	LFRC	3+
RBFD	RCAH	4
RBFD	LFRC	3

PAL 1. Without the throttle director, I was able to keep dynamic pressure within the desired range by making power changes in response to deviations and using guidelines I learned from observing PAL 4, 3, and 2 throttle requirements. My performance for this task with PAL 1 was probably as good as with PAL 2, but this was due to my being well up on the learning curve with this particular task. However, given different initial conditions with different power demands, my performance would have been much better with PAL 2 (CHR 4).

PAL 0. With the conventional display and LFRC flight control law, I could not achieve even adequate performance. Altitude could be maintained to within about 1000 ft of target and dynamic pressure within 100 lb/ft^2 of target. Load factor varied $\pm 0.5g$ from the desired factor. Attitude and flight path inconsonance prevented me from maintaining precise control of the aircraft (CHR 7).

With conventional HUD and RCAH flight control laws, my performance was only slightly better in terms of *g*-control but still well outside of adequate performance criteria (CHR 7).

During this simulation session, my performance of cruise turns with lower PAL's appeared to be significantly better than during my previous session. This was because I had recent practice and was familiar with power settings and attitudes required to accomplish the maneuvers.

Table C4. Pilot B Cooper-Harper Ratings With Preferred HUD and Response Type

PAL	Rating
3	3
2	4
1	4
0	7

Pilot C Comments

Experiment Part 1

HUD. The conventional flight director was preferred over the resolver-based flight director (RBFD) because errors and error rates in roll and pitch were more easily perceived. The RBFD was disliked because of symbology clutter which obscured the exact position of the lift vector tip and required that longitudinal and lateral errors be somewhat large before they could be detected. The load factor circle, the lift vector arrowhead, and the bank angle director form a large fuzzy mass of intersecting white lines where exact positioning of any single element cannot be determined.

When a bank angle error exists, the conventional flight director HUD requires the pilot to apply some visual extrapolation of the wing line of the flight path marker (FPM) symbol so that the height of the flight director diamond above or below the wing level can be used as a measure of the longitudinal inputs needed. This process seems to be easy to accomplish, however, and no noticeable degradation in performance was observed with this scheme compared with the conceptually better (in my judgment) RBFD scheme.

When the error in load factor and bank angle are moderate to small, the conventional flight director gives superior error and error rate cues, in part, because of having more symbol surfaces and corners to examine for alignment with each other.

Command response. The N_V rate command and N_V hold (LFRC) was preferred to the pitch-rate-command–attitude-hold (RCAH) system because between roll-in into the turn and roll-out from the turn, the longitudinal stick forces could be released once a steady solution was reached. This permitted more pilot attention to making bank angle corrections.

Experiment Part 2

PAL settings. The PAL 4 (fully automated) setting was not very interesting except that a carefully flown PAL 2 seemed to hold altitude and dynamic pressure closer to target values. The same result applies to a comparison between the PAL 3 and PAL 2 settings. PAL 2 provided better altitude and dynamic pressure holding. The cost of the improved performance with PAL 2 is an increased demand for pilot attention. Any side task loading could result in very different outcomes.

The throttle cues were useful. The throttle gain was about right for manual control, but its feel was sticky and abrupt, so steplike changes were made of necessity. In spite of this, good control of thrust was possible. With PAL 1, good control was possible just by watching dynamic pressure values and responding to them.

The PAL 0 setting was possible to fly from the start of the task up until somewhere during the roll-out on the new heading. Practice would probably permit that part to be flown as well. My approach was to try to keep the flight path marker on the horizon and to adjust bank angle to keep it there (correcting altitude errors). I set about 1.98*g*, let the control system hold it there, and varied thrust around the value that I knew to be about right. The roll-out was difficult for two reasons. First, my attitude reference on roll-out seemed to go away. Not enough time was available to understand what was happening here. Secondly, capturing the heading exactly involved knowing a lead point and a roll-and-push technique.

General comment. My control strategy was to be very attentive to small errors and error rates and then try to quickly and smoothly null them. This required much attention and would not allow distractions to dilute the pilot effort applied to the task.

Table C5. Pilot C Cooper-Harper Ratings for PAL 3 (autothrottles on):

[HUD and response type preference: RBFD and LFRC]

HUD	Response type	Rating
Conventional	RCAH	3
Conventional	LFRC	2.5
RBFD	RCAH	4
RBFD	LFRC	4

Table C6. Pilot C Cooper-Harper Ratings With Preferred HUD and Response Type

PAL	Rating
3	2.5
2	3
1	3
0	7

Pilot D Comments

Experiment Part 1

I chose the conventional HUD-LFRC control system. My belief was that the resolver-based flight director (RBFD) moved the pilot's focus away from the flight path of the vehicle because of the compelling nature of the RBFD load factor circle. The pilot finds himself striving to fly the lift vector arrow with relation to the

load factor circle rather than concentrating on the flight path. With such narrow flight path deviations acceptable in hypersonic flight, an omission of gamma as a primary scan item may prove disastrous. The net effect is to reduce the overall situational awareness of the pilot. The conventional HUD with its flight path director permits the pilot to maintain situational awareness as one flies the flight path marker to the flight path director.[2]

The LFRC response type was selected because of the ease of sustaining the proper load factor and ultimately the proper altitude during the sustained turn maneuver. The RCAH response type was inferior in the roll-in and roll-out of the turn, and the workload was higher during the sustained turn to maintain altitude control. The LFRC response type did require forward stick during the roll-out, which was not an intuitive input and is considered to be a minor deficiency of the response type.

Experiment Part 2

The PAL 4 configuration is totally automated, and therefore, no CHR's were provided. I had the opportunity to observe the autothrottle movements (the autothrottles are backdriven) for eyeball calibration and to observe the throttle director. PAL 3 was the same configuration flown to evaluate the most preferred HUD-response type combination. The desired performance criteria were met, and I rated the task a CHR of 3. The roll-axis required a little more effort than was desirable, and the necessity of pushing forward on the side-arm controller (SAC) during roll-out was a little annoying. PAL 2 was interesting as the throttle director appeared to make the task more difficult because it tended to cause me to manipulate the throttles at a higher gain level with the result of chasing the q-bar at times. I found that a better technique for me was to use the throttle bowtie display in conjunction with the dynamic pressure display to more smoothly control the q-bar. Using the throttle director, I gave the task a CHR of 4 while ignoring the throttle director resulted in a CHR of 3. This was essentially the PAL 1 configuration. The PAL 0 configuration (no flight director) did not lend itself to the use of the LFRC response type, so I preferred the RCAH configuration. Because of the compounding problems of centrifugal relief, path and attitude decoupling, and dynamic pressure sensitivity, just maintaining control was an effort without a flight director. The CHR of 8 reflects this.

[2]Author's comment: Note that the director symbols for both HUD symbologies were driven by the same load factor error signal. When the pilot nulled the flight director error on the conventional HUD, the pilot was not directly flying the flight path marker to the director but rather was zeroing the director offset from the flight path marker by achieving the desired load factor.

Table C7. Pilot D Cooper-Harper Ratings for PAL 3 (autothrottles on):

[HUD and response type preference: RBFD and LFRC]

HUD	Response type	Rating
Conventional	RCAH	4
Conventional	LFRC	3
RBFD	RCAH	4
RBFD	LFRC	3

One other comment deserves mention. The motion cueing of the Langley VMS provided an excessive beta signal during the cruise turns. The cruise turns are balanced turns, yet the simulator provided a significant sideslip motion cue which was clearly discernible to the pilot.

Table C8. Pilot D Cooper-Harper Ratings With Preferred HUD and Response Type

PAL	Rating
3	3
2	4
1	3
0	8

References

1. Walton, James T.: Performance Sensitivity of Hypersonic Vehicles to Changes in Angle of Attack and Dynamic Pressure. AIAA-89-2463, July 1989.

2. Shaughnessy, John D.; and Raney, David L.: *Response of a Hypersonic Vehicle to Atmospheric Disturbances During Ascent*. NASP TM-1061, NASP JPO, Wright-Patterson AFB, 1989.

3. Berry, Donald T.: *National Aero-Space Plane Flying Qualities Task Definition Study.* NASP TM-1039, NASP JPO, Wright-Patterson AFB, 1988.

4. Berry, Donald T.: *National Aero-Space Plane Flying Qualities Requirements*. NASP TM-1084, NASP JPO, Wright-Patterson AFB, 1989.

5. McRuer, Duane T.; Ashkenas, Irving L.; and Johnston, Donald E.: *Flying Qualities and Control Issues/Features for Hypersonic Vehicles*. NASP CR-1063, NASP JPO, Wright-Patterson AFB, 1989.

6. Chalk, C. R.: *Flying Qualities Criteria Review, Assessment and Recommendations for NASP.* NASP CR-1065, NASP JPO, Wright-Patterson AFB, 1989.

7. McRuer, Duane T.; and Myers, Thomas T.: *Considerations for the Development of NASP Flying Qualities Specifications*. WL-TR-92-3042, U.S. Air Force, 1991. (Also available from DTIC as AD B170 015L.)

8. Lallman, Frederick J.; and Raney, David L.: *Dynamic Pressure/Energy Regulator for NASP.* NASP TM-1032, NASP JPO, Wright-Patterson AFB, 1988.

9. Lallman, Frederick J.; and Raney, David L.: *Altitude-Velocity Regulator for NASP.* NASP TM-1053, NASP JPO, Wright-Patterson AFB, 1989.

10. Lallman, Frederick J.; and Raney, David L.: *Energy/Dynamic Pressure Regulator for NASP.* NASP TM-1066, NASP JPO, Wright-Patterson AFB, 1989.

11. Lallman, Frederick J.; and Raney, David L.: *Velocity/Dynamic Pressure Regulator for NASP.* NASA TM-1089, NASP JPO, Wright-Patterson AFB, 1989.

12. Lallman, Frederick J.; and Raney, David L.: *Altitude-Energy Regulator for NASP.* NASP TM-1098, NASP JPO, Wright-Patterson AFB, 1990.

13. Raney, David L.; and Lallman, Frederick J.: *Control Integration Concept for Hypersonic Cruise-Turn Maneuvers*. NASA TP-3136, 1992.

14. Bonner, E.; Clever, W.; and Dunn, K.: *Aerodynamic Preliminary Analysis System II. Part I—Theory.* NASA CR-182076, 1991.

15. Shaughnessy, John D.; Pinckney, S. Zane; McMinn, John D.; Cruz, Christopher I.; and Kelley, Marie-Louise: *Hypersonic Vehicle Simulation Model: Winged-Cone Configuration*. NASA TM-102610, 1990.

16. Hahne, David E.; Luckring, James M.; Covell, Peter F.; Phillips, W. Pelham; Gatlin, Gregory M.; Shaughnessy, John D.; and Nguyen, Luat T.: Stability Characteristics of a Conical Aerospace Plane Concept. SAE Tech. Paper Ser. 892313, Sept. 1989.

17. Chavez, Frank R.; and Schmidt, David K.: Dynamics of Hypersonic Flight Vehicles Exhibiting Significant Aeroelastic and Aeropropulsive Interactions. AIAA-93-3763, Aug. 1993.

18. Chan, Samuel Y.; Cheng, Peter Y.; Pitt, Dale M.; Myers, Thomas T.; Klyde, David H.; Magdaleno, Raymond E.; and McRuer, Duane T.: *Aeroservoelastic Stabilization Techniques for Hypersonic Flight Vehicles*. NASA CR-187614, 1991.

19. Spain, Charles V.; Zeiler, Thomas A.; Gibbons, Michael D.; Soistmann, David L.; Pozefsky, Peter; DeJesus, Rafael O.; and Brannon, Cyprian P.: Aeroelastic Character of a National Aerospace Plane Demonstrator Concept. AIAA-93-1314, Apr. 1993.

20. Grantham, William D.: *Comparison of Flying Qualities Derived From In-Flight and Ground-Based Simulators for a Jet-Transport Airplane for the Approach and Landing Pilot Tasks*. NASA TP-2962, 1989.

21. Martin, D. J., Jr.: *A Digital Program for Motion Washout on Langley's Six-Degree-of-Freedom Motion Simulator.* NASA CR-145219, 1977.

22. McFarland, Richard E.: *A Standard Kinematic Model for Flight Simulation at NASA-Ames*. NASA CR-2497, 1975.

23. Rollins, John D.: *Description and Performance of the Langley Visual Landing Display System*. NASA TM-78742, 1978.

Table 1. Geometric Characteristics of Vehicle Concept Used in Real-Time Simulation

Wing:	
Reference area (includes area projected to fuselage centerline), ft^2	3603
Aspect ratio	1.00
Span, ft	60.0
Leading-edge sweep angle, deg	75.97
Trailing-edge sweep angle, deg	0.0
Mean aerodynamic chord, ft	80.0
Airfoil section	Diamond
Airfoil thickness to chord ratio, percent	4.0
Incidence angle, deg	0.0
Dihedral angle, deg	0.0
Wing flap (elevon):	
Area (each), ft^2	92.3
Chord (constant), ft	7.22
Inboard section span location, ft	15.0
Outboard section span location, ft	27.78
Vertical tail, body centerline:	
Exposed area, ft^2	645.7
Theoretical area, ft^2	1248.8
Span, ft	32.48
Leading-edge sweep angle, deg	70.0
Trailing-edge sweep angle, deg	38.13
Airfoil section	Diamond
Airfoil thickness to chord ratio, percent	4.0
Rudder:	
Area, ft^2	161.4
Span, ft^2	22.8
Chord to vertical tail chord ratio, percent	25.0
Axisymmetric fuselage:	
Theoretical length, ft	200.0
Cone half angle, deg	5.0
Cylinder radius (maximum), ft	12.87
Cylinder length, ft	12.88
Boattail half angle, deg	9.0
Boattail length, ft	40.0
Moment reference center, ft	124.01

Table 2. Performance Limits of Langley Visual/Motion Simulator

[See ref. 20]

Degree of freedom	Position, deg	Velocity, deg/sec	Acceleration, deg/sec^2
Pitch	+30 to –20	±15	±50
Roll	±22	±15	±50
Yaw	±32	±15	±50
	Position, ft	Velocity, ft/sec	Acceleration, *g* units
Vertical	+2.5 to –3.25	±2	±0.6
Lateral	±4.0	±2	±0.6
Longitudinal.	+4.1 to –4.0	±2	±0.6

Table 3. Feel System Settings of McFadden Control Loader Used for Side Stick

Parameter	Pitch axis	Roll axis
Breakout force, lb	±1.0	0.75 left, 1.0 right
Displacement limits, deg	18 fwd, 20 aft	±20
Maximum force, lb	12 fwd, 13 aft	5.0 left, 6.5 right
Velocity limit, in/sec	35	35
Frequency, rad/sec	23	16
Damping	0.85	1.4

Table 4. Task Completion Criteria Used in Hypersonic Cruise Turn Maneuver

Parameter	Completion criteria
Heading	Maintain within ±2° of target heading for 5 sec
Bank angle	Maintain magnitude of $\phi < 3°$ for 3 sec
Altitude	Maintain within ±80 ft of target altitude for 5 sec
Dynamic pressure	Maintain within ±20 lb/ft^2 of target value for 5 sec

Table 5. Definition of Pilot Assistance Level (PAL) Designations

PAL designation	Flight director	Throttle director	Autothrottle	Autopilot	Description
0	OFF	OFF	OFF	OFF	Manual control, unassisted
1	ON	OFF	OFF	OFF	Manual control with flight director
2	ON	ON	OFF	OFF	Manual control with flight and throttle directors
3	ON	ON	ON	OFF	Manual stick with auto-throttle and both directors
4	ON	ON	ON	ON	Fully automated control: autopilot and autothrottle

Table 6. Designations for Response Type and HUD Combinations

Control response type	HUD symbology	
	Conventional	RBFD
RCAH	RCAH-1	RCAH-2
LFRC	LFRC-1	LFRC-2

Table 7. Pilot Preferences for Response Type and HUD Combination

Pilot	Response type		HUD symbology		Preferred combination
	RCAH	LFRC	Nominal	RBFD	
A		√		√	LFRC-2
B		√		√	LFRC-2
C		√	√		LFRC-1
D		√	√		LFRC-1

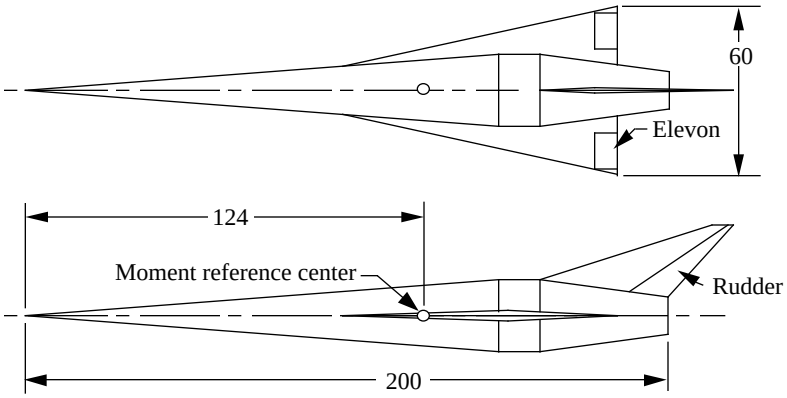

Figure 1. Hypersonic vehicle concept used in real-time simulation. All dimensions are in feet.

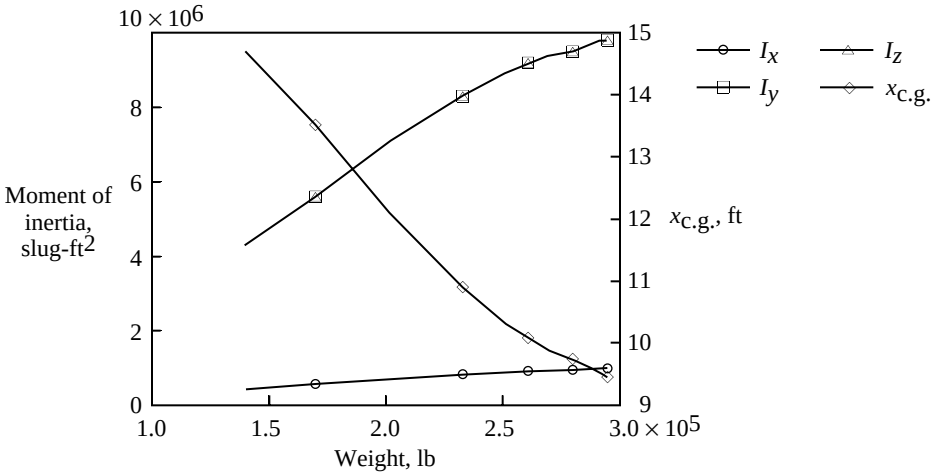

Figure 2. Variation of vehicle inertial characteristics and center of gravity with weight.

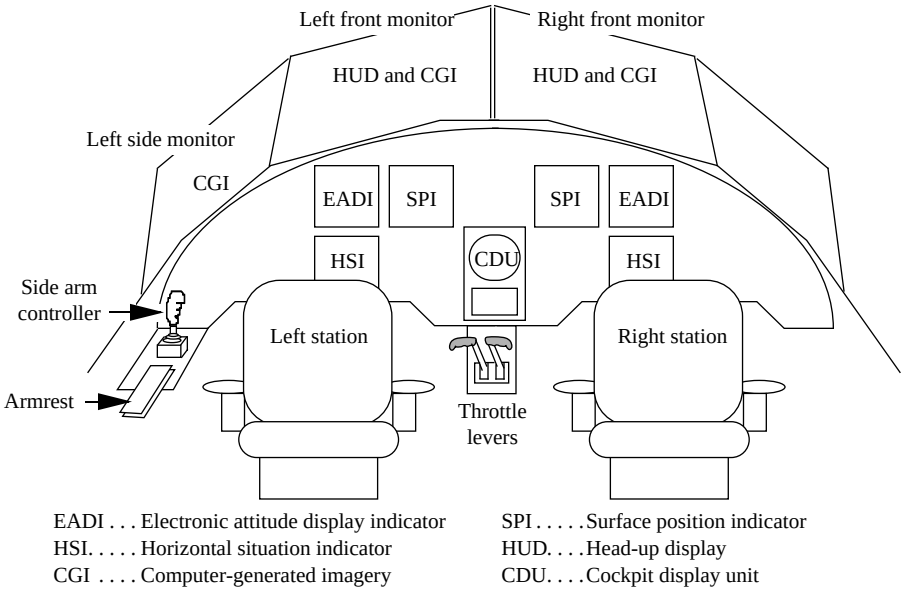

Figure 3. Interior layout of simulator cockpit.

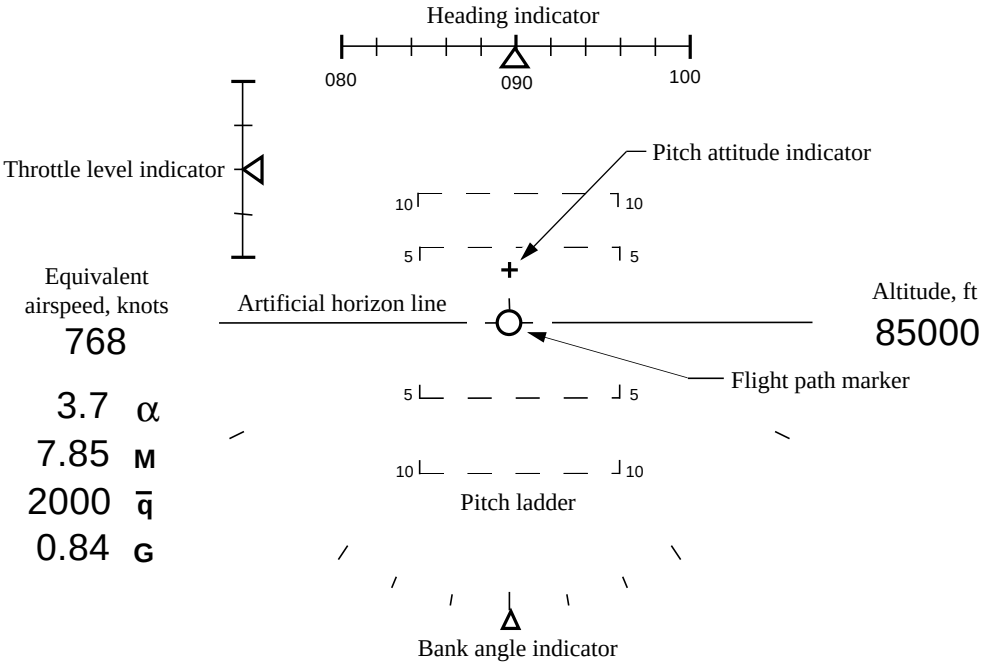

Figure 4. Symbology for baseline head-up display used in real-time simulation.

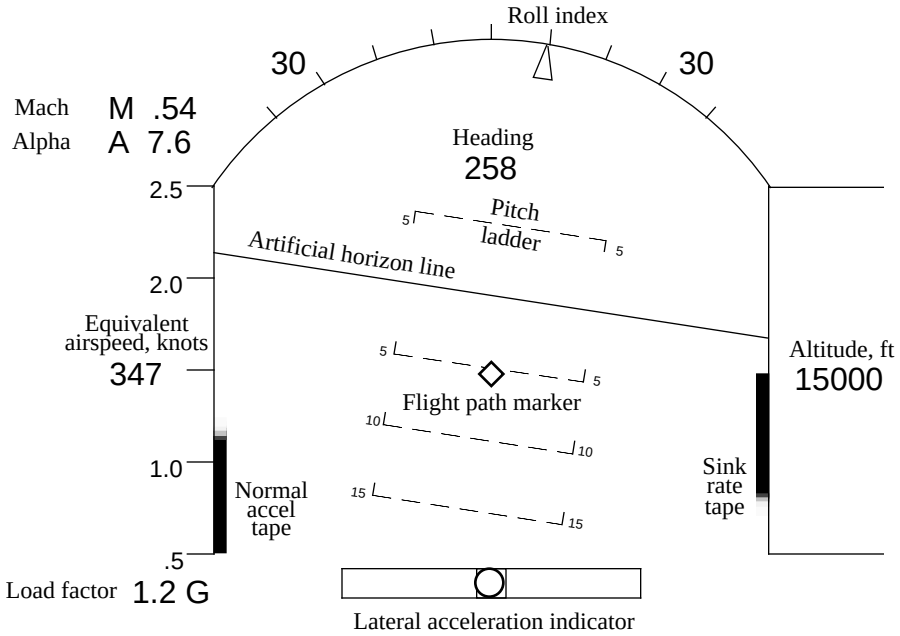

Figure 5. Diagram of head-down electronic attitude display indicator (EADI).

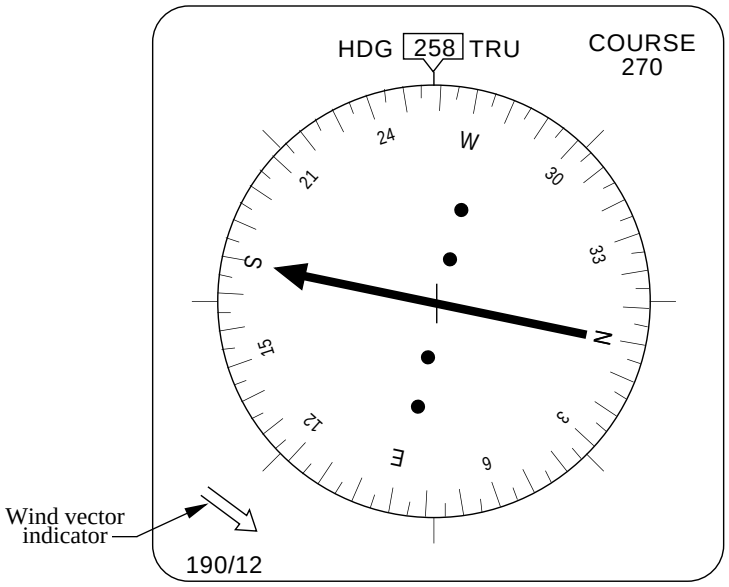

Figure 6. Diagram of head-down horizontal situation indicator (HSI) display.

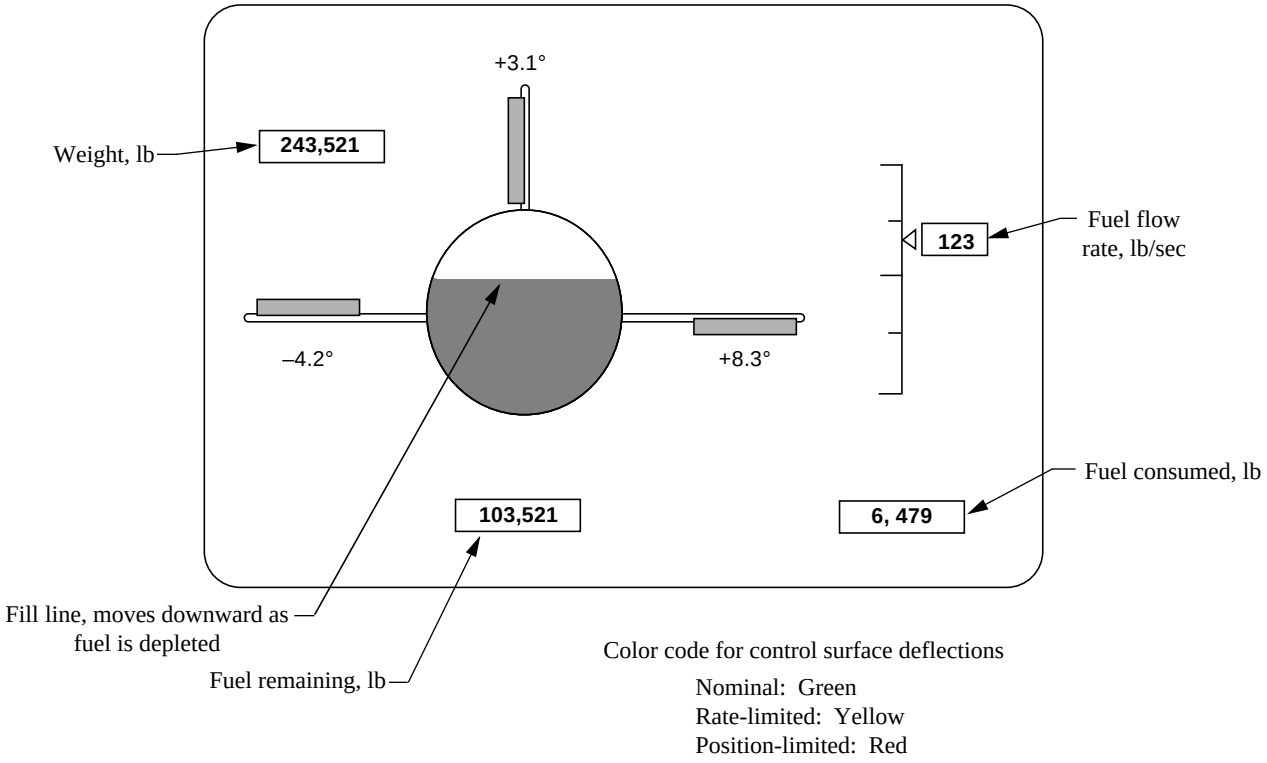

Figure 7. Diagram of head-down surface position indicator (SPI) display.

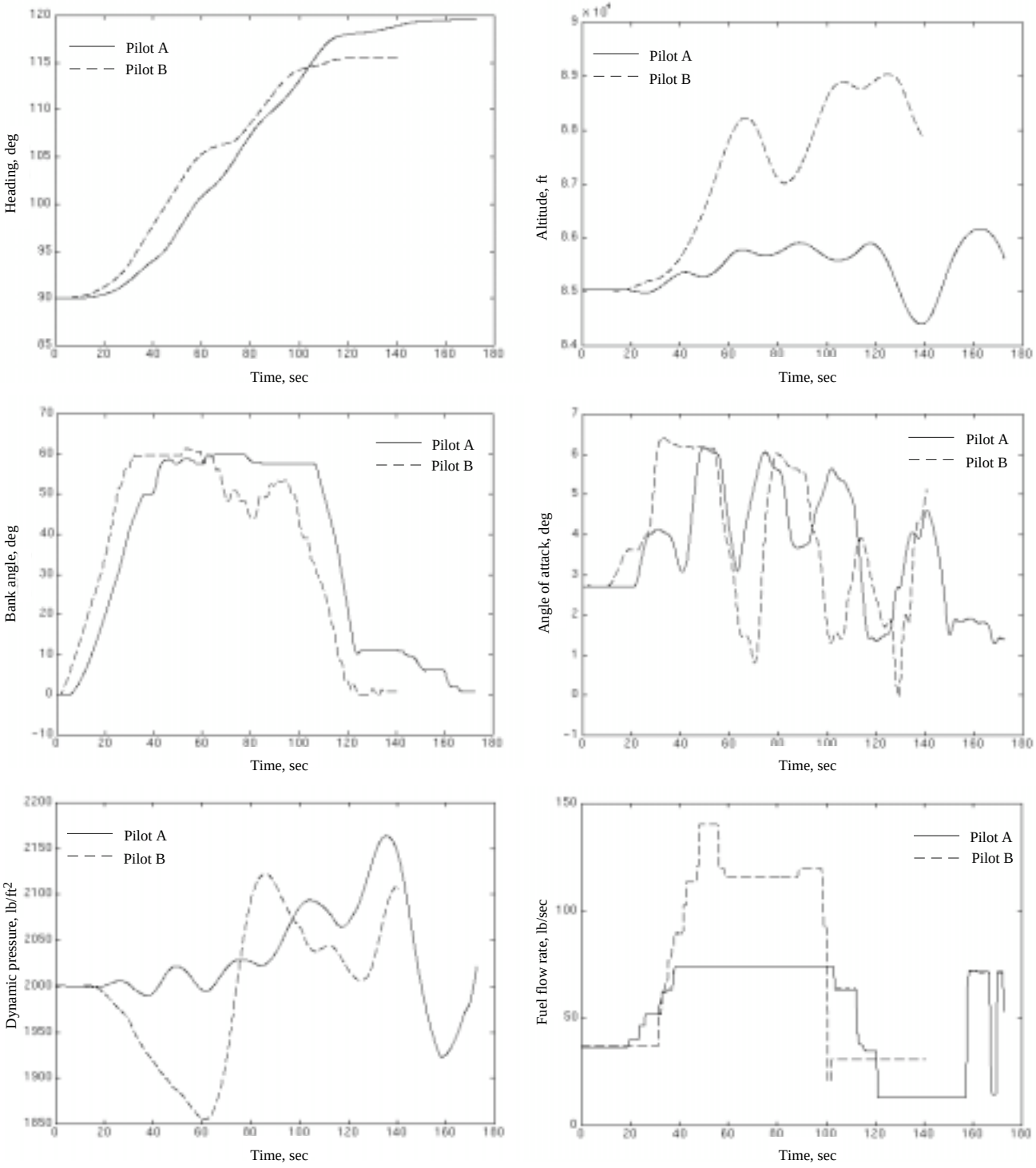

Figure 8. Time history of two typical cruise turn maneuvers executed during preliminary simulation sessions at Mach 7.86 and 85 000 ft.

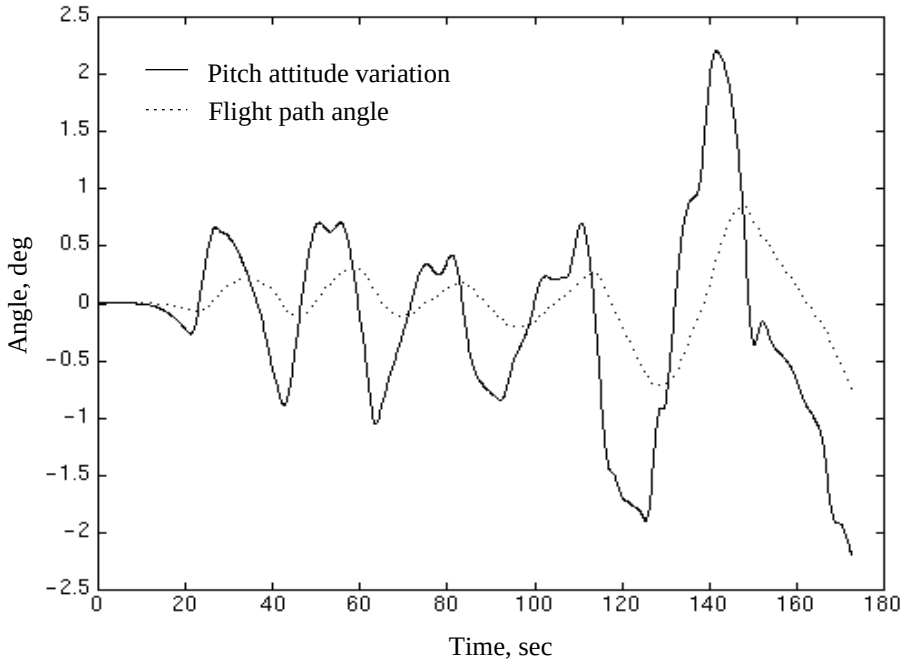

(a) Pilot A.

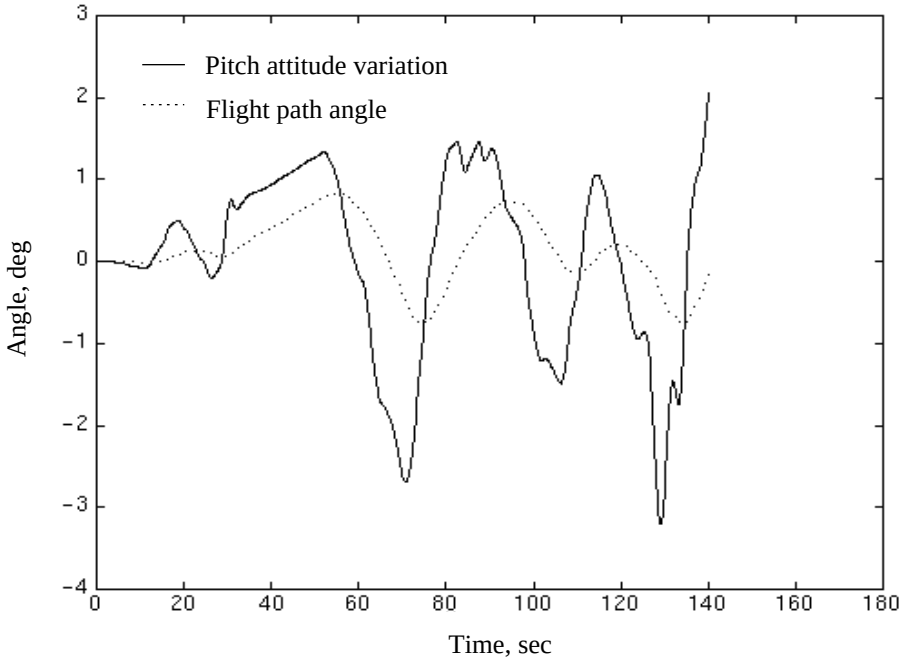

(b) Pilot B.

Figure 9. Variation in pitch attitude and flight path angle for typical cruise turn maneuvers executed during preliminary simulation sessions at Mach 7.86 and 85 000 ft.

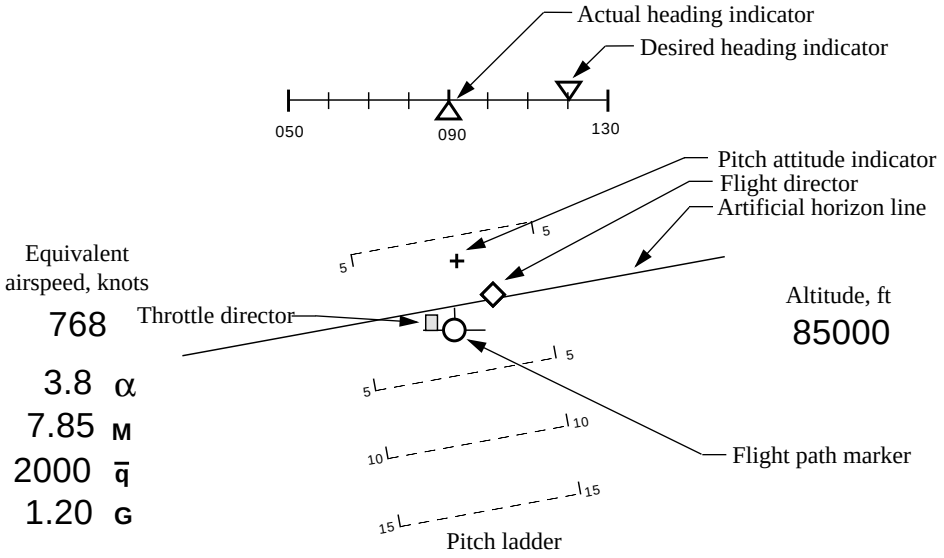

Figure 10. Symbology for conventional flight director.

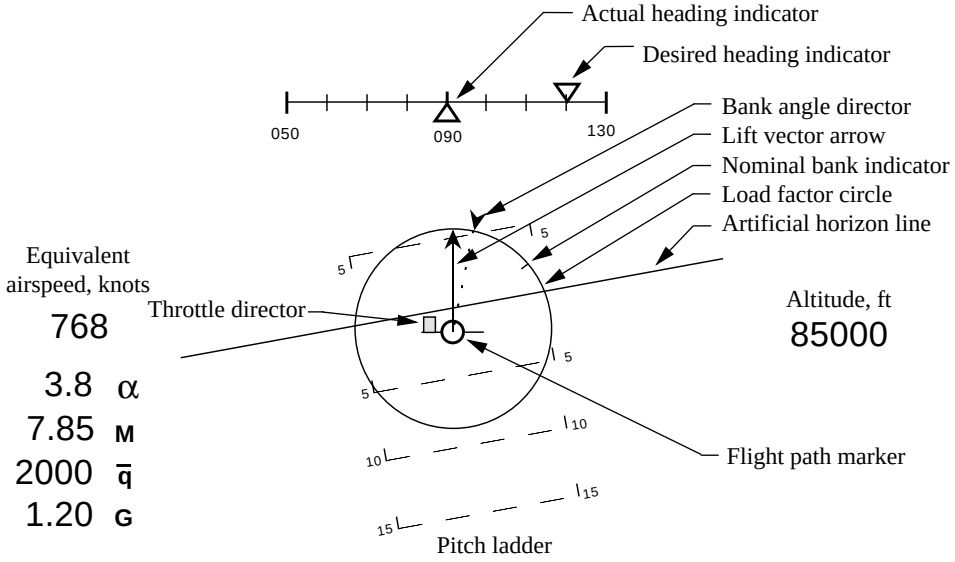

Figure 11. Symbology for resolver-based flight director (RBFD).

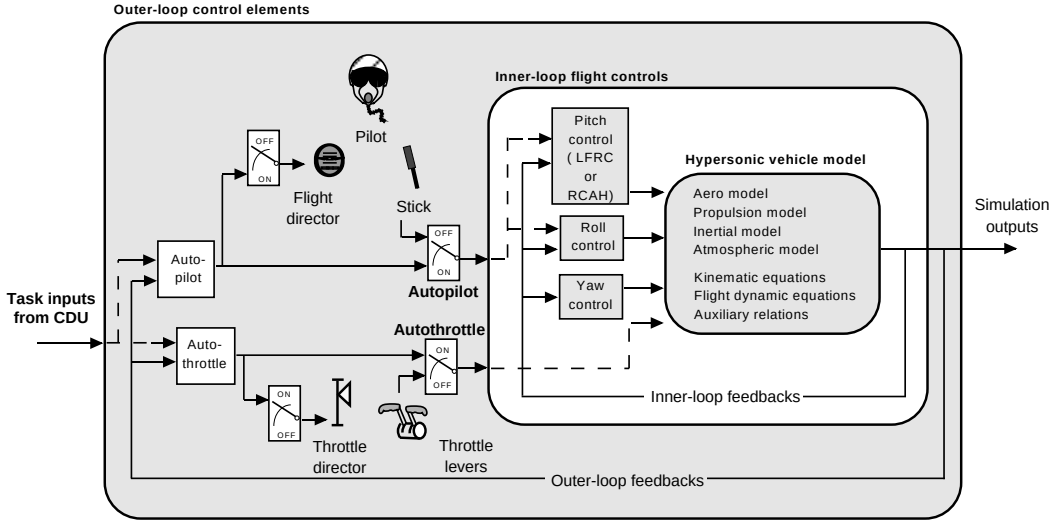

Figure 12. Flowchart showing elements of real-time simulation setup.

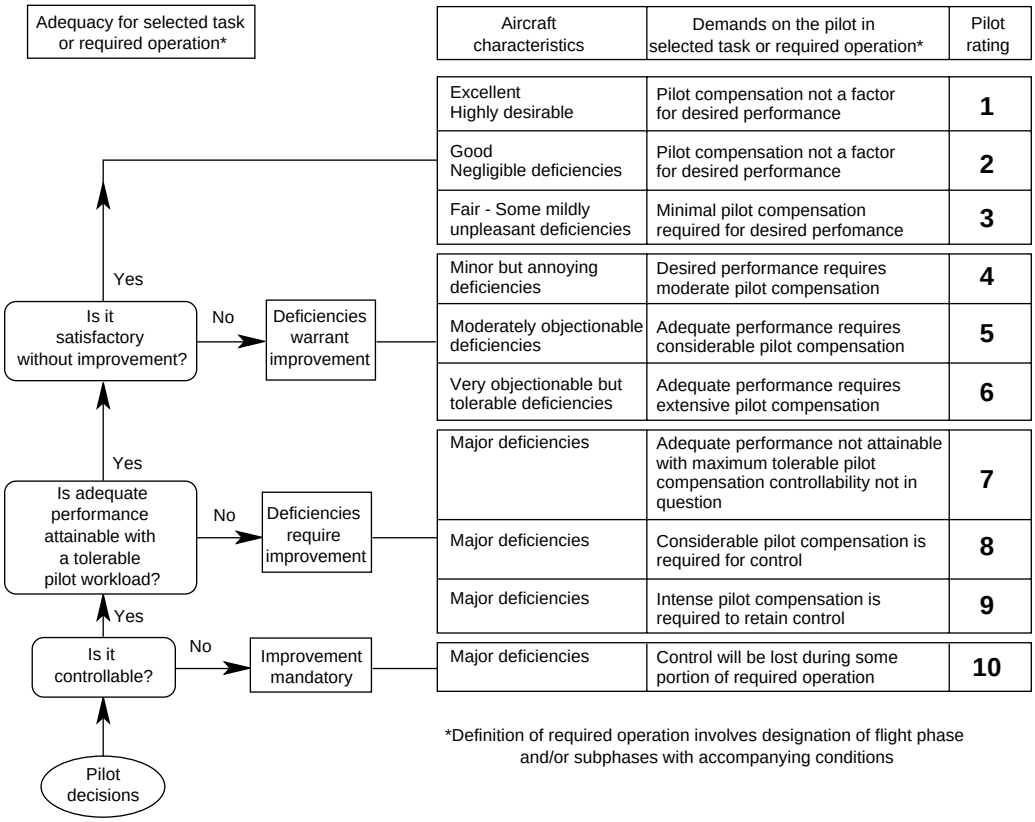

Figure 13. Cooper-Harper flying qualities rating scale.

Real Time Session -- **Itinerary**	Hypersonic Simulation Pilot: Date:

Session itinerary for up & away maneuver tasks:

Part I: Execute cruise-turn comparing 4 Response Type/ HUD combinations using PAL 3; select preferred combination.

a) Command Response Types: RCAH, LFRC
b) HUD Types: HUD 0a (conventional), HUD 2 (RBFD)

Part II: Execute cruise-turn using successively lower PAL settings with preferred response type and HUD combination; note perfomance degradation with PAL reduction.

c) PAL Settings:

PAL	Flight Director	Throttle Director	Autothrottle	Autopilot
4	X	X	X	X
3	X	X	X	--
2	X	X	--	--
1	X	--	--	--
0	--	--	--	--

Cruise-Turn Task Defintion: 30 deg. heading change; 2-g turn from 090 to 120
(Initiate from level flight at Mach= 7.90, dynamic pressure= 2000 psf, h= 85,040 ft)
Hold dynamic pressure and altitude
Bank to initiate maneuver
Establish steady 2g turn
Attain required heading change
Roll out on desired heading

Flight Director Tracking Tolerances:

	Desired	Adequate
Normal Load Factor	± 0.10 g	± 0.20 g
Bank Angle	± 5.0 deg	± 10.0 deg

Target Parameter Acquisition/ Regulation Tolerances:

	Desired	Adequate
Dynamic Pressure	± 20.0 psf	± 30.0 psf
Altitude	± 200 ft	± 300 ft
Heading	± 0.5 deg	± 1.0 deg

Figure 14. Itinerary for typical real-time simulation session.

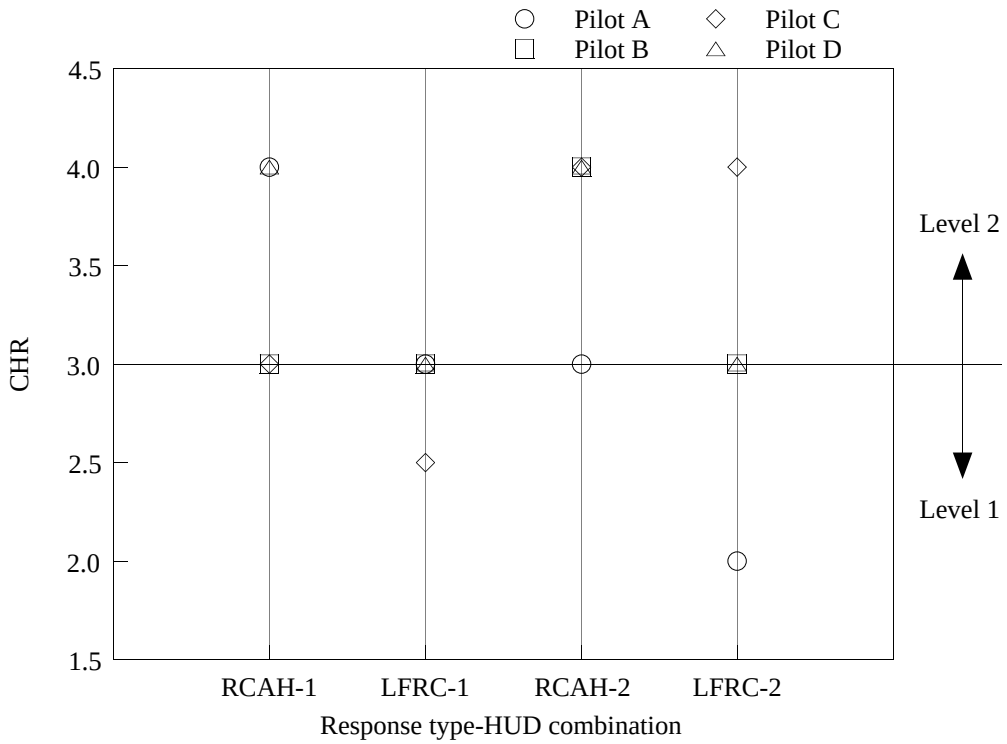

Figure 15. Cooper-Harper ratings of response type and HUD combination with PAL 3.

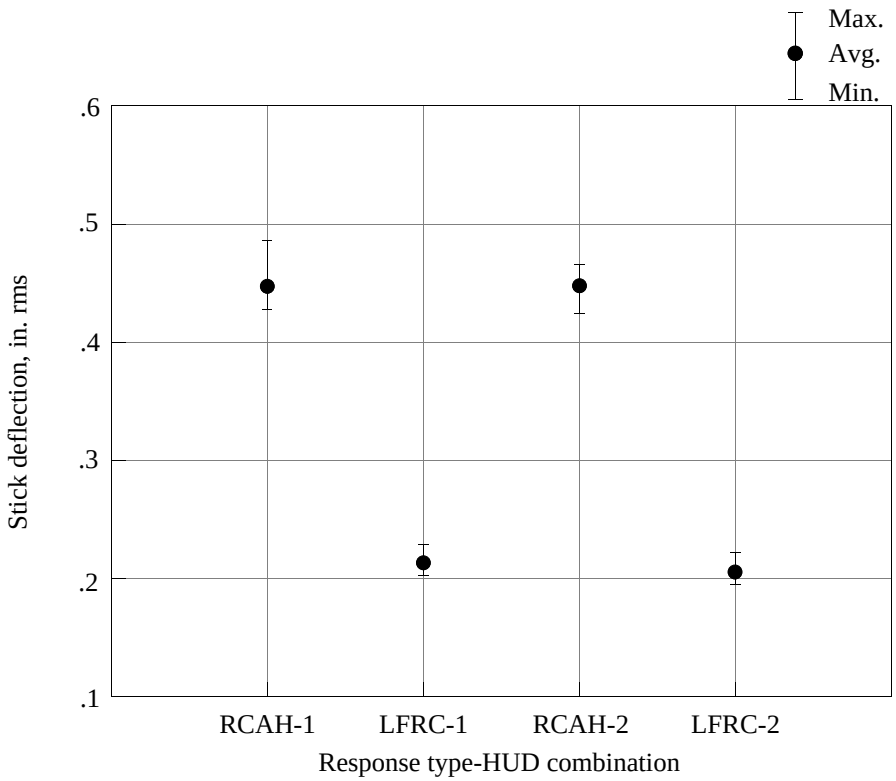

Figure 16. Stick deflection (rms) versus response type and HUD combination with PAL 3.

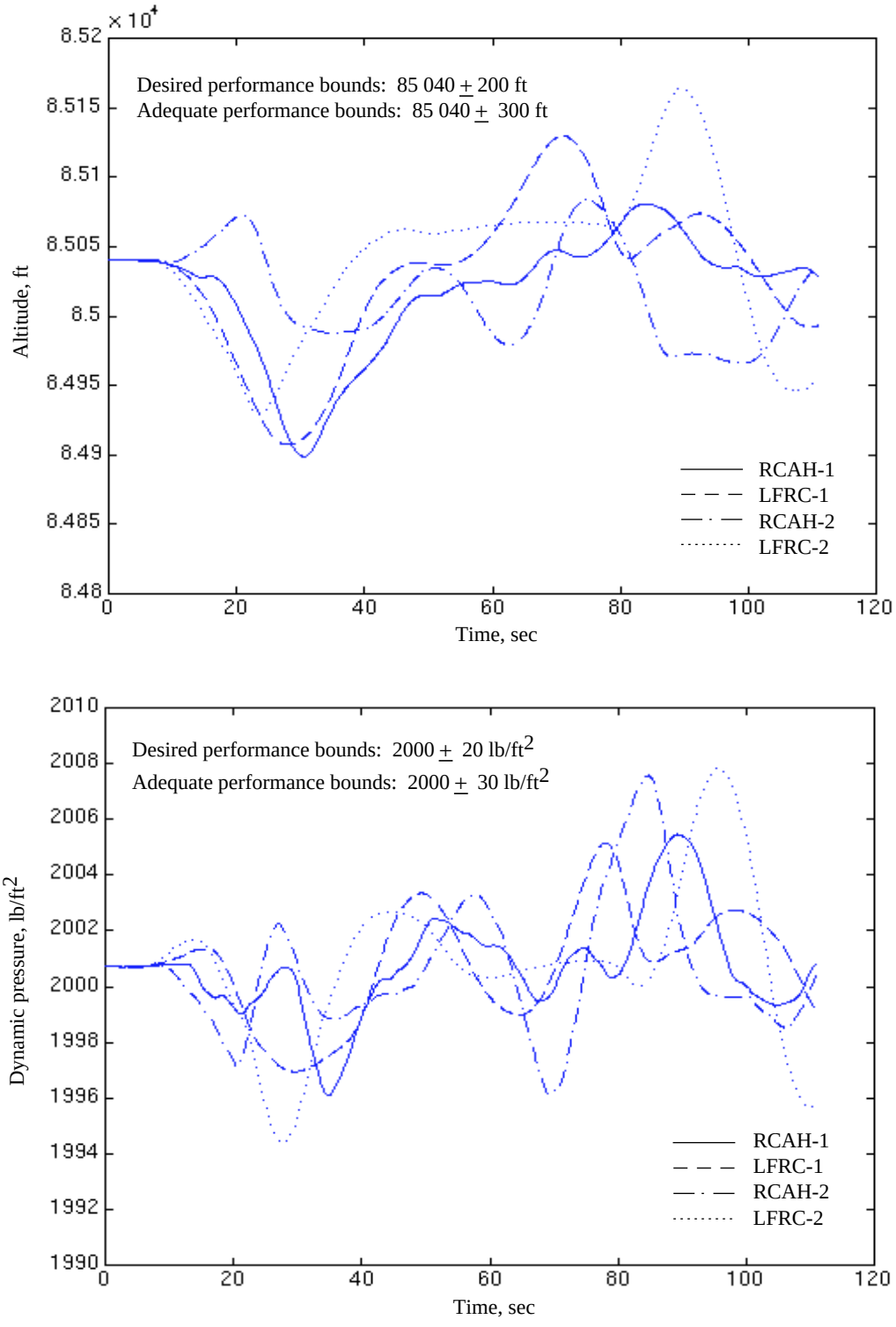

Figure 17. Time histories of typical maneuvers conducted by pilot A using each of four response type and HUD combinations.

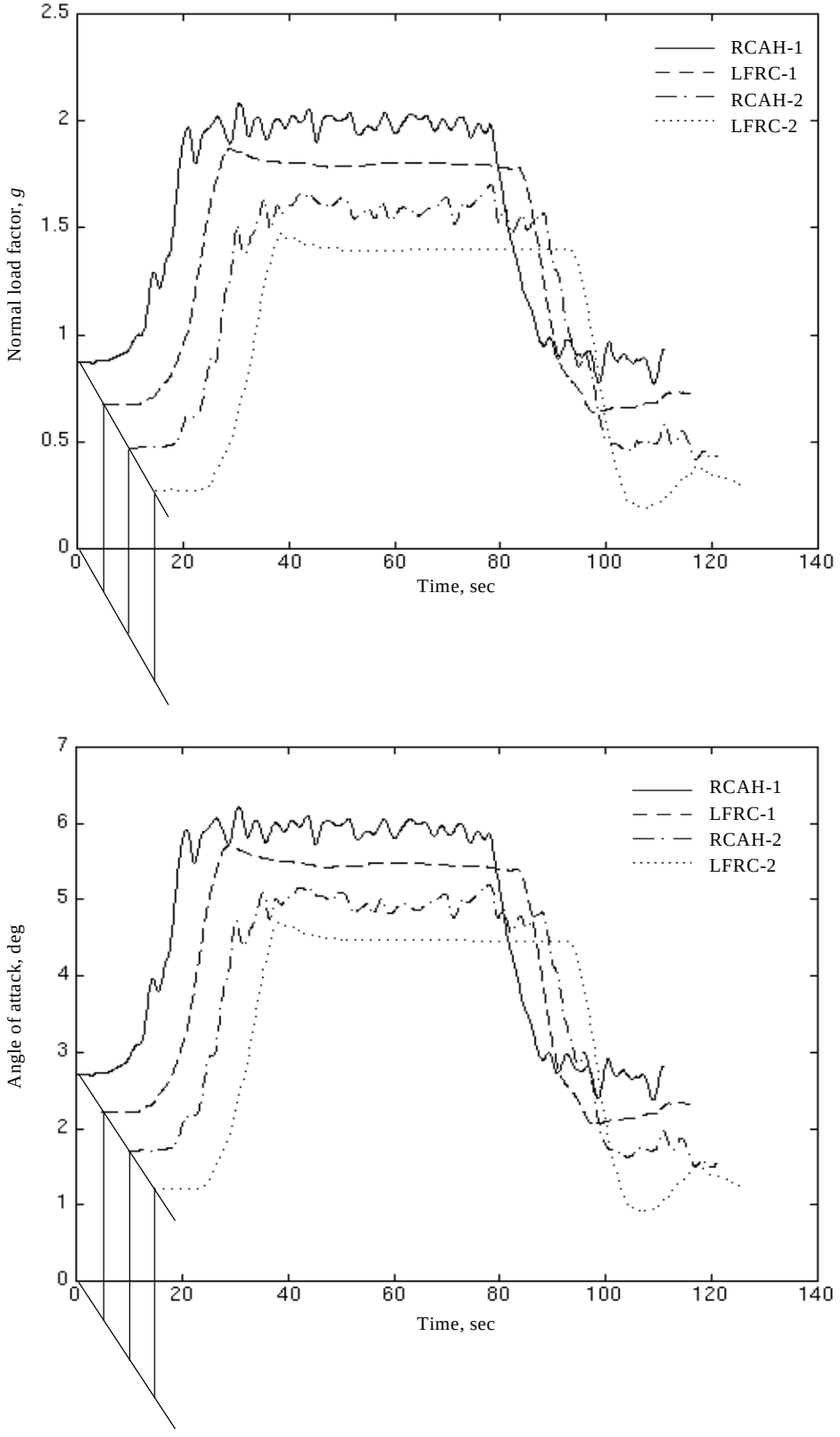

Figure 17. Continued.

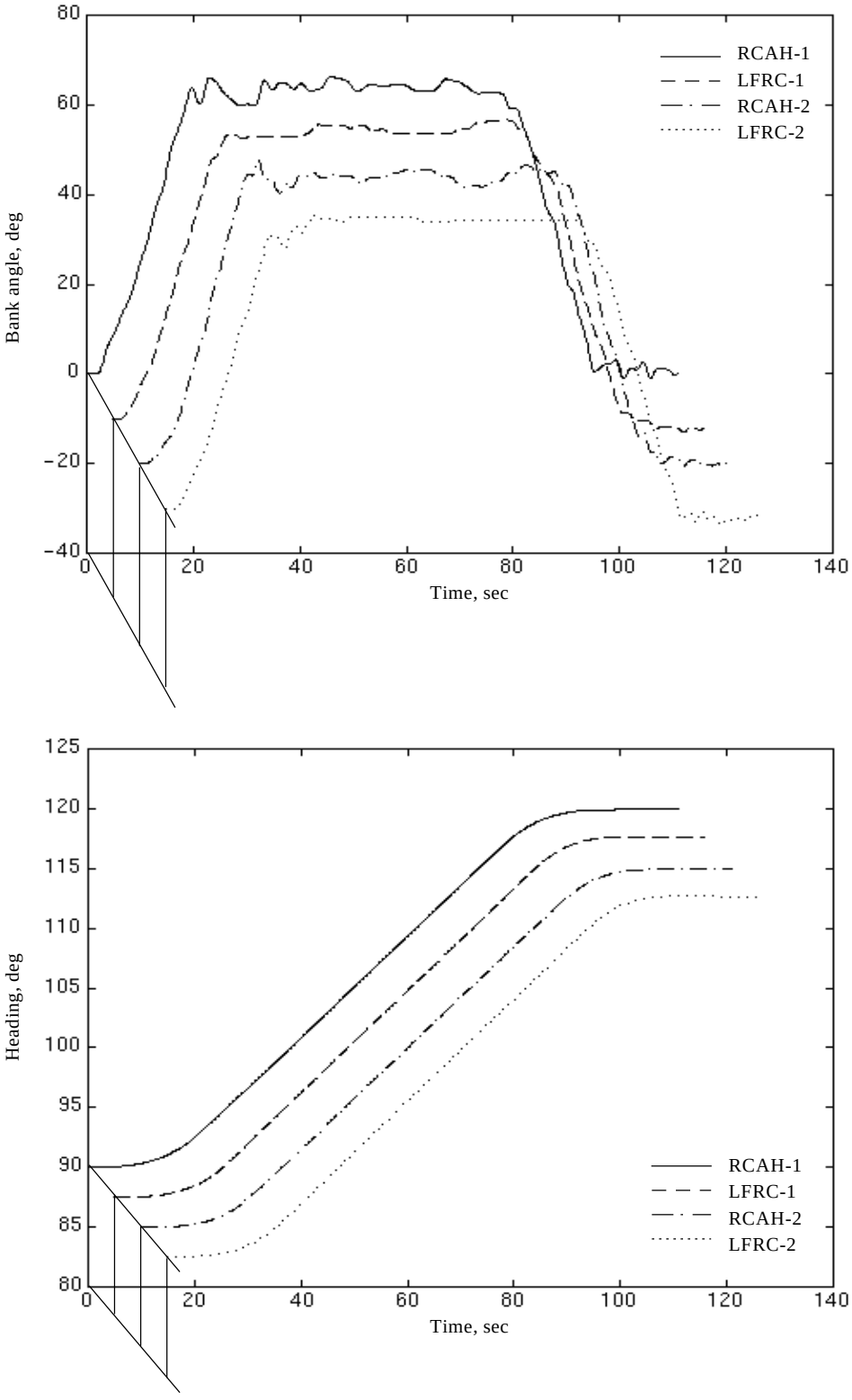

Figure 17. Concluded.

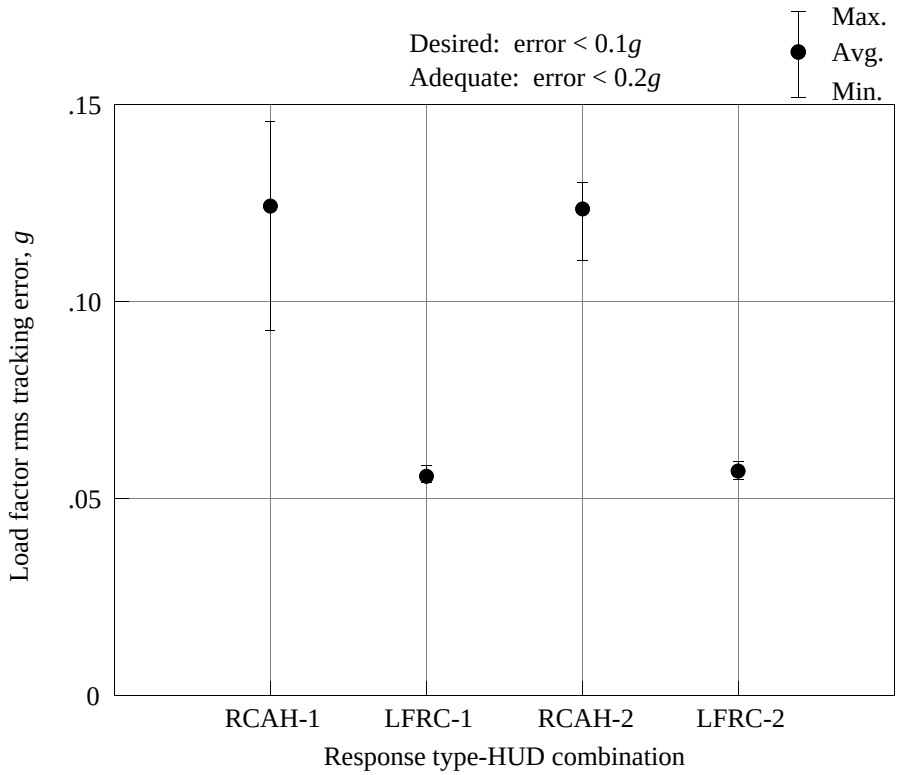

Figure 18. Normal load factor rms tracking error versus response type and HUD combination with PAL 3.

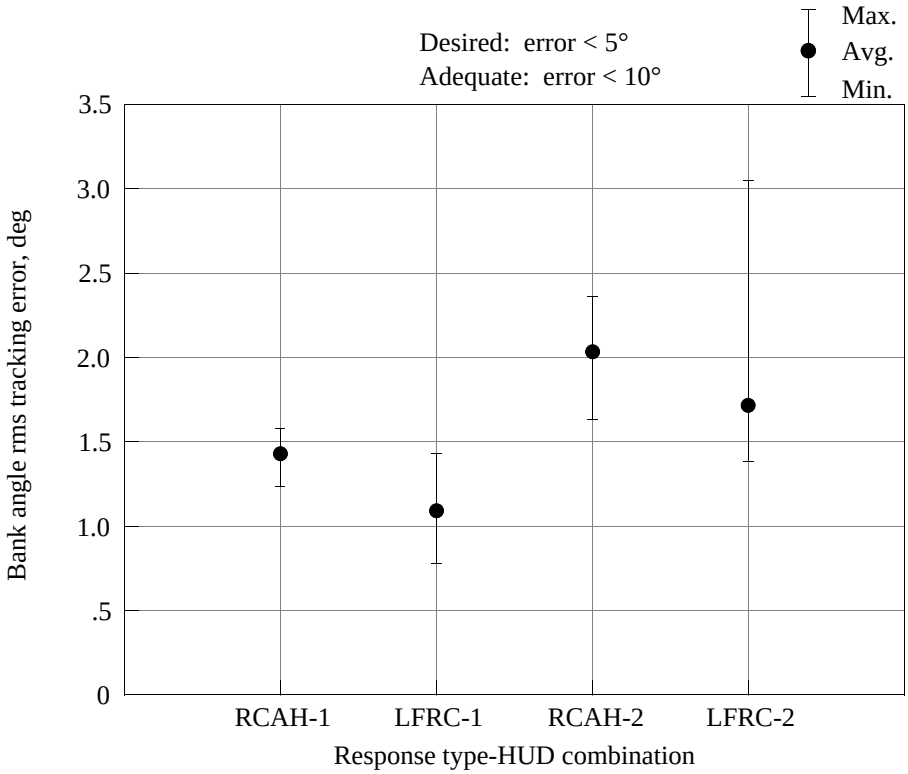

Figure 19. Bank angle rms tracking error versus response type and HUD combination with PAL 3.

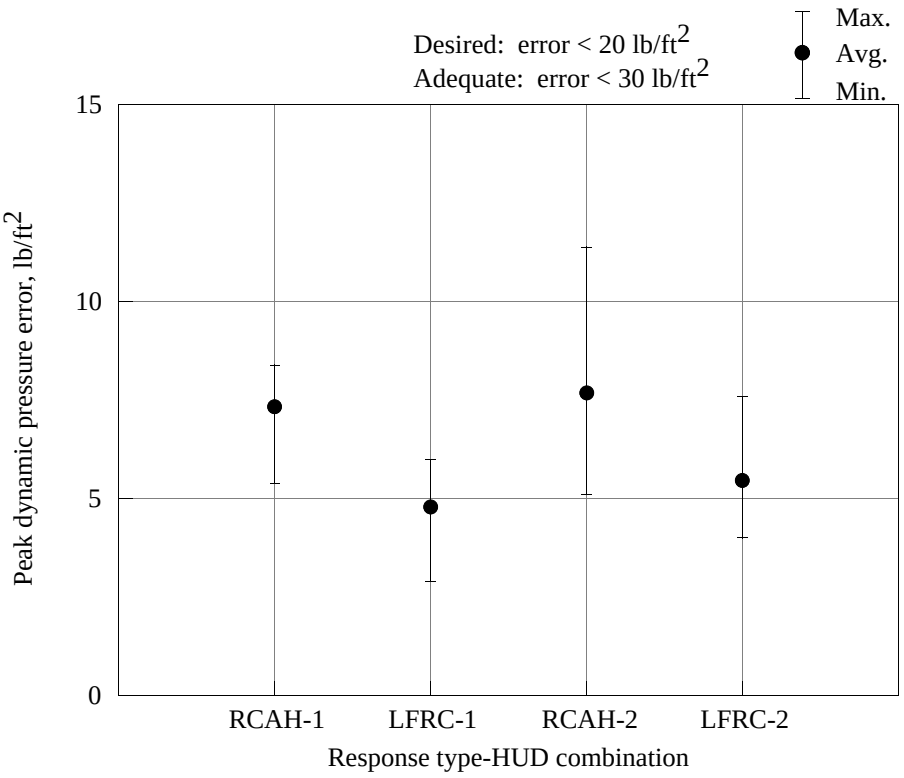

Figure 20. Peak absolute dynamic pressure error versus response type and HUD combination with PAL 3.

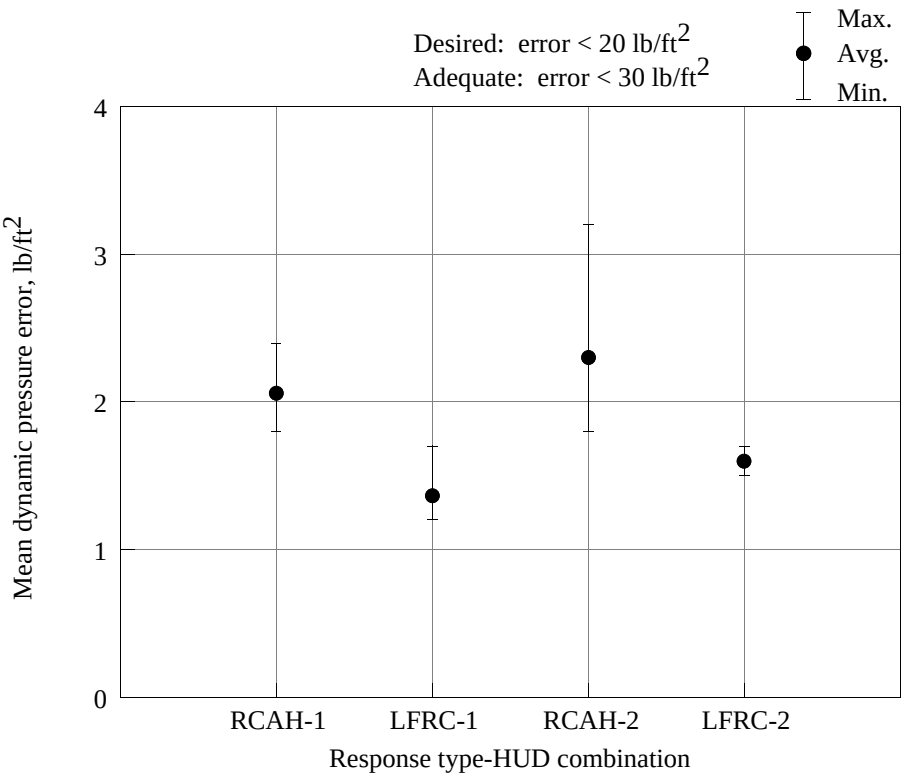

Figure 21. Mean absolute dynamic pressure error versus response type and HUD combination with PAL 3.

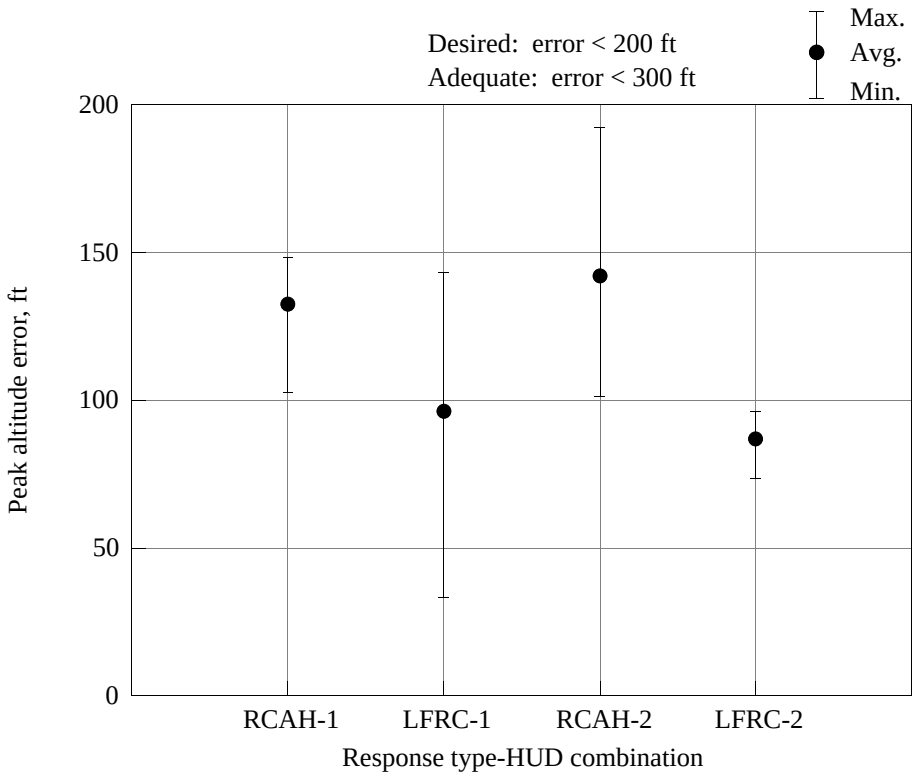

Figure 22. Peak absolute altitude error versus response type and HUD combination with PAL 3.

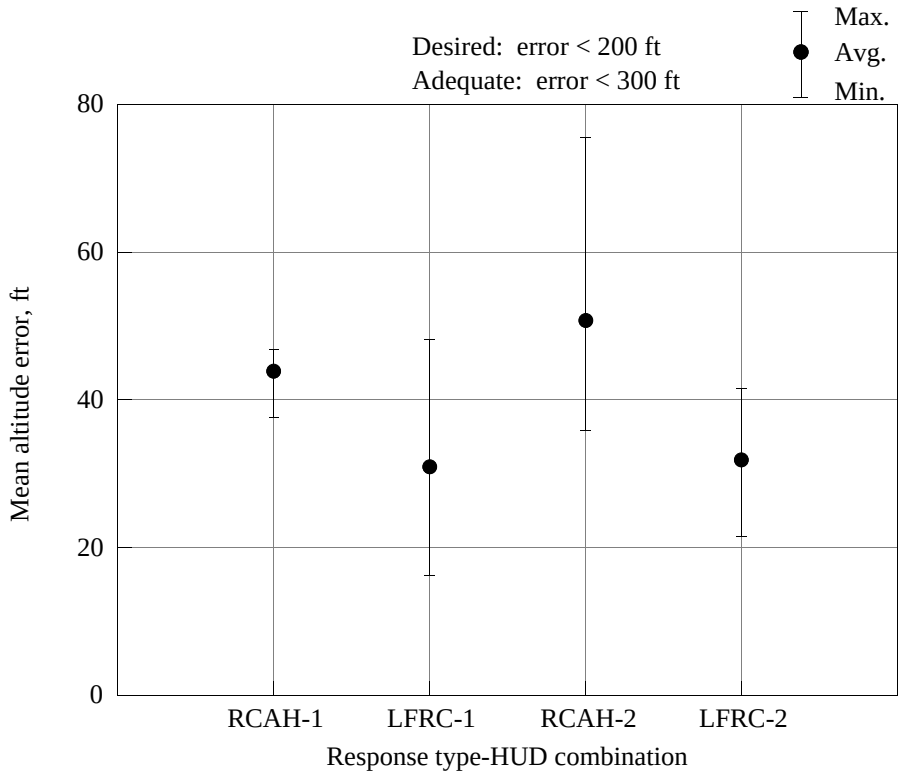

Figure 23. Mean absolute altitude error versus response type and HUD combination with PAL 3.

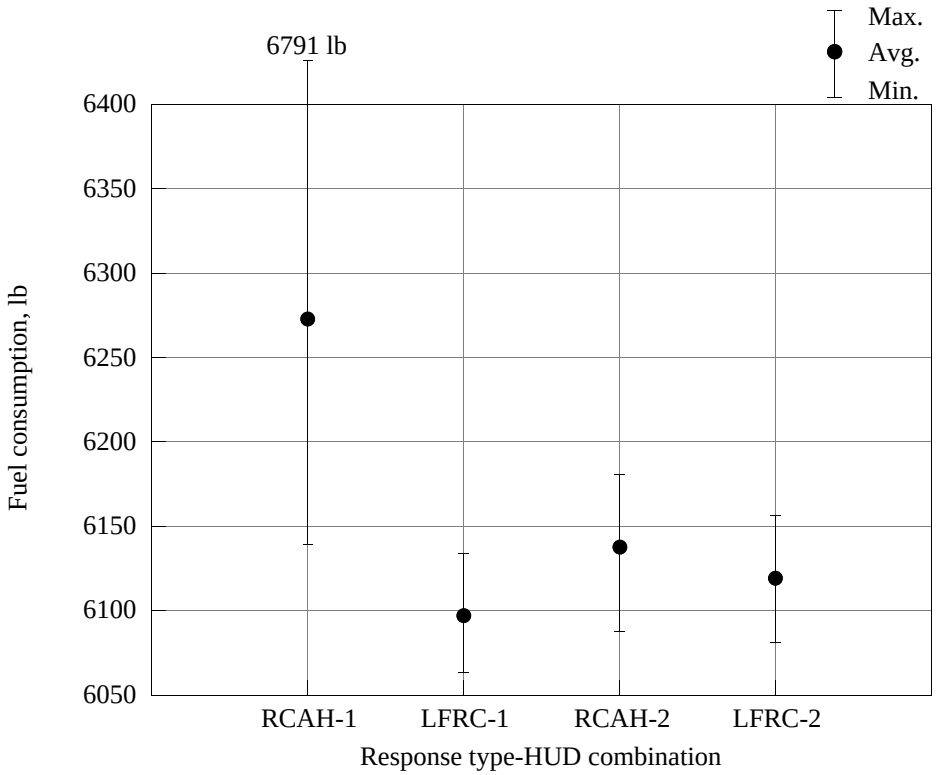

Figure 24. Fuel consumption versus response type and HUD combination with PAL 3.

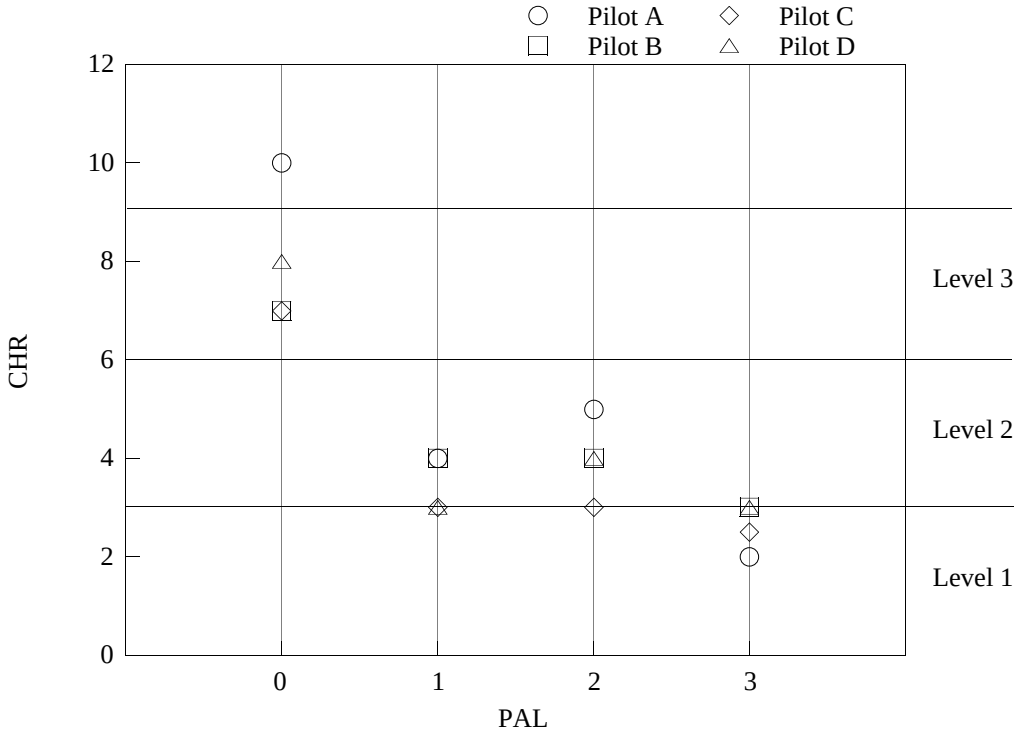

Figure 25. Cooper-Harper ratings with pilot assistance levels.

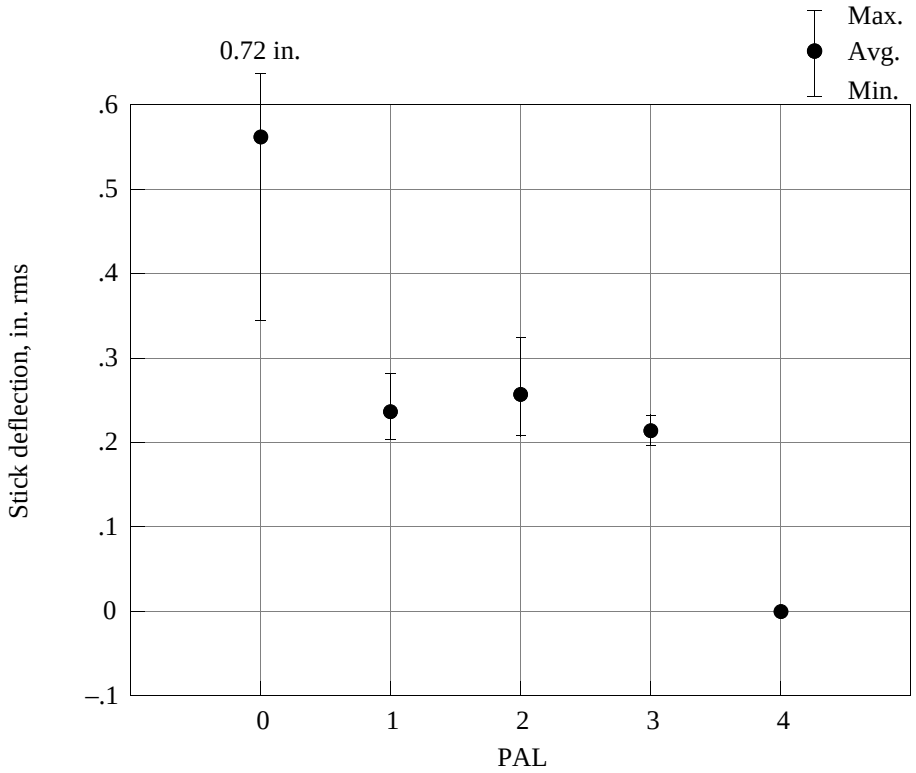

Figure 26. Stick deflection (rms) versus pilot assistance level.

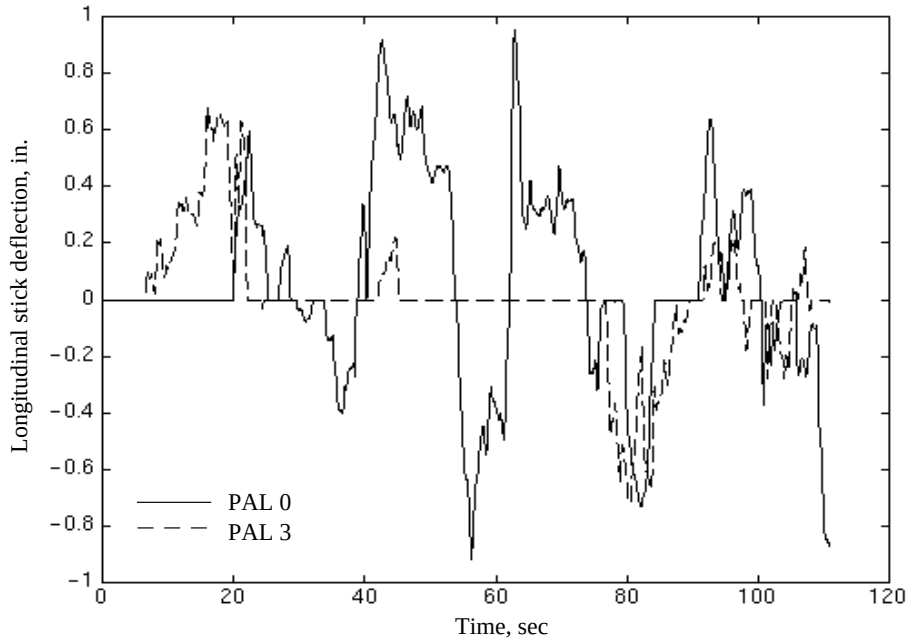

Figure 27. Time histories of longitudinal stick deflection from two maneuvers conducted by pilot B using the LFRC response type with PAL 0 and PAL 3.

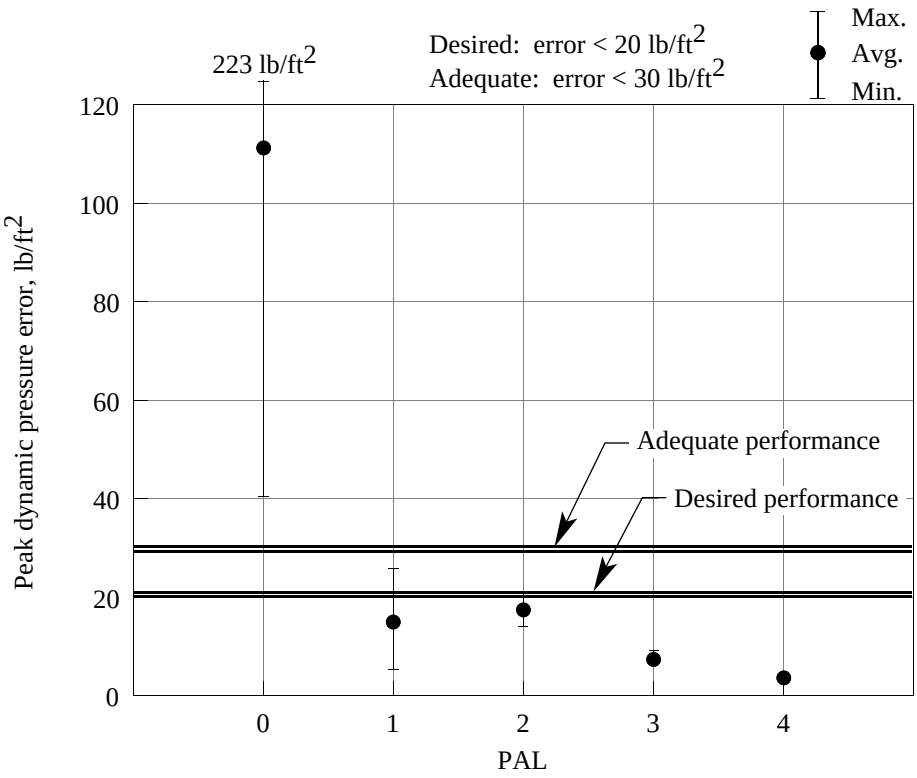

Figure 28. Peak absolute dynamic pressure error versus pilot assistance level.

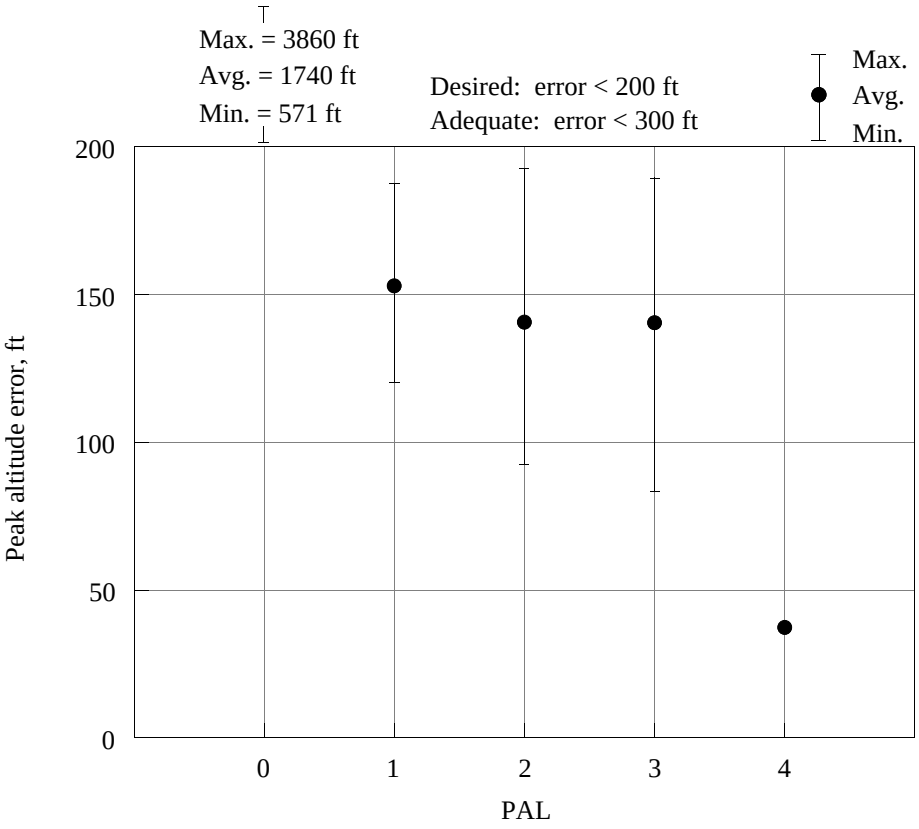

Figure 29. Peak absolute altitude error versus pilot assistance level.

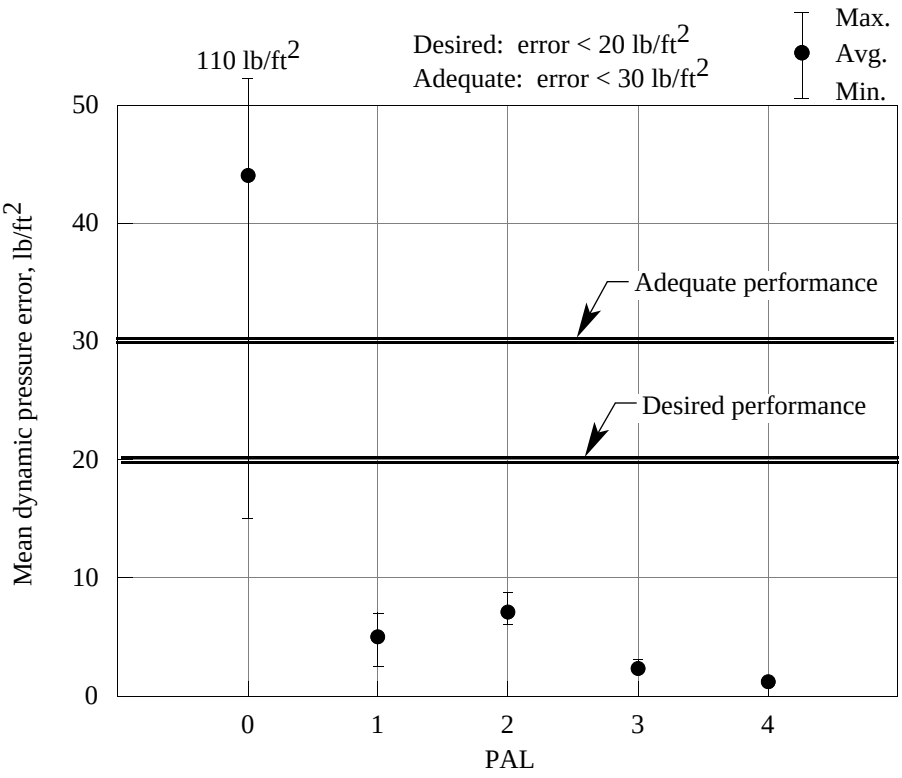

Figure 30. Mean absolute dynamic pressure error versus pilot assistance level.

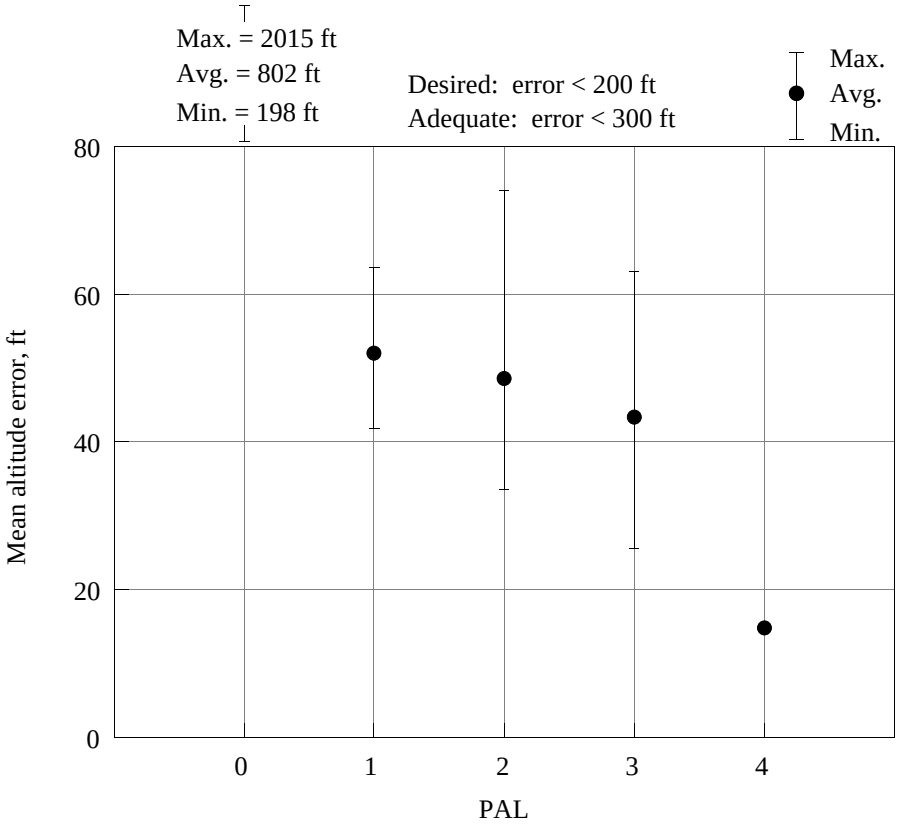

Figure 31. Mean absolute altitude error versus pilot assistance level.

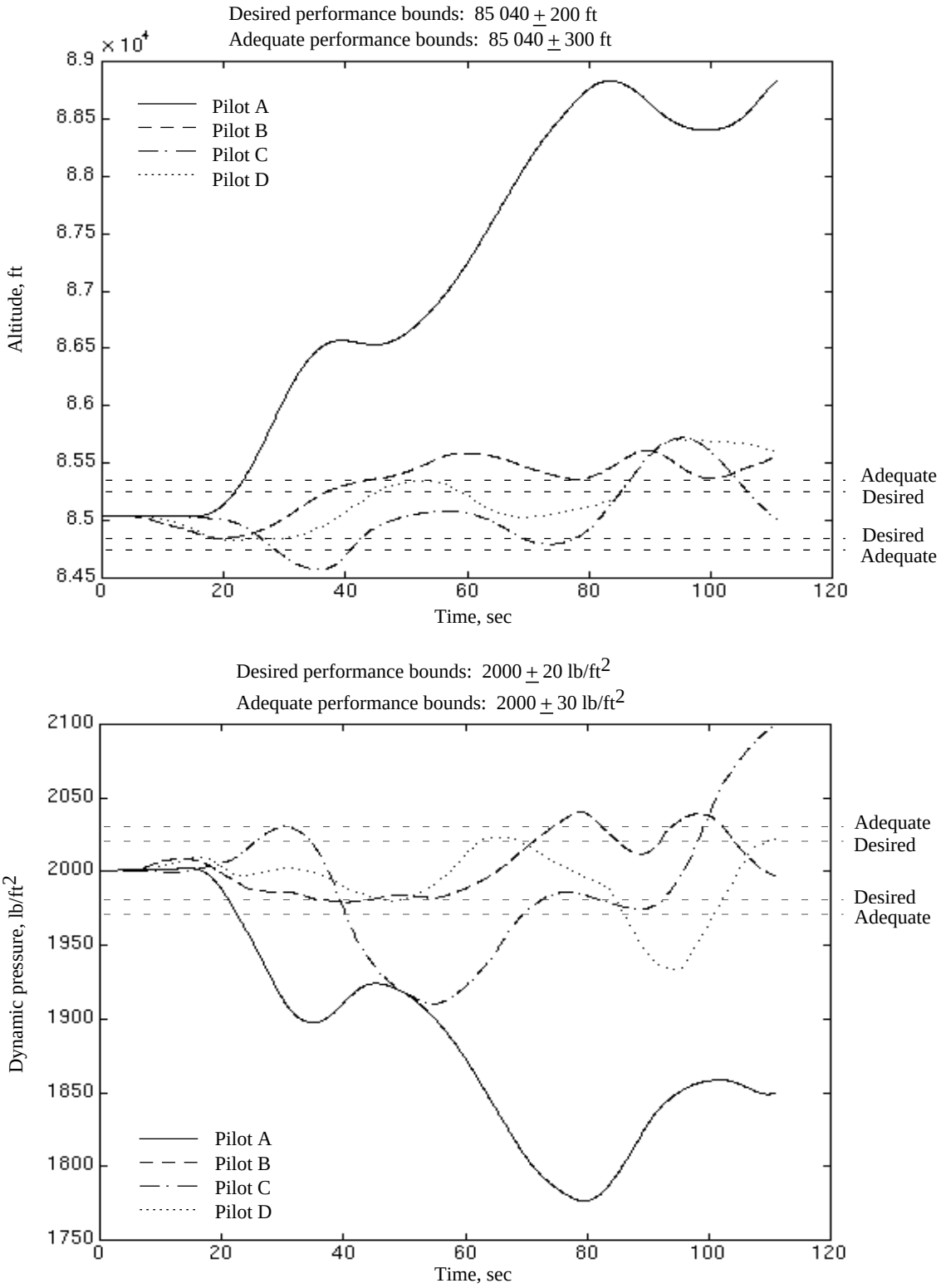

Figure 32. Time histories of typical maneuvers conducted by each of four pilots in PAL 0 using their preferred response type and HUD combination.

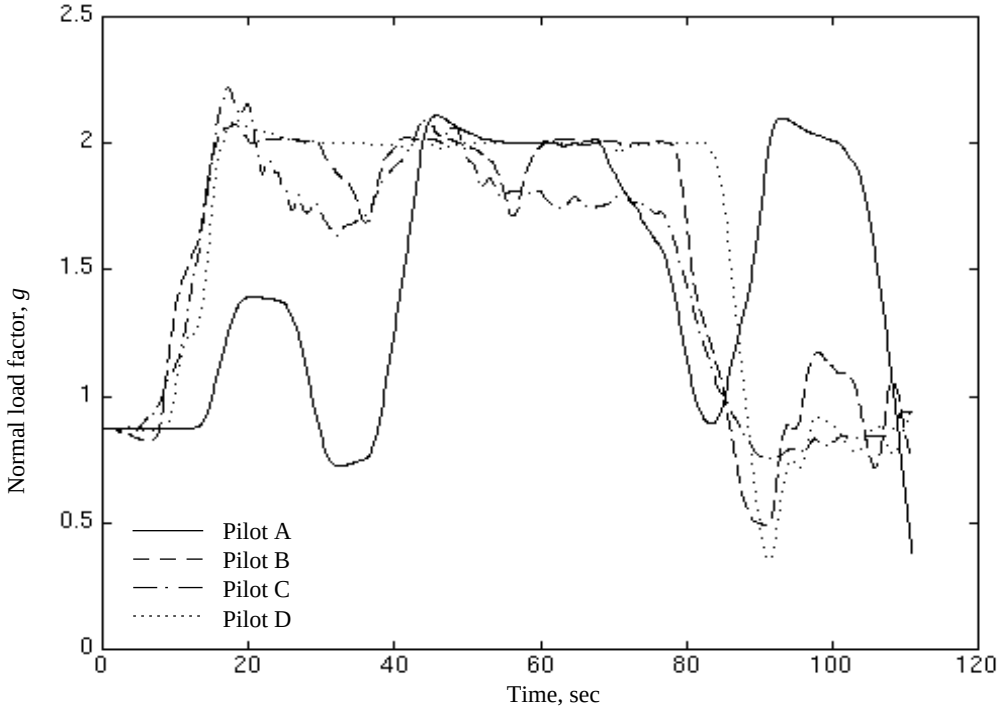

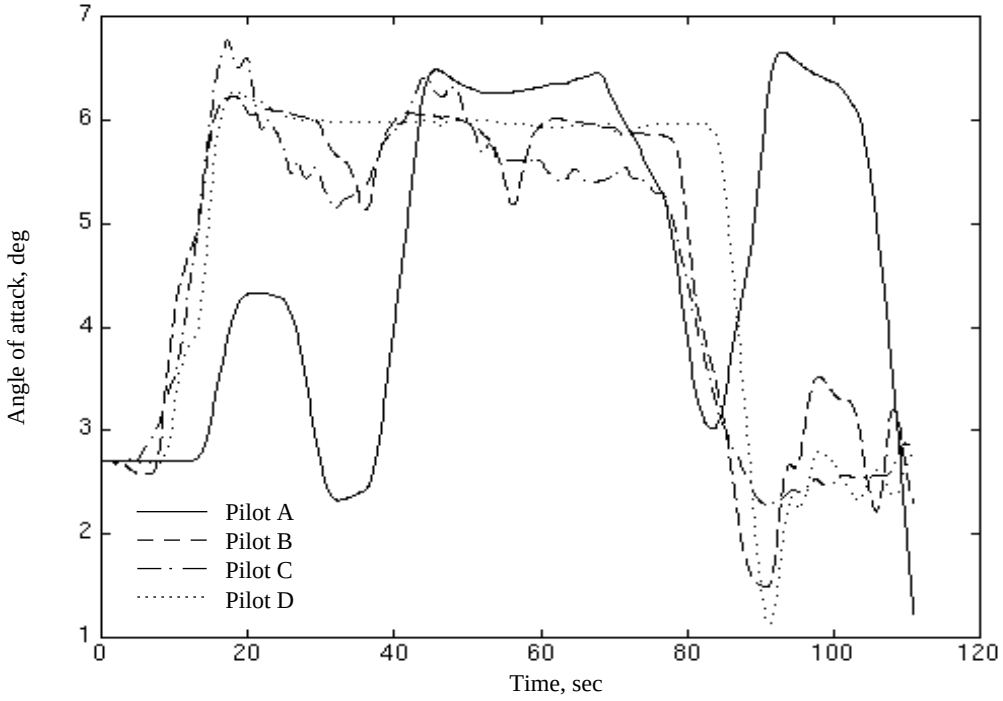

Figure 32. Continued.

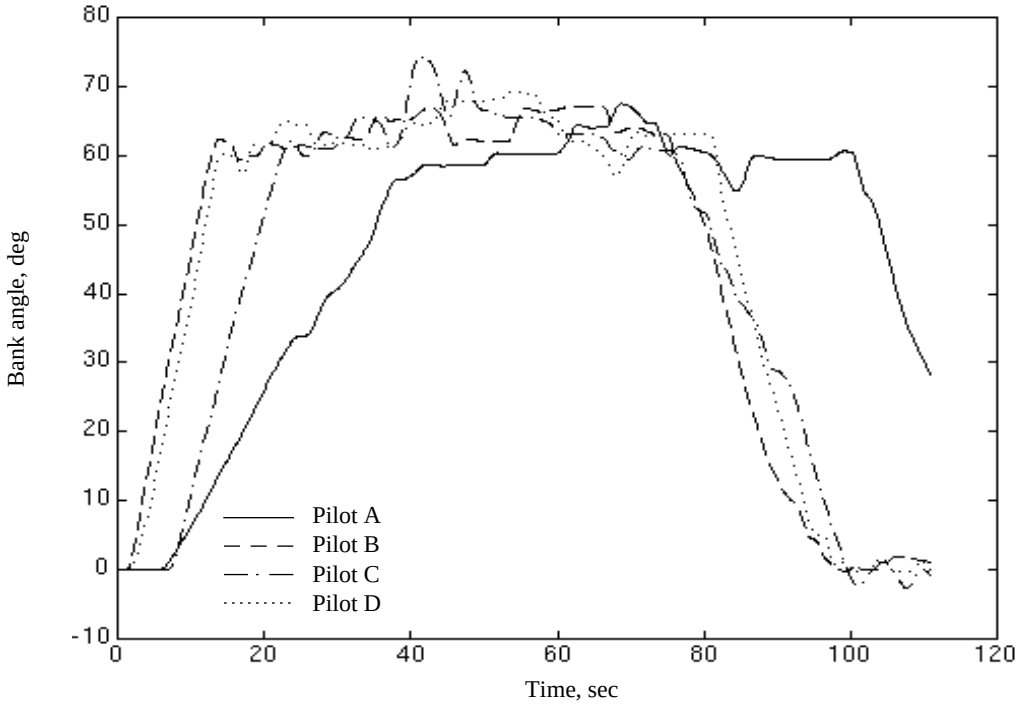

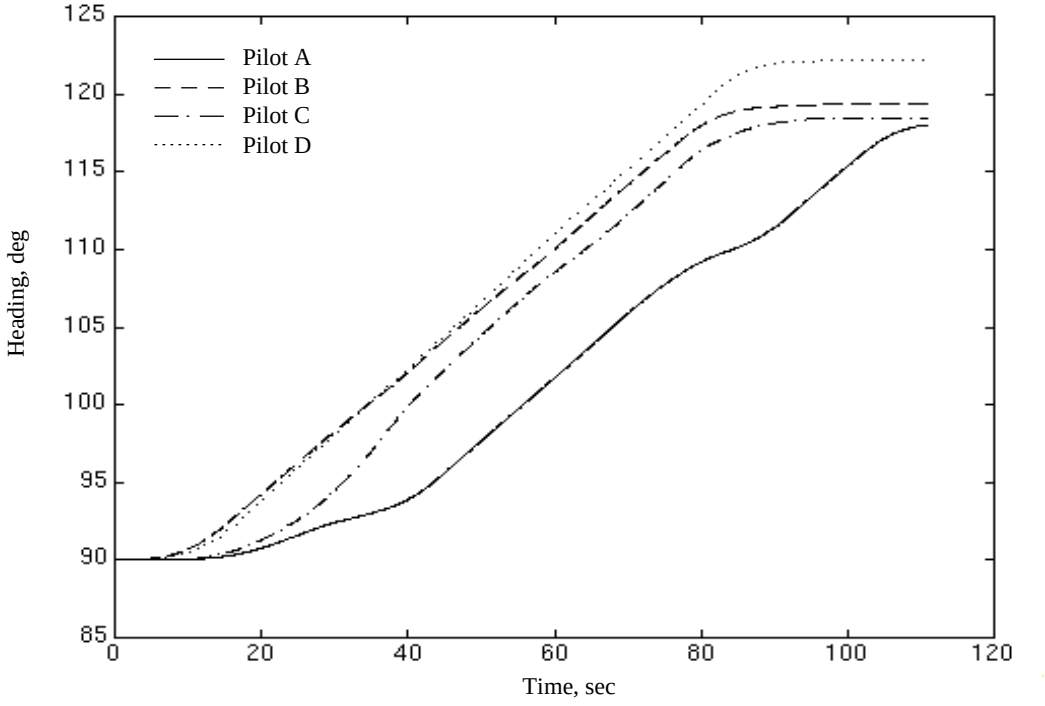

Figure 32. Continued.

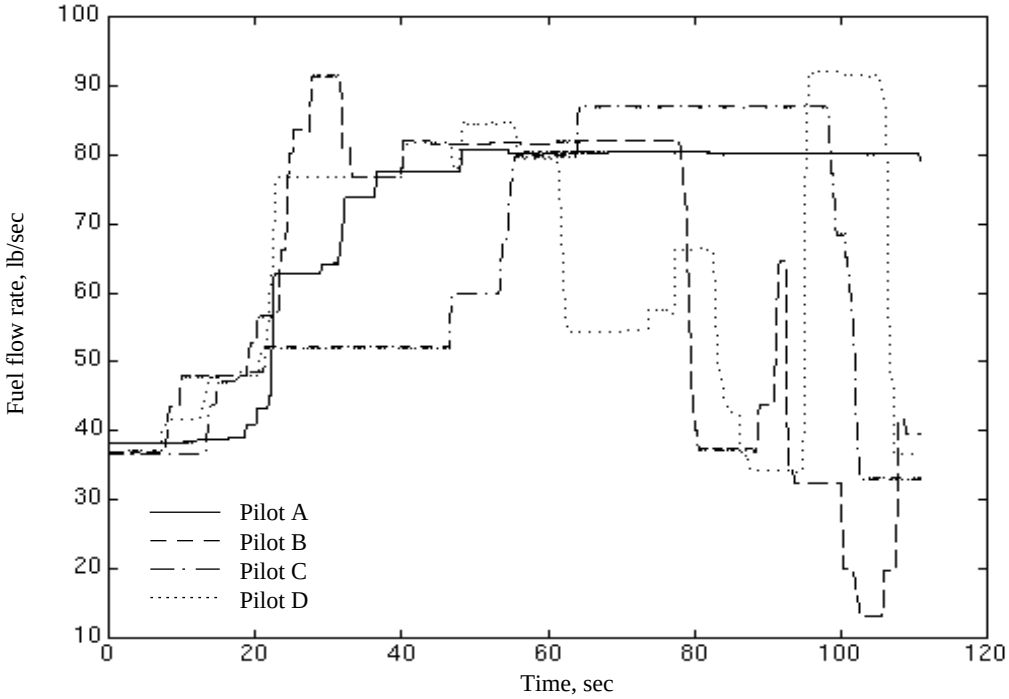

Figure 32. Concluded.

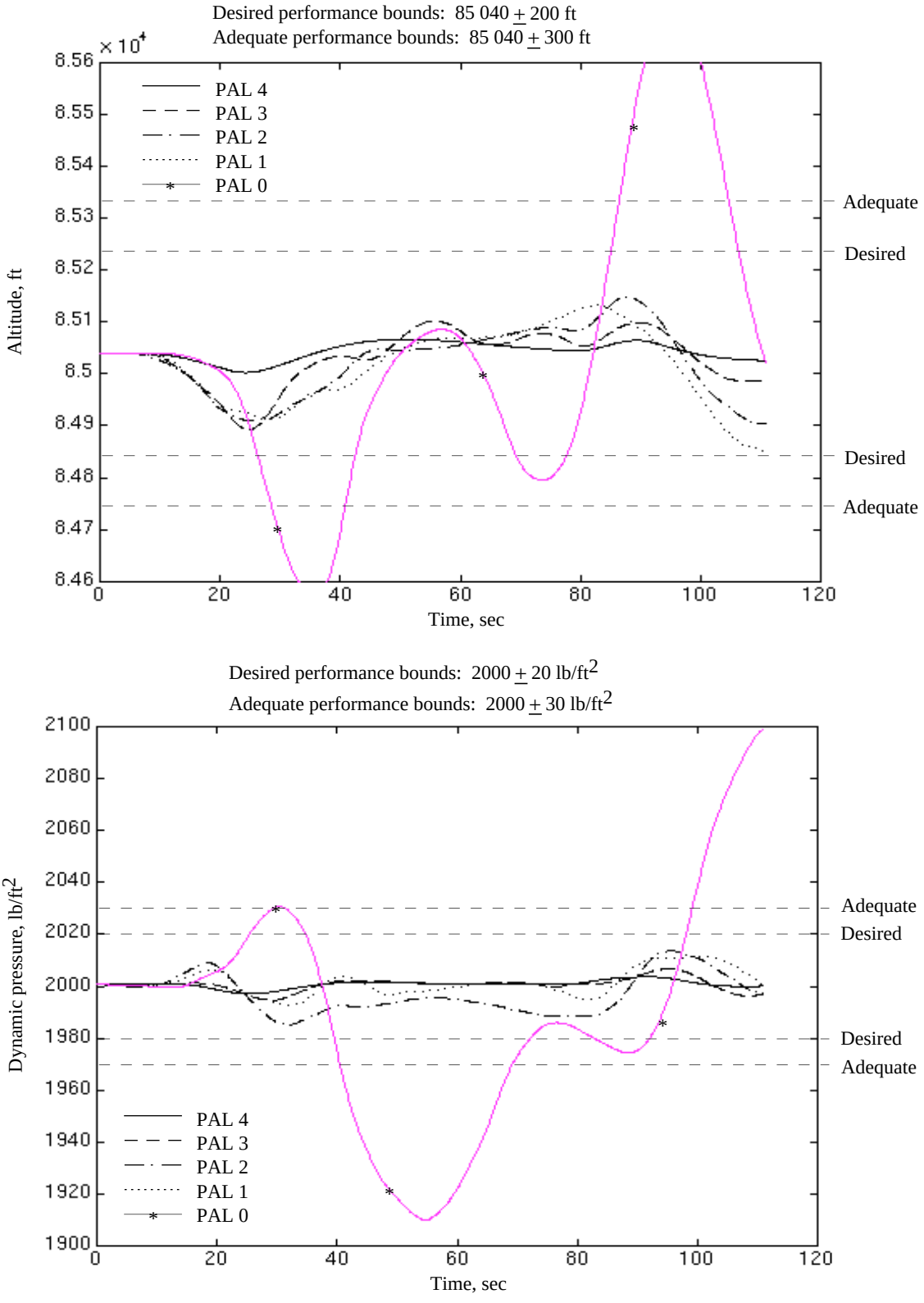

Figure 33. Time histories from typical maneuvers conducted by pilot D with all pilot assistance levels.

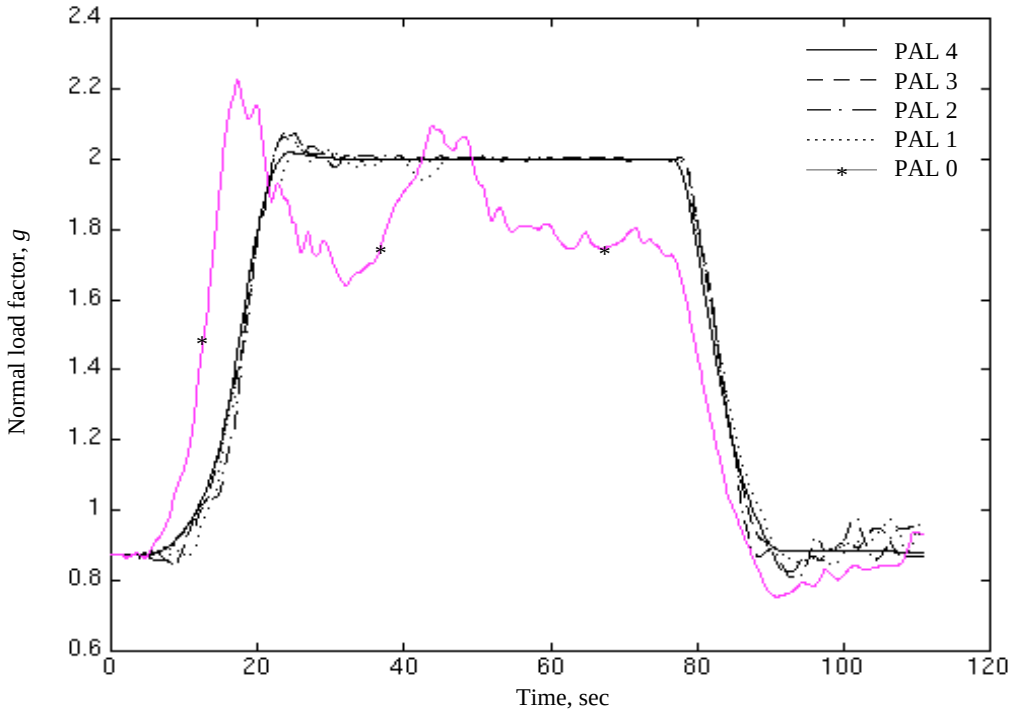

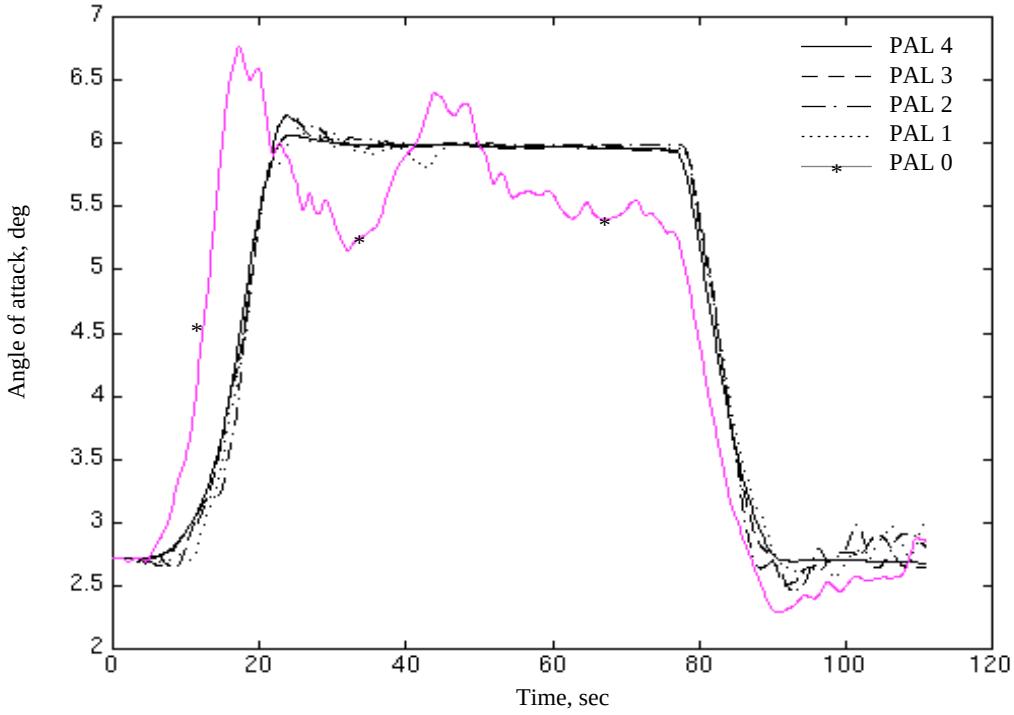

Figure 33. Continued.

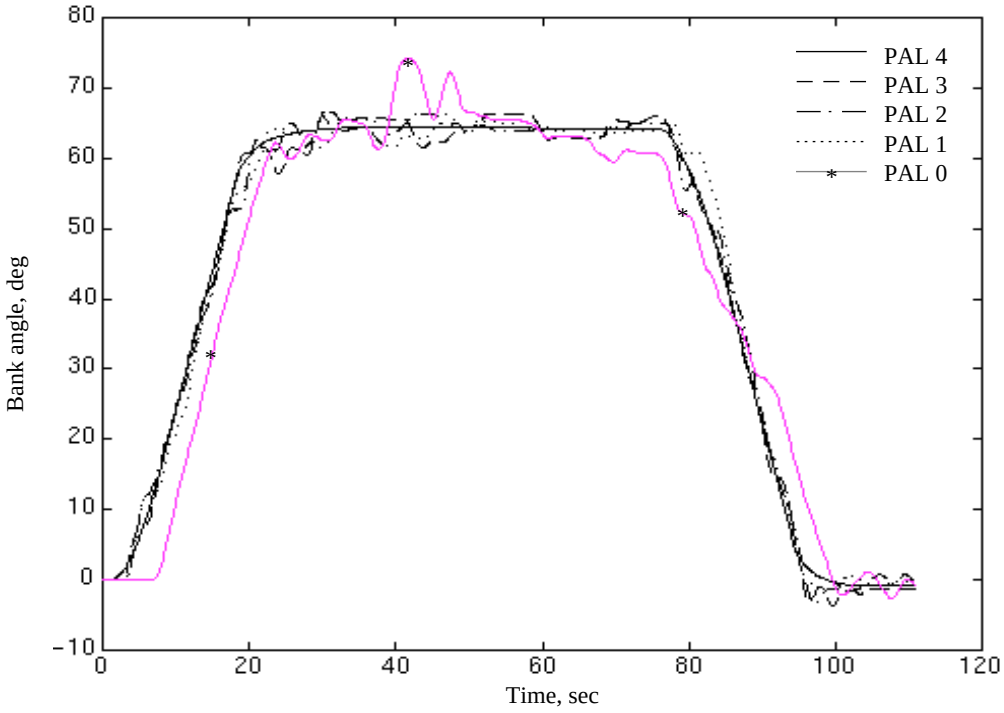

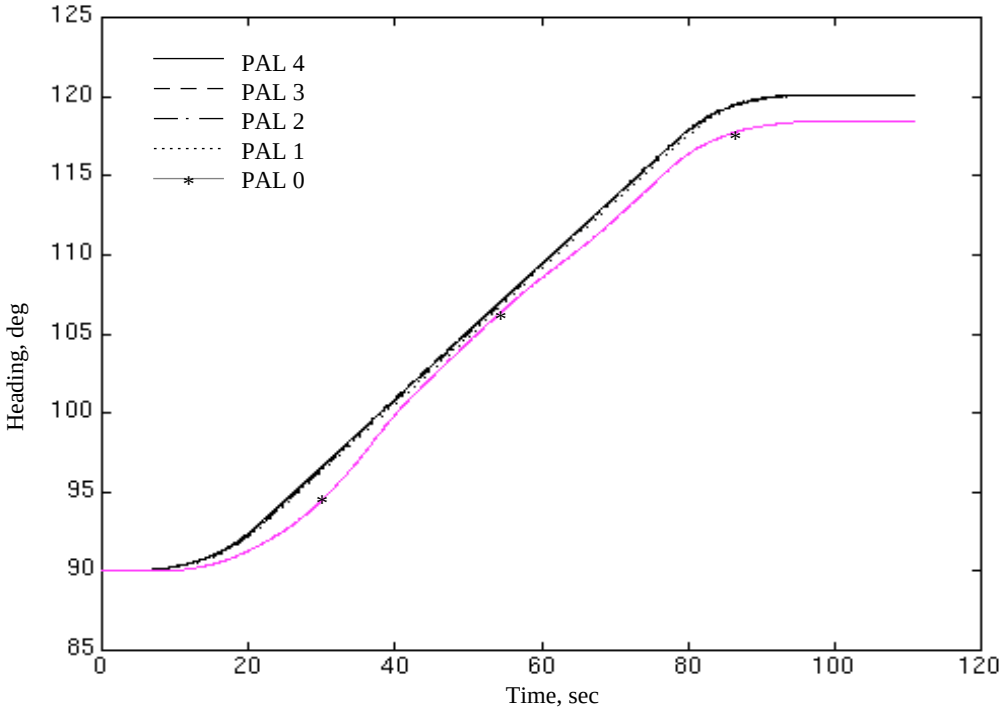

Figure 33. Continued.

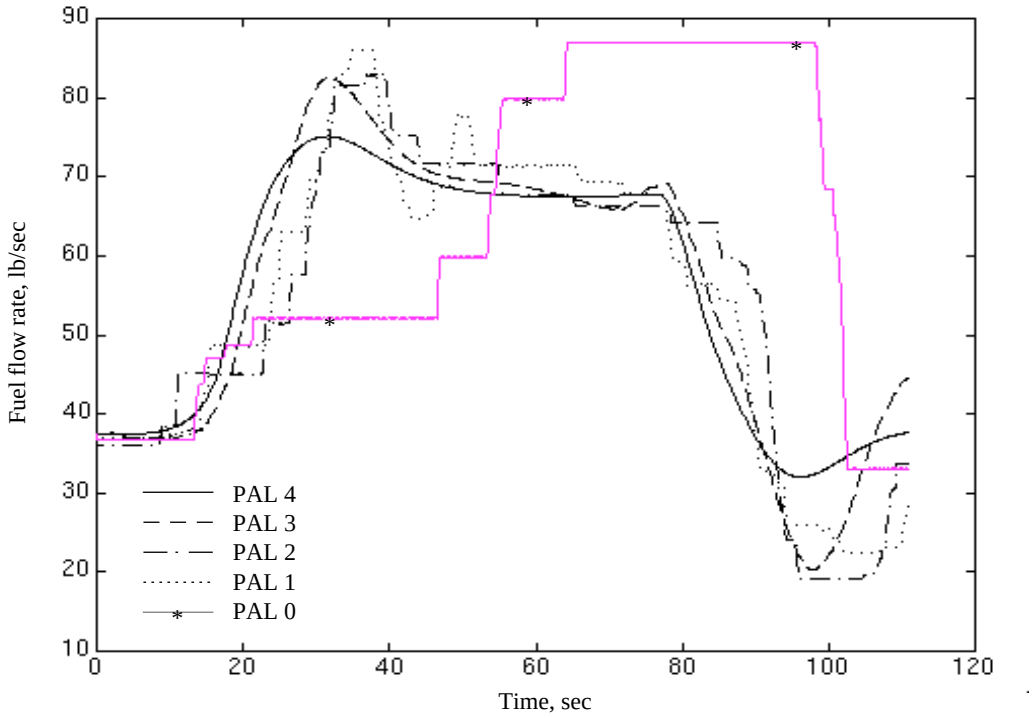

Figure 33. Concluded.

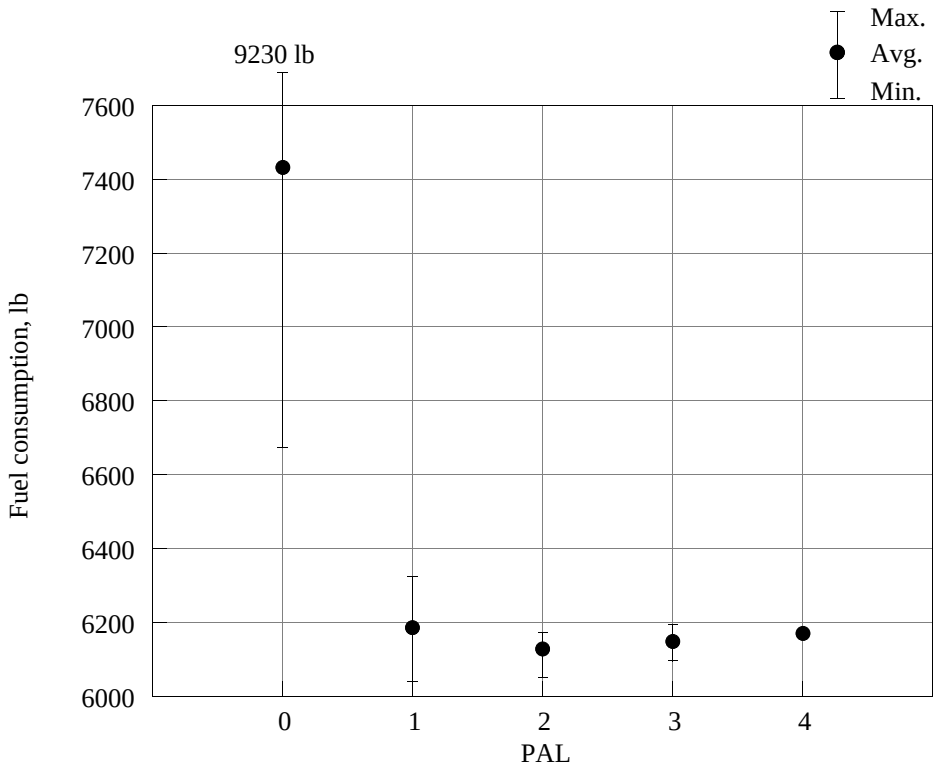

Figure 34. Fuel consumption versus pilot assistance level.

REPORT DOCUMENTATION PAGE

Form Approved
OMB No. 0704-0188

1. AGENCY USE ONLY *(Leave blank)*	2. REPORT DATE	3. REPORT TYPE AND DATES COVERED
	October 1995	Technical Paper

4. TITLE AND SUBTITLE
Investigation of Piloting Aids for Manual Control of Hypersonic Maneuvers

5. FUNDING NUMBERS
WU 505-70-64-01

6. AUTHOR(S)
David L. Raney, Michael R. Phillips, and Lee H. Person, Jr.

7. PERFORMING ORGANIZATION NAME(S) AND ADDRESS(ES)
NASA Langley Research Center
Hampton, VA 23681-0001

8. PERFORMING ORGANIZATION REPORT NUMBER
L-17446

9. SPONSORING/MONITORING AGENCY NAME(S) AND ADDRESS(ES)
National Aeronautics and Space Administration
Washington, DC 20546-0001

10. SPONSORING/MONITORING AGENCY REPORT NUMBER
NASA TP-3525

11. SUPPLEMENTARY NOTES

12a. DISTRIBUTION/AVAILABILITY STATEMENT
Unclassified–Unlimited
Subject Category 08
Availability: NASA CASI (301) 621-0390

12b. DISTRIBUTION CODE

13. ABSTRACT *(Maximum 200 words)*

An investigation of piloting aids designed to provide precise maneuver control for an air-breathing hypersonic vehicle is described. Stringent constraints and nonintuitive high-speed flight effects associated with maneuvering in the hypersonic regime raise the question of whether manual control of such a vehicle should even be considered. The objectives of this research were to determine the extent of manual control that is desirable for a vehicle maneuvering in this regime and to identify the form of aids that must be supplied to the pilot to make such control feasible. A piloted real-time motion-based simulation of a hypersonic vehicle concept was used for this study, and the investigation focused on a single representative cruise turn maneuver. Piloting aids, which consisted of an autothrottle, throttle director, autopilot, flight director, and two head-up display configurations, were developed and evaluated. Two longitudinal control response types consisting of a rate-command–attitude-hold system and a load-factor-rate–load-factor-hold system were also compared. The complete set of piloting aids, which consisted of the autothrottle, throttle director, and flight director, improved the average Cooper-Harper flying qualities ratings from 8 to 2.6, even though identical inner-loop stability and control augmentation was provided in all cases. The flight director was determined to be the most critical of these aids, and the cruise turn maneuver was unachievable to adequate performance specifications in the absence of this flight director.

14. SUBJECT TERMS
Hypersonic maneuvers; Automatic flight control; Hypersonic vehicles; Hypersonic flight; Flight dynamics; Hypersonic flying qualities

15. NUMBER OF PAGES
64

16. PRICE CODE
A04

17. SECURITY CLASSIFICATION OF REPORT	18. SECURITY CLASSIFICATION OF THIS PAGE	19. SECURITY CLASSIFICATION OF ABSTRACT	20. LIMITATION OF ABSTRACT
Unclassified	Unclassified	Unclassified	